Temporal compartmentalization of viral infection in bacterial cells

Audrey Labarde, Lina Jakutyte, Cyrille Billaudeau, Beatrix Fauler, Maria López-Sanz, Prishila Ponien, Eric Jacquet, Thorsten Mielke, Silvia Ayora, Rut Carballido-López, et al.

Temporal Compartmentalization of Viral Infection in Bacterial Cells

Audrey Labarde[a], Lina Jakutyte[b,1], Cyrille Billaudeau[c, 1], Beatrix Fauler[d], Maria López-Sanz[e], Prishilla Ponien[f], Eric Jacquet[f], Thorsten Mielke[d], Silvia Ayora[e], Rut Carballido-López[c], Paulo Tavares[a,*]

[a] Université Paris-Saclay, CEA, CNRS, Institute for Integrative Biology of the Cell (I2BC), 91198, Gif-sur-Yvette, France

[b] Laboratoire de Virologie Moléculaire et Structurale, Centre de Recherche de Gif, CNRS UPR 3296 and IFR 115, Avenue de la Terrasse, Bâtiment 14B, CNRS, 91198 Gif-sur-Yvette, France

[c] Université Paris-Saclay, INRAE, AgroParisTech, Micalis Institute, 78350, Jouy-en-Josas, France

[d] Max-Planck-Institut für Molekulare Genetik, Microscopy and Cryo-Electron Microscopy Group, Ihnestraße 63-73, 14195 Berlin, Germany

[e] Department of Microbial Biotechnology, Centro Nacional de Biotecnología, CNB-CSIC, Madrid, Spain

[f] Université Paris-Saclay, CNRS, Institut de Chimie des Substances Naturelles, UPR 2301, 91198, Gif-sur-Yvette, France

Published July 13 2021 in *Proc Natl Acad Sci U S A*, **118**(28):e2018297118

https://doi.org/10.1073/pnas.2018297118

PMID: 34244425

PNAS
www.pnas.org

Main Manuscript for

Temporal Compartmentalization of Viral Infection in Bacterial Cells

Audrey Labarde[a], Lina Jakutyte[b,1], Cyrille Billaudeau[c, 1], Beatrix Fauler[d], Maria López-Sanz[e], Prishilla Ponien[f], Eric Jacquet[f], Thorsten Mielke[d], Silvia Ayora[e], Rut Carballido-López[c], Paulo Tavares[a,*]

[a] Université Paris-Saclay, CEA, CNRS, Institute for Integrative Biology of the Cell (I2BC), 91198, Gif-sur-Yvette, France

[b] Laboratoire de Virologie Moléculaire et Structurale, Centre de Recherche de Gif, CNRS UPR 3296 and IFR 115, Avenue de la Terrasse, Bâtiment 14B, CNRS, 91198 Gif-sur-Yvette, France

[c] Université Paris-Saclay, INRAE, AgroParisTech, Micalis Institute, 78350, Jouy-en-Josas, France

[d] Max-Planck-Institut für Molekulare Genetik, Microscopy and Cryo-Electron Microscopy Group, Ihnestraße 63-73, 14195 Berlin, Germany

[e] Department of Microbial Biotechnology, Centro Nacional de Biotecnología, CNB-CSIC, Madrid, Spain

[f] Université Paris-Saclay, CNRS, Institut de Chimie des Substances Naturelles, UPR 2301, 91198, Gif-sur-Yvette, France

[1] - L.J. and C.B. contributed equally to this work.
[*] - To whom correspondence may be addressed. Email: paulo.tavares@i2bc.paris-saclay.fr.

Classification
Major classification: Biological Sciences
Minor classification: Microbiology

Keywords
bacteriophage; phage infection; virus infection; viral DNA replication; phage DNA replication; virus assembly; bacterial cell compartmentalization; Gram-positive bacterium; phage-host interaction; virus-host interaction

Author contributions
A.L., L.J., C.B., B.F., M.L.-S., P.P., E.J., and P.T. conducted experiments. C.B. developed image analysis tools. All authors interpreted data. A.L., C.B., E.J., L.J., and B.F. prepared Figures. P.T., A.L., R.C-L., and S.A. wrote the manuscript.

This PDF file includes:

Main Text

Figures 1 to 6

Abstract

Virus infection causes major rearrangements in the subcellular architecture of eukaryotes but its impact in prokaryotic cells was much less characterized. Here, we show that infection of the bacterium *Bacillus subtilis* by bacteriophage SPP1 leads to hijacking of host replication proteins to assemble hybrid viral-bacterial replisomes for SPP1 genome replication. Their biosynthetic activity doubles the cell total DNA content within 15 min. Replisomes operate at several independent locations within a single viral DNA focus positioned asymmetrically in the cell. This large nucleoprotein complex is a self-contained compartment whose boundaries are delimited neither by a membrane nor by a protein cage. Later during infection, SPP1 procapsids localize at the periphery of the viral DNA compartment for genome packaging. The resulting DNA-filled capsids do not remain associated to the DNA transactions compartment. They bind to phage tails to build infectious particles that are stored in warehouse compartments spatially independent from the viral DNA. Free SPP1 structural proteins are recruited to the dynamic phage-induced compartments following an order that recapitulates the viral particle assembly pathway. These findings show that bacteriophages restructure the crowded host cytoplasm to confine at different cellular locations the sequential processes that are essential for their multiplication.

Significance Statement

Virus lytic infection disrupts host cell homeostasis and takes over cell space for virus multiplication. . Viral-induced reorganization of prokaryotic cells must meet the challenge to restructure the cytoplasm open space of a small-sized cell. We discovered that the bacterial siphovirus SPP1 builds two types of independent compartments in the host cytoplasm to confine viral DNA enzymatic reactions and to store viral particles. This spatial partition responds to the requirements for exponential replication of SPP1 genomes and for assembly of hundreds of viral particles. Its similarities to remodelling of the cell nucleus by herpesviruses led to the hypothesis that ancestral strategies used by viruses to invade the cell space were conserved to infect hosts of different Domains of Life.

Main Text

Introduction

Organization of the cellular space is a common feature of living systems. Cell compartments delimited by membranes were observed in eukaryotic cells at the dawn of cell biology. More recently, membrane-less self-organizing compartments were identified, adding further spatial order to the cell.

Bacterial cells mainly rely on the latter type of strategy to structure their “open-space” cytoplasm because they rarely feature intracellular membranes (1), although some notable exceptions exist (2). One well-documented case of membrane-free compartmentalization is self-assembly of protein cages that confine biochemical reactions (3) or store specific cargo (4) in the bacterial cytoplasm. Considering their increasing variety, cell compartments are collectively defined here as a self-contained space that concentrates a set of macromolecular components inside the cell. Their boundaries can be established by membranes, a protein cage, or by the physicochemical properties of their components.

Lytic viral infection disrupts host cell homeostasis, re-allocating extensive resources for virus multiplication. In eukaryotic viruses this takeover correlates with the formation of virus replication compartments either in the host cytoplasm or in the nucleus (5). These viral factories can be membrane-associated structures as in case of several RNA virus families (6), membrane-less viral DNA replication compartments (5), or liquid compartments formed by phase separation (7). Re-structuration of bacterial cell architecture upon infection by bacterial viruses (phages or bacteriophages) is much less documented. DNA replication has been reported to occur at particular positions of the bacterial cytoplasm for four *Caudovirales*, a widely distributed order of double-stranded DNA (dsDNA) viruses also known as tailed bacteriophages. Phage ϕ29 uses the actin-like MreB cytoskeleton and the bacterial nucleoid to position protein-primed replication of its ~20 kbp genome at the periphery of the host cytoplasm (8, 9). Jumbo phages compartmentalize replication and transcription of their >200 kbp genome inside a viral proteinaceous nucleus-like cage that is positioned at mid-cell by a tubulin-related spindle (10–12). These are rare cases within the tailed phagosphere because of their particular mode of protein-primed replication (ϕ29) and of their genome size (ϕ29 and jumbo phages). The genomes of sequenced tailed phages have a median length of 51 kbp and those of the *Siphoviridae* family, which accounts for more than 55% of *Caudovirales*, are 48 kbp-long on median (13). λ and SPP1, which typify the siphoviruses, accumulate their replicated DNA in a defined focus localized asymmetrically in the cell during lytic infection (14, 15) but further investigation is critical to assess the impact of their infection on cell biology.

Here we investigate cell host takeover by the well-characterized bacteriophage SPP1 (16–20), which infects the Gram-positive model bacterium *Bacillus subtilis* (Fig. 1*A*). We discovered that phage infection leads to an extensive reorganization of the *B. subtilis* cytoplasmic space. SPP1 is shown to assemble two temporally and spatially independent types of compartments in the bacterial cytoplasm. A single compartment harbors viral genome replication and packaging while the others are storage regions of viral particles (or virions).

Results

DNA biosynthetic challenge imposed by bacteriophage SPP1 infection to the host cell. Genome replication and virion assembly are the key steps of virus multiplication (Fig. 1*A*) accounting for most of phage infection biosynthetic costs. To investigate their impact on the architecture of infected cells, we used a phage that carries an array of ~64 *lacO* operator sites inserted in its genome (SPP1*delX110lacO64*). By infecting *B. subtilis* cells producing the cognate LacI binding protein fused to a fluorescent protein (FP), phage DNA can be visualized during infection (15). SPP1*delX110lacO64* produces ~2 to 3-fold less progeny virions than SPP1 wild-type but impacts neither the phage temporal infection program nor the timing of phage lysis (*SI Appendix*, Fig. S1*A*) (15, 16). SPP1*delX110lacO64*, abbreviated SPP1*lacO64* from hereafter, and the *B. subtilis* strain producing LacI-mCherry are the parental viral and bacterial strains, respectively, used throughout the present study unless stated otherwise.

The DNA mass in SPP1*lacO64*-infected cells rose sharply after 15 min post-infection (p.i.) (*SI Appendix* Fig. S1*B*). At 30 min p.i., when lysis initiates in rich medium cultures grown at 37°C, total DNA increased ~2-fold relative to non-infected cells. The mean cell surface did not vary significantly during infection (2.71±0.78 μm^2 (n=2464) in infected cells *vs* 2.85±0.79 μm^2 (n=1160) in non-infected cells), indicating that the DNA/cytoplasmic space ratio was doubled. We next quantified bacterial and viral DNA during infection by qPCR. Viral genome replication was detectable at 10 min p.i. and increased exponentially until 30 min p.i. (Fig. 1*B*). At this stage of infection each bacterium contained an average of 318 copies of the phage genome (Fig. 1*B*, empty circles) accounting for 13.4 Mbp of viral DNA, which exceeds the ~11 Mbp of bacterial DNA present in the cell (equivalent to 2.7 copies of the 4.06 Mbp *B. subtilis* YB886 genome (*SI Appendix* Fig. S1 *C* and *D*) (21)).

Genome encapsidation quantified by qPCR of DNAse-protected DNA was detected at 20 min p.i. (Fig. 1*B*, filled circles) due to its temporal delay relative to DNA replication (16). Only a fraction of the SPP1 DNA synthesized (reaching ~60% at 30 min p.i.) was encapsidated inside viral particles (Fig. 1*B*, filled circles and Fig. 1*C*). The majority of those particles (~75% at 30 min p.i.) were infectious as quantified in a phage titration plaque assay (Fig. 1*B*, squares). The non-infectious viral particles were likely DNA-filled capsids that did not yet attach tails in their assembly pathway (22) and possibly some defective tailed phage particles. Interestingly, SPP1 DNA synthesis was reduced in infections with a phage defective in the DNA packaging enzyme gp2 (SPP1*delX110lacO64sus19* (Table S1) (23), hereafter abbreviated as SPP1*lacO64gp2*$^-$) that does not encapsidate DNA (Fig. 1*D*), indicating a regulatory feedback between genome encapsidation and DNA replication.

***B. subtilis* replisome proteins are recruited into hybrid phage-host replisomes at the viral DNA compartment.** Mono-infected *B. subtilis* cells display a single phage DNA focus (*SI Appendix* Fig. S2 *A*

and *B*), hereinafter referred to as the viral DNA compartment, which increases in size during infection (*SI Appendix* Fig. S2*B*) (15). Since SPP1 requires several host proteins for replication of its genome (Table S2) (24-26), we investigated the sub-cellular localization of both SPP1 DNA and FP fusions to *B. subtilis* replisome components (Fig. 2*A* and *SI Appendix* Fig. S2*C*). In non-infected bacteria the DNA polymerase PolC, the clamp loader subunit DnaX, the sliding clamp DnaN, and the single-stranded DNA binding protein SsbA localized into small foci, presumably the *B. subtilis* replisomes assembled at replication forks (arrowheads in Fig. 2*A* and *SI Appendix* Fig. S2*C*) (27). Foci of the primosome protein DnaB and of the DNA polymerase DnaE were also detected in some cells, while the primase DnaG displayed a diffuse distribution (*SI Appendix* Fig. S2*C*, left) (27, 28). Interestingly, in infected bacteria all seven host proteins co-localized with SPP1 DNA, irrespectively of being essential (PolC, DnaE, DnaX, DnaN and DnaG) or dispensable (SsbA and DnaB) for SPP1 multiplication (Fig. 2 and *SI Appendix* Fig. S2*C* and Table S2). The co-localization of DnaE and DnaB fluorescent protein fusions with phage DNA was more prominent early p.i. while the other host replisome components associated persistently to phage DNA during infection. Small foci of SsbA and more rarely of DnaX were also detected outside the viral DNA compartment in some infected cells (arrows in Fig. 2*A* and *SI Appendix* Fig. S2*C*) possibly associated to host DNA. The *B. subtilis* replicative helicase DnaC showed a homogeneous distribution both in non-infected and in infected bacteria (Fig. 2*B* and *SI Appendix* Fig. S2*C*).

SPP1 infection led to a loss of the regular distribution of bacterial DNA replication origins in the cell (*SI Appendix* Fig. S1*E*) but replication of the *B. subtilis* genome continued at least early during phage infection (*SI Appendix* Fig. S1*F*). Nevertheless, the prominent spatial concentration of bacterial DNA replication effectors in the SPP1 DNA compartment correlated with a strong viral genome replication activity (Fig. 1*B* and *SI Appendix* Fig. S1*G*) that outperforms DNA replication in the bacterial nucleoid (Fig. 1*B*). We concluded that the DNA replication machinery of *B. subtilis* is biochemically and spatially re-programmed for SPP1 genome replication.

We next investigated how the host replisome is recruited to the phage DNA compartment in three-color imaging experiments in which SPP1 DNA, *B. subtilis* replication proteins, and SPP1 replication proteins were simultaneously labelled. SPP1 DNA replication is initiated by gp38 binding and melting of the phage origins of replication (29). Then, gp39 loads the helicase gp40 to the open origins (26, 30). Gp40 is known to interact with the host clamp loader subunits DnaX (31) and with the primase DnaG (32, 33). The finding that a gp40-mCitrine fusion produced in non-infected *B. subtilis* displayed a replisome-like localization and co-localized with mCFP-DnaX (Fig. 3*A*) is consistent with those previously identified interactions. Thus, the SPP1 helicase is recruited to the *B. subtilis* replisome in the absence of other phage proteins. In infected cells, both gp40 and DnaX relocalized into two or more foci inside the SPP1 DNA compartment (Fig. 3*B*), as also observed for other host replisome

components (Fig. 2*A* and *SI Appendix* Fig. S2*C*). These results indicate that viral DNA replication factories composed of hybrid phage-host replisomes assemble at distinct positions within the viral DNA compartment.

Upon entry into the host cell, the SPP1 genome is circularized and undergoes several cycles of circle-to-circle (theta) replication, leading to an exponential increase of phage DNA template molecules, and then switches to a linear sigma replication mode to generate genome concatemers (Fig. 3*E*). The gp40 helicase is essential for SPP1 DNA synthesis in both modes (25, 26) providing a hallmark for localization of SPP1 replication throughout infection (Fig. 3*F*). The SPP1 recombinase gp35 is essential for the theta-to-sigma replication mode switch and the 5'-3' exonuclease gp34.1 is the other major phage effector of this step (17, 34). We were unable to determine the subcellular localization of gp35 due to aggregation of different FP fusions to gp35, but we obtained a functional gp34.1-mCitrine fusion. Gp34.1-mCitrine formed a small focus that increased in size and co-localized with phage DNA in infections with a SPP1 mutant defective for production of gp34.1 (Fig. 3*G*). Thus, the complete sequential program of SPP1 replication is compartmentalized in the phage DNA compartment.

Viral DNA occupies a self-contained dynamic compartment. Presence of a single viral DNA compartment in mono-infected bacteria indicates that replication of the SPP1 DNA molecule, which entered the cell at the beginning of infection (Fig. 1*A*), occurs at a specific location in the cytoplasm where descendent viral genomes accumulate throughout infection (*SI Appendix* Fig. S2 *A* and *B*). We then analyzed quantitatively this compartment position and shape in hundreds of mono-infected cells. The compartment grew as infection proceeded (Fig. 4*A*) and had a center of mass at about 1.2 µm from the cell proximal pole regardless its size (Fig. 4*B*). The cell diameter of *B. subtilis* (~1 µm) rapidly constrained radial growth of the compartment leading to an elongated shape. Its area increased by longitudinal growth as DNA synthesis ensued (Fig. 4 *C-E*). Phage DNA accessible for LacI-mCherry labeling occupied, on average, 25% of the cell area late in infection (Fig. 4*A*, blue). This accounted only for ~40% of the total SPP1 DNA synthesized because the remaining DNA shielded inside viral particles (Fig. 1*B,C*) was stripped-off of LacI-mCherry during its packaging into phage procapsids through a 30 Å-wide portal channel. To visualize the total SPP1 DNA synthesized we infected cells with SPP1*lacO64gp2*$^{-}$ that is defective in DNA packaging. In absence of genome encapsidation, the viral DNA compartment grew into a significantly more elongated shape (Fig. 4 *C-E*) revealing that SPP1 DNA can occupy more that 35% of the cell area (Fig. 4*A*, magenta).

In order to visualize this impact of SPP1 infection on DNA spatial distribution within the cell ultrastructure we carried out immunoelectron microscopy (immunoEM) of thin sections from *B. subtilis* YB886, an isogenic strain without fluorescent markers. DNA was localized using an anti-DNA

monoclonal antibody decorated with 5 nm colloidal gold (small dots in Fig. 5 *A*,*B*,*E* and *F*) or DNAse treatment (Fig. 5 *C* and *D*) (35). In non-infected cells two separated, symmetrically positioned, bacterial nucleoids were readily observable (Fig. 5 *A*,*C* and *E*), consistent with DAPI fluorescence staining (Fig. 5*G*). SPP1*lacO64gp2*$^{-}$ infection led to a major reorganization of the cytoplasmic space where DNA occupied a much larger region (Fig. 5*D*). Loss of the bacterial nucleoids typical position and organization in the cell (Fig. 5 *B*,*D*,*F* and *H*) correlated with re-positioning of *B. subtilis* chromosome origins away from the viral DNA compartment (*SI Appendix* Fig. S1*E*).

Membrane staining shows that no membrane separates the SPP1 DNA compartment from the cytoplasm (*SI Appendix* Fig. S2*B*) (15). The unpackaged ~125 genome copies (5.3 Mbp) of SPP1*lacO64* DNA late p.i. (Fig. 1*B*) occupy no more than ~25% of the cytoplasm open space area (Fig. 4*A*). To investigate if integrity of this viral DNA compartment requires active DNA replication and is energy-dependent we arrested DNA polymerase III activity with 6 (*p*-Hydroxyphenylazo)-Uracil (HPUra) (15, 36) and collapsed the proton motive force with 2,4-dinitrophenol (DNP) (37), respectively. Both HPUra and DNP prevented formation of the viral DNA compartment at the beginning of infection. When the drugs were added after appearance of the SPP1 DNA focus, they did not disrupt its morphological integrity (Fig. 3 *C* and *D*; SPP1 DNA panels). In HPUra-treated cells, proteins of the hybrid viral-bacterial replisome (visualized by gp40 and DnaX) lost, however, their typical pattern of discrete small foci within the DNA compartment and re-localized all over the SPP1 DNA (Fig. 3*C*). We concluded that maintenance of SPP1 replication factories, but not of the viral DNA compartment, required active DNA synthesis. In DNP-treated cells, DnaX lost most of its association with the compartment and displayed a patchy pattern in the cytoplasm while gp40 maintained its co-localization with SPP1 DNA (Fig. 3*D*). Thus, energy depletion leads to hybrid replisomes disassembly and dissociation of DnaX, but not of gp40, from the viral DNA compartment.

A sub-population of SPP1 procapsids localizes at the edges of the viral DNA compartment. The goal of viral genome replication is to provide a nucleic acid substrate suitable for viral particles construction. In tailed bacteriophages, as in numerous viruses, replicated DNA is packaged into procapsids that are virion precursors without DNA (Fig. 5*K*), prompting investigation of their position relative to DNA in the cell. Procapsids accumulate in the cytoplasm of bacteria infected with SPP1 mutants defective for genome packaging like SPP1*lacO64gp2*$^{-}$ (18). Reliable imaging of individual phage procapsids and virions by EM of infected bacteria was hampered by sample fixation, in spite of extensive optimization work. However, immuno-labeling of thin sections with anti-(pro)capsid antibodies showed that those structures (thick dots in Fig. 5 *B*,*D* and *F*) accumulate at the periphery of DNA (thin dots in Fig. 5 *B* and *F*) in *B. subtilis* YB886 cells infected with SPP1*lacO64gp2*$^{-}$. Procapsid labeling was

reproducibly enhanced by digestion of DNA (Fig. 5*D*) and of trypsin-sensitive non-assembled proteins (Fig. 5*F*) in the thin sections.

We then imaged specifically SPP1 DNA with LacI-mCherry and the procapsid scaffolding protein gp11 fused to mCitrine in live cells. Gp11 is a rod-like internal chaperone that scaffolds multimerization of the major capsid protein gp13 to build functional procapsids (38). Gp11 then exits the procapsid through holes of ~3 x 2.2 nm in the gp13 protein lattice to leave space for DNA packing (Fig. 5*K*) (39). Infection of cells producing mCitrine-gp11 with phages coding for gp11 but defective in DNA packaging (e.g. SPP1*lacO64gp2*$^{-}$ in Fig. 5*K*) led to accumulation of procapsids in the bacterium. Their sedimentation behavior and shape were similar to SPP1 wild-type procapsids although they carry the two gp11 forms (*SI Appendix* Fig. S3 *A* and *B*), showing that mCitrine-gp11 is incorporated into correctly-shaped procapsids during assembly. Unexpectedly, CsCl-purified phage particles produced during infection with SPP1*lacO64* contained mCitrine but not the full-length mCitrine-gp11 fusion (*SI Appendix* Fig. S3*C*). We posited that the mCitrine β-barrel dimensions (~3 x 4 nm size in case of mCitrine (40)) precluded exit of mCitrine-gp11 through the procapsid holes and interpreted that the fusion protein was proteolyzed when its gp11 moiety left the procapsid prior to DNA packaging, leaving mCitrine stuck inside. Collectively, the data show that mCitrine-gp11 is incorporated into procapsids and that mCitrine remains inside functional structures during their subsequent maturation steps until the end of viral particle assembly.

MCitrine-gp11 distributed homogeneously in the cytoplasm of either non-infected cells (Fig. 5*I*) or cells infected with SPP1*lacO64gp13*$^{-}$ (*SI Appendix* Fig. S3*D*), a mutant defective in the major capsid protein gp13 that does not build procapsids (Fig. 5*K*). When procapsids assembled during infection, mCitrine-gp11 formed foci in the cell consistent with its incorporation in viral structures. In absence of DNA packaging these foci accumulated at the phage DNA compartment periphery (Fig. 5*J* and *SI Appendix* Fig. S3 *E* and *F*) as found in immunoEM experiments (Fig. 5 *B*,*D* and *F*). To follow the localization of procapsids during infection without the space constraints imposed by the cells small size, we performed time-lapse observation of mCitrine-gp11 in filamentous *B. subtilis* bacteria infected by SPP1*lacO64gp2*$^{-}$. Septation was inhibited by adding the FtsZ-inhibitor PC190723 to exponentially growing cells prior to infection, leading to the formation of long, aseptated filaments (41). The SPP1 DNA compartment became several micrometer-long in the filamentous cells before procapsids progressively accumulated at the compartment edges as well as at SPP1 DNA-free regions near the cell poles (Fig. 5*L*). Procapsids lacking the portal protein gp6 (42) showed a similar distribution (Fig. 5*M*). Interestingly, when the bacterium lysed procapsids maintained their cluster organization in the agarose pad gel used to immobilize the cells while the SPP1 DNA compartment lost its organization (Fig. 5*L*, bottom panel arrow).

The localization pattern of mCitrine-gp11 had some distinctive features in cells infected by SPP1*lacO64*, in which the assembly pathway of viral particles is complete. Fluorescent foci that flank the SPP1 DNA compartment are significantly better individualized and separated from the DNA compartment (*SI Appendix* Fig. S3*G*) than those observed when only procapsids accumulate in the infected cell (*SI Appendix* Fig. S3 *E* and *F*). Since the fluorescent protein reports the localization of both procapsids and DNA-filled capsids (see above) its assignment to the distribution of specific viral structures in the cell was not made.

SPP1 DNA-filled particles accumulate in spatially independent compartments. In order to image SPP1 capsids specifically at the post-DNA packaging state, we fused mCitrine to the non-essential capsid accessory protein gp12 (Fig. 6*A*). The binding sites of gp12 in the gp13 capsid lattice are generated during DNA encapsidation (39, 43). Consistently, when *B. subtilis* cells expressing gp12-mCitrine were infected with a DNA packaging defective mutant, gp12 displayed a diffuse localization in the cytoplasm (Fig. 6*B*). During productive infections, gp12-mCitrine bound to DNA-filled viral particles and localized to foci flanking the phage DNA compartment both in the absence (Fig. 6*C*) and in the presence (Fig. 6*D*) of phage-encoded gp12. This spatial distribution correlated with the presence of two electrondense regions near the poles of infected cells in immunoEM thin sections that were labelled with anti-DNA and anti-capsid antibodies (Fig. 6 *E* and *G*). Infections for EM and DAPI DNA-labeling experiments (Fig. 6 *E-H*) were carried out in an isogenic strain producing no fluorescent proteins to exclude the possibility that reporter fusion proteins affect the formation or properties of foci containing DNA-filled capsids. Therefore, formation of such foci and their stronger prominence in absence of gp12 are inherent features of SPP1 viral particles at the post-DNA packaging state (compare Fig. 5 *A*,*B*,*G* and *H* to Fig. 6 *E-H*). In thin sections, those particles were almost certainly sectioned during preparation rendering their DNA accessible to labeling (Fig. 6 *E* and *G*). The less compact DNA present at more central regions of the cell corresponds presumably to both SPP1 and host free DNA (Fig. 6 *E* and *G*).

We then made triple-labeling experiments to follow the spatial distribution of capsids in the cell during their maturation from the DNA packaging step to the formation of mature virions after addition of the tail (Fig. 6*A*). Capsids were labeled with gp12-mCFP and tails with the major protein gp17.1 (44) fused to mCitrine in filamented cells infected with SPP1 mutants impairing different assembly steps of the viral particle (Fig. 6*A* and *SI Appendix* Fig. S4). When DNA packaging was arrested, gp12-mCFP remained homogenous in the bacterial cytoplasm while foci of gp17.1-mCitrine flanked the SPP1 DNA compartment (*SI Appendix* Fig. S4*A*). These foci, which were absent in the infection with a SPP1 mutant defective in tail formation (*SI Appendix* Fig. S4*B*), reveal regions of tail structures clustering. During infection with SPP1*lacO64gp16*$^{-}$ the post-DNA packaging step that leads to formation of the

capsid connector interface necessary for tail binding is disrupted (45). In such situation, both capsids (gp12-mCFP label) and tails (gp17.1-mCitrine label) formed foci outside the region occupied by the SPP1 DNA compartment. Those foci were mostly spatially independent, as can be best appraised on the rightmost overlay of gp12-mCFP (blue) and gp17.1-mCitrine (yellow) signals in *SI Appendix* Fig. S4*C*. We conclude that capsids and tails accumulate predominantly in different discrete locations within the cell when their interaction is impaired. In contrast, such segregation is not detectably observed when assembly of tailed phage particles occurs in cells infected with SPP1*lacO64* (Fig. 6*I*). Time-lapse experiments showed that DNA-filled capsids and tails co-localize as soon as they become detectable, revealing a rapid capsid-tail association in wild-type infection conditions (*SI Appendix* Fig. S4*D*). Therefore, the spatial distribution of SPP1 capsids and tails recapitulates precisely the post-DNA packaging sequential assembly steps (Fig. 6 *A* and *I* and *SI Appendix* Fig. S4). We defined the compartments where mature virions are stored as warehouses.

At early infection times, the SPP1 DNA overlapped with the most proximal warehouse identified by the gp12 focus in ~50% of the cells (Fig. 6*J*). Late in infection, most gp12-mCitrine had re-localized to positions distant from the SPP1 DNA (Fig. 6 *C*,*D* and *J*). Automated segmentation of fluorescent gp12-mCitrine foci in mono-infected cells confirmed that there are multiple foci early in infection, which likely merge afterwards to form two or three warehouses (*SI Appendix* Fig. S5*A*). In cells containing two warehouses, these were generally found on either side of the viral DNA compartment (*SI Appendix* Fig. S5*B*) at different relative distances (*SI Appendix* Fig. S5 *C* and *D*). Their fluorescence intensity revealed a roughly similar distribution of DNA-filled particles between the two warehouses (*SI Appendix* Fig. S5*E*). We next analyzed the gp12-mCitrine focus proximal to the viral DNA compartment to follow the evolution of warehouses during infection. The surface of the warehouses increased moderately during infection (*SI Appendix* Fig. S5*F*) and they remained quasi-spherical (*SI Appendix* Fig. S5*G*). However, their fluorescence intensity raised significantly (*SI Appendix* Fig. S5*H*) indicating that DNA-filled particles adopt a more compact organization in the warehouse with time. Gp12-mCitrine foci formed in the absence of phage-encoded gp12 were more compact and brighter than the ones built in the presence of phage-encoded gp12 (*SI Appendix* Fig. S5 *F-H*).

We next visualized the complete spatio-temporal program of viral DNA compartment and virion warehouses formation during infection of gp12-mCitrine-producing cells with SPP1*lacO64gp12*$^{-}$ in real time using a microfluidics device (Fig. 6*K* and Movie S1). Quasi-circular phage DNA compartments formed first and then elongated throughout infection until cell lysis. Flanking, spatially independent, warehouses of DNA-filled particles appeared later. They grew initially to a defined circular shape and then became more intense without major change in their size. Interestingly, bacteria continued to elongate and to divide during infection (white arrow in Fig. 6*K*), although their growth in liquid medium

was slightly reduced relative to non-infected bacteria (*SI Appendix* Fig. S1*B*). In some cells, the division septum sectioned the viral DNA compartment partitioning phage genome copies between daughter cells in which SPP1 DNA continued to replicate (Fig. 6*L*).

Discussion

We have discovered that bacteriophage SPP1 infection generates compartments in the crowded bacterial cytoplasm that have neither membrane nor protein cage boundaries. The spatio-temporal independent compartments confine viral DNA transactions and storage of viral particles. This spatial partition responds to the requirements for accommodating exponential replication of the viral genome and assembly of hundreds of infectious viral particles, the two central processes of the viral lytic cycle. The resulting major quantitative perturbation is the amount of viral DNA synthesized, which rises >2-fold the total cell DNA mass (Fig. 1*B*; Dataset S1). Concomitantly, bacterial nucleoids lose their regular position and condensed organization in the cell (Fig. 5 *A*-*H* and *SI Appendix* Fig. S1*E*). These changes in the *B. subtilis* chromosomes organization can be attributed to arrest of its replication (46) by hijacking bacterial replisomes to replicate SPP1 DNA (Fig. 2 and *SI Appendix* Fig. S2*C*), although some bacterial DNA synthesis still proceeds during infection (*SI Appendix* Fig. S1*F*). The area occupied by DNA in infected bacteria increases without a detectable change on average cell size in spite of the mechanism that maintains a constant nucleocytoplasmic ratio across bacteria, including *B. subtilis* (47). Hence, viral DNA can occupy more than 35% of the cell area (Figs. 4*A* and 5*D*). Such spatial stress is relieved by DNA packaging, which stripps-off proteins bound to the viral DNA to tightly pack it in capsids at a concentration of ~415 mg/mL, liberating space for higher yield DNA synthesis (Fig. 1*D*).

The single SPP1 DNA molecule entering the cytoplasm of mono-infected bacteria seeds the viral-induced DNA compartment found at a unique asymmetric position in the cell. This finding shows that the 44 kbp circular molecules generated by initial theta replication of the SPP1 genome (Fig. 3*E*) do not segregate to establish independent replication compartments. They rather stay confined together at a defined position of the cell. Similarly, eukaryotic herpesviruses, which are phylogenetically related to tailed phages (48) assemble discrete DNA replication compartments in the cell nucleus, each originating from a single incoming genome (49). Biogenesis of the viral DNA compartment can be partially explained by accumulation of replicated SPP1 DNA at a defined position of the cytoplasm. Polymer dynamics simulations predict that long DNA molecules fold to a compact globular shape in a crowded confined space like the cellular environment (1). Further compaction is likely achieved by protein-DNA interactions (e.g. with nucleoid-associated proteins), while binding of other proteins may antagonize it to ensure accessibility of genome sequences to DNA transactions like DNA replication, recombination, transcription, or encapsidation into viral procapsids (1, 50–52). These combined effects

can explain formation of a self-contained compartment with neither membrane nor protein cage boundaries. Its constrained metastable state is nearly instantaneously lost upon infection-induced cell lysis and death (e.g. 82 min p.i. in Fig. 6*K* and Movie S1), probably due to reduction of cytoplasmic crowding following leakage of the cell content. We also showed that the division septum can cut through the SPP1 DNA compartment during cell division, delivering viral genomes to the two daughter cells (Fig. 6*L*). This is advantageous for the phage, rendering superfluous an occlusion mechanism similar to the one employed by bacteria to prevent sectioning of their chromosome (53).

We found that SPP1-host hybrid replisome components co-localize at multiple discrete foci inside the viral DNA compartment. In contrast to the compartment integrity, stable maintenance of those punctuate hybrid replisome foci is DNA replication and energy-dependent (Fig. 3 *B-D*). We posit that they correspond to parallelized factories synthesizing DNA from several independent templates (Fig. 3*E*), which are necessary to sustain the viral genome replication rate during infection. Considering that SPP1/*acO64* synthesizes 278 copies of its 42.3 kbp genome within 15 min (15-30 min p.i. in Fig. 1*B*) this corresponds to an average synthesis rate of 13.1 kbp/s. There are thus at least 13 fully operative DNA replication machines synthesizing at a rate of 1000 bp/s (54) distributed at different locations within the DNA compartment ultrastructure. The localization of procapsids at the periphery of the SPP1 DNA compartment (Fig. 5) identifies the most likely position of replicated DNA packaging reactions into procapsids. A related spatial organization was found in the nucleus of cells infected by the human herpes simplex virus 1 (HSV-1) whose procapsids cluster at positions adjacent to the virus DNA replication centers (55). Presence of DNA replication and of DNA packaging molecular machineries in the same compartment provides a cytological basis for their cross-talk as reported for phages T4 (56) and SPP1 (57), as well as for the regulatory feed-back we observed between the two processes (Fig. 1*D*). The two machineries must also work together in bacteriophages T3, T7 and T5, which require re-synthesis of DNA concomitantly with genome packaging to generate terminal repetitions of identical sequence in the DNA molecules encapsidated (58). Collectively, our data rationalize previous observations in several viral systems, defining the viral-induced DNA compartment as the central industrial hub to sequester the proteins required for DNA transactions and to couple spatially their reactions in the infected cell. It also reveals a strategy to confine viral DNA processes different from the protein cage used by jumbo phages to compartmentalize their DNA at mid-cell (10,11).

SPP1 capsids do not remain associated with the viral DNA compartment after DNA packaging, a morphogenetic step that is characterized by transition from the procapsid to the DNA-filled capsid state. This transition creates the binding sites for the non-essential auxiliary protein gp12 at the capsid surface (39, 43) and the interface for tails binding to the capsid connector. The latter reaction leads to formation of infectious virions (Fig. 6*A*). Virions accumulate in a different type of compartment, the

warehouse (Fig. 6 and *SI Appendix* Figs. S4 and S5), irrespectively of gp12 binding to capsids. Particles lacking gp12 form warehouses significantly more compact than those with gp12 do (Fig. 6 *C-H*). This finding shows that the properties of the phage icosahedral capsid surface play a main role on warehouse organization and possibly also on its biogenesis. We hypothesize that it is the smooth (59), albeit more electronegative surface of capsids lacking gp12 (43), that facilitates their tighter association in warehouses when compared to capsids decorated with arrays of flexible, symmetrically arranged, gp12 trimers (39, 59). Orderly packing of a large number of phage particles through their capsid icosahedral lattices is certainly disturbed by the presence of tail structures. Such constrain makes it unlikely to reach a crystal-like arrangement of viral particles as found for HSV-1 and polyomavirus capsids in the nucleus of infected eukaryotic cells (60, 61). The formation of phage warehouses fulfills, nevertheless, their putative function to minimize the storage space of viral particles in the cell.

The SPP1 DNA is in direct contact with the cytoplasm rendering it vulnerable to cellular defenses like CRISPR-Cas (62), in contrast to the nucleus-like protein cage used by jumbo-phages to protect their DNA (12, 63). Although this is a limitation for SPP1 exploration of hosts landscape, such cost is plausibly compensated by the competitive advantage of its much higher burst size and shorter infection period when compared to jumbo phages multiplication parameters (64). A different way to exploit the cytoplasm open space is typified by bacteriophage phage ϕ29 that targets the MreB bacterial cytoskeleton to structure its DNA replication at the periphery of the cell interior (8, 9). This strategy allows for production of a high burst of infectious virions but might be limited to the few viruses that replicate their DNA by a protein-primed replication mechanism. The SPP1 compartments properties offer a cost and time-effective way to exchange protein effectors between the cellular pool and viral compartments to fulfill the needs for phage multiplication. Proteins enrollment follows a defined order. This principle is well illustrated by assembly of SPP1 viral particles. Their building blocks are recruited from homogeneous cytoplasmic pools to a defined sub-cellular localization, following an order that recapitulates the program of viral particle sequential assembly. That is shown in our study for the scaffolding protein gp11 at the procapsid assembly stage (*SI Appendix* Fig. S3 *D-G*), the capsid accessory protein gp12 at the post-DNA packaging state (Fig. 6 *B-D*), and the tail fixation to the capsid connector interface (*SI Appendix* Fig. S4).

The ways how SPP1 restructures the infected cell are most probably used by a large number of phages. SPP1 partition of cytoplasmic space has also a number of striking similarities with remodeling of the eukaryotic cell nucleus during infection by herpesviruses (see above) (49, 55 and references therein). Those changes of cell architecture concur with common molecular mechanisms of recombination-dependent DNA replication (17) and packaging into viral procapsids (65). We propose

that SPP1 typifies ancestral strategies used by viruses to organize the cellular space that were conserved to infect hosts of different Domains of Life.

Materials and Methods

A complete list of bacterial strains, phages, plasmids, antibodies and primers used in this work is presented in *SI Appendix, Table S3*.

A detailed description of all the methods is provided in *SI Appendix, Materials and Methods* that includes bacterial, phages and plasmids construction; phages amplification and infection studies; purification and characterization of phage particles; qPCR, fluorescence microscopy, microfluidics, and quantitative imaging of infected bacteria; electron microscopy, and statistical analyses. The MatLab scripts used in this work and a tutorial were uploaded to a repository in GitHub for open access: https://github.com/CyrilleBillaudeau/TemporalCompartmentalization_ofViral_Infection_inBactCells.

ACKNOWLEDGMENTS. This work is part of Audrey Labarde's PhD thesis. Naima Nhiri is acknowledged for her most helpful support on qPCR and Qubit experiments. We are very thankful to Mart Krupovic for providing up-to-date quantitative information on tailed phages genome size. We acknowledge Laetitia Maroc for participation on the analysis of procapsids composition. We are also grateful to Arnaud Chastanet for advice to setup the microfluidics experiments. We thank Etienne Dervyn, Alan D Grossman, Catherine Ann Lee, Jeff Errington, Heath Murray, Ling Juan Wu, Adriano Henriques, David Rudner, Thierry Doan, Dan Zeigler and the Bacillus Genetic Stock Center (BGSC), for providing strains used in this study. We are grateful to Neal Brown, George Wright and Neal Agneta (GLSynthesis) for HPUra. Sandrine Brasilès is acknowledged for anti-SPP1 procapsids rabbit serum. We thank Arnaud Chastanet, Marta de Frutos, and Eric Cascales for fruitful discussions. Thanks also to Magali Ventroux for comments on the manuscript. We acknowledge Marta de Frutos (Laboratoire de Physique des Solides, Université Paris-Saclay, Orsay) for rendering available one of the fluorescence microscopes used in this work. This microscope was funded by the CNRS - Actions interdisciplinaires, Interface physique-chimie-biologie : Soutien à la prise de risque (2011) and by the Université of Paris-Sud - Appel d'offre Attractivité (2010). Microscopes upgrade and acquisition of a Cellasics microfluidics was funded by Fondation pour la Recherche Médicale (FRM). L.J. was supported by the University of Vilnius, the Université Paris-Sud, the French embassy in Lithuania, the program Egide Gilibert between France and Lithuania, the European Union Erasmus Program, and the Région Ile-de-France (SETCI).This work was funded by grants from FRM (to P.T.), ANR BacVirFactory and BacVirRemodel (to P.T. and R.C.-L.), MINECO and MCIU (to S.A.), and institutional funding from CNRS (P.T.), INRA (R.C.-L.), and MPIMG (T.M.).

Competing interests

The authors declare that they have no competing interests.

References

1. I. Surovtsev, C. Jacobs-Wagner, Subcellular Organization : A Critical Feature of Bacterial Cell Replication. *Cell* **172**, 1271–1293 (2018).
2. E. Cornejo, N. Abreu, A. Komeilo, Compartmentalization and Organelle Formation in Bacteria. *Curr. Opin. Cell Biol.* **26**, 132–138 (2014).
3. C. V Iancu, *et al.*, Organization, Structure, and Assembly of α-Carboxysomes Determined by Electron Cryotomography of Intact Cells. *J. Mol. Biol.* **396**, 105–117 (2010).
4. C. A. McHugh, *et al.*, A virus capsid-like nanocompartment that stores iron and protects bacteria from oxidative stress. *EMBO J.* **33**, 1896–1911 (2014).
5. M. Schmid, T. Speiseder, T. Dobner, A. Gonzalez, DNA Virus Replication Compartments. *J. Virol.* **88**, 1404–1420 (2014).
6. C. Risco, *et al.*, Three-Dimensional Imaging of Viral Infections. *Annu. Rev. Virol.* **1**, 453–473 (2014).
7. J. Nikolic, *et al.*, Negri bodies are viral factories with properties of liquid organelles. *Nat. Commun.* **8**, 1–12 (2017).
8. D. Muñoz-Espín, *et al.*, The actin-like MreB cytoskeleton organizes viral DNA replication in bacteria. *Proc. Natl. Acad. Sci.* **106**, 13347–13352 (2009).
9. D. Muñoz-Espín, I. Holguera, D. Ballesteros-Plaza, R. Carballido-Lopez, M. Salas, Viral terminal protein directs early organization of phage DNA replication at the bacterial nucleoid. *Proc. Natl. Acad. Sci. U. S. A.* **107**, 16548–16553 (2010).
10. V. Chaikeeratisak, *et al.*, Assembly of a nucleus-like structure during viral replication in bacteria. *Science (80-.).* **355**, 194–197 (2017).
11. V. Chaikeeratisak, *et al.*, Viral Capsid Trafficking along Treadmilling Tubulin Filaments in Bacteria. *Cell* **177**, 1771–1780 (2019).
12. L. M. Malone, *et al.*, A jumbo phage that forms a nucleus-like structure evades CRISPR – Cas DNA targeting but is vulnerable to type III RNA-based immunity. *Nat. Microbiol.* **5**, 48–55 (2020).
13. M. Krupovic, V. Cvirkaite-Krupovic, J. Iranzo, D. Prangishvili, E. V. Koonin, Viruses of archaea: Structural, functional, environmental and evolutionary genomics. *Virus Res.* **244**, 181–193 (2018).
14. R. Edgar, *et al.*, Bacteriophage infection is targeted to cellular poles. *Mol. Microbiol.* **68**, 1107–1116 (2008).
15. L. Jakutyte, *et al.*, Bacteriophage infection in rod-shaped Gram-positive bacteria: Evidence for a preferential polar route for phage SPP1 entry in Bacillus subtilis. *J. Bacteriol.* **193**, 4893–4903 (2011).
16. J. C. Alonso, P. Tavares, R. Lurz, T. A. Trautner, Bacteriophage SPP1. R. *Calendar (ed.), Bacteriophages, 2nd edn.*, pp. 331–349 (2006).

17. A. Lo Piano, M. I. Martínez-Jiménez, L. Zecchi, S. Ayora, Recombination-dependent concatemeric viral DNA replication. *Virus Res.* **160**, 1–14 (2011).

18. L. Oliveira, P. Tavares, J. C. Alonso, Headful DNA packaging: Bacteriophage SPP1 as a model system. *Virus Res.* **173**, 247–259 (2013).

19. E. Tzipilevich, M. Habusha, S. Ben-Yehuda, Acquisition of Phage Sensitivity by Bacteria through Exchange of Phage Receptors. *Cell* **168**, 186–199 (2017).

20. L. M. Godinho, *et al.*, The Revisited Genome of Bacillus subtilis Bacteriophage SPP1. *Viruses* **10**, 1–28 (2018).

21. H. Murray, J. Errington, Dynamic Control of the DNA Replication Initiation Protein DnaA by Soj/ParA. *Cell* **135**, 74–84 (2008).

22. P. Tavares, The bacteriophage head-to-tail interface in *Subcellular Biochemistry*, (2018), pp. 305–328.

23. S. Chai, *et al.*, Molecular Analysis of the Bacillus subtilis Bacteriophage SPP1 Region Encompassing Genes 1 to 6 SPP1 - The Products of Gene 1 and Gene 2 are Required for pac Cleavage. *J. Mol. Biol.* **224**, 87–102 (1992).

24. X. Pedré, F. Weise, S. Chai, G. Lüder, J. C. Alonso, Analysis of Cis and Trans acting elements required for the initiation of DNA replication in the Bacillus subtilis bacteriophage SPP1. *J. Mol. Biol.* **236**, 1324–1340 (1994).

25. E. M. Seco, *et al.*, Bacteriophage SPP1 DNA replication strategies promote viral and disable host replication in vitro. *Nucleic Acids Res.* **41**, 1711–1721 (2013).

26. E. M. Seco, S. Ayora, Bacillus subtilis DNA polymerases, PolC and DnaE, are required for both leading and lagging strand synthesis in SPP1 origin-dependent DNA replication. *Nucleic Acids Res.* **45**, 8302–8313 (2017).

27. J. C. Meile, L. J. Wu, S. D. Ehrlich, J. Errington, P. Noirot, Systematic localisation of proteins fused to the green fluorescent protein in Bacillus subtilis: Identification of new proteins at the DNA replication factory. *Proteomics* **6**, 2135–2146 (2006).

28. E. Dervyn, *et al.*, Two Essential DNA Polymerases at the Bacterial Replication Fork. *Science* **294**, 1716–1719 (2001).

29. R. Missich, F. Weise, S. Chai, R. Lurz, J. C. Alonso, The Replisome Organizer (G38P) of Bacillus subtilis Bacteriophage SPP1 Forms Specialized Nucleoprotein Complexes with two Discrete Distant Regions of the SPP1 Genome. *J. Mol. Biol.* **15**, 50–64 (1997).

30. S. Ayora, A. Stasiak, J. C. Alonso, The Bacillus subtilis bacteriophage SPP1 G39P delivers and activates the G40P DNA helicase upon interacting with the G38P-bound replication origin. *J. Mol. Biol.* **288**, 71–85 (1999).

31. M. I. Martínez-Jiménez, P. Mesa, J. C. Alonso, Bacillus subtilis τ subunit of DNA polymerase III interacts with bacteriophage SPP1 replicative DNA helicase G40P. *Nucleic Acids Res.* **30**, 5056–5064 (2002).

32. S. Ayora, U. Langer, J. C. Alonso, Bacillus subtilis DnaG primase stabilises the bacteriophage SPP1 G40P helicase-ssDNA complex. *FEBS Lett.* **439**, 59–62 (1998).

33. G. Wang, *et al.*, The structure of a DnaB-family replicative helicase and its interactions with primase. *Nat. Struct. Mol. Biol.* **15**, 94–100 (2008).

34. A. Valero-Rello, M. López-Sanz, A. Quevedo-Olmos, A. Sorokin, S. Ayora, Molecular mechanisms that contribute to horizontal transfer of plasmids by the bacteriophage SPP1. *Front.*

Microbiol. **8**, 1–13 (2017).

35. B. Bohrmann, E. Kellenberger, Immunostaining of DNA in Electron Microscopy : An Amplification and Staining Procedure for Thin Sections as Alternative to Gold Labeling. *J. Histochem. Cytochem.* **42**, 635–643 (1994).

36. S. D. Rowley, N. C. Brown, Bacillus subtilis DNA polymerase III is required for the replication of DNA of bacteriophages SPP-1 and ϕ105. *J. Virol.* **21**, 493–496 (1977).

37. A. Lamsa, W.-T. Liu, P. C. Dorrestein, K. Pogliano, The Bacillus subtilis cannibalism toxin SDP collapses the proton motive force and induces autolysis. *Mol Microbiol* **84**, 1–24 (2012).

38. S. L. Poh, *et al.*, Oligomerization of the SPP1 Scaffolding Protein. *J. Mol. Biol.* **378**, 551–564 (2008).

39. A. Ignatiou, *et al.*, Structural transitions during the scaffolding-driven assembly of a viral capsid. *Nat. Commun.* **10**, 1–11 (2019).

40. O. Griesbeck, G. S. Baird, R. E. Campbell, D. A. Zacharias, R. Y. Tsien, Reducing the environmental sensitivity of yellow fluorescent protein. Mechanism and applications. *J. Biol. Chem.* **276**, 29188–29194 (2001).

41. D. J. Haydon, *et al.*, An Inhibitor of FtsZ with Potent and Selective anti-Staphylococcal Activity. *Science* **321**, 1673–1676 (2008).

42. A. Dröge, *et al.*, Shape and DNA packaging activity of bacteriophage SPP1 procapsid: protein components and interactions during assembly. *J. Mol. Biol.* **296**, 117–132 (2000).

43. M. Zairi, A. C. Stiege, N. Nhiri, E. Jacquet, P. Tavares, The Collagen-like Protein gp12 is a Temperature-dependent Reversible Binder of SPP1 Viral Capsids. *J. Biol. Chem.* **289**, 27169–27181 (2014).

44. I. Auzat, A. Dröge, F. Weise, R. Lurz, P. Tavares, Origin and function of the two major tail proteins of bacteriophage SPP1. *Mol. Microbiol.* **70**, 557–569 (2008).

45. E. V. Orlova, *et al.*, Structure of a viral DNA gatekeeper at 10 Å resolution by cryo-electron microscopy. *EMBO J.* **22**, 1255–1262 (2003).

46. M. Marbouty, *et al.*, Condensin- and Replication-Mediated Bacterial Chromosome Folding and Origin Condensation Revealed by Hi-C and Super-resolution Imaging. *Mol. Cell 59*, 588–602 (2015).

47. W. T. Gray, *et al.*, Nucleoid Size Scaling and Intracellular Organization of Translation across Bacteria. *Cell* **177**, 1632–1648 (2019).

48. J. Iranzo, M. Krupovic, E. V. Koonin, The double-stranded DNA virosphere as a modular hierarchical network of gene sharing. *MBio* **7**, 1–21 (2016).

49. O. Kobiler, P. Brodersen, M. P. Taylor, E. B. Ludmir, L. W. Enquist, Herpesvirus replication compartments originate with single incoming viral genomes. *MBio* **2**, 1–9 (2011).

50. J. K. Fisher, *et al.*, Four dimensional imaging of E. coli nucleoid organization and dynamics in living cells. *Cell* **153**, 882–895 (2013).

51. S. Cunha, C. L. Woldringh, T. Odijk, Polymer-mediated compaction and internal dynamics of isolated Escherichia coli nucleoids. *J. Struct. Biol.* **136**, 53–66 (2001).

52. S. C. Verma, Z. Qian, S. L. Adhya, Architecture of the Escherichia coli nucleoid. *PLoS Genet.* **15**, 1–35 (2019).

53. D. W. Adams, L. J. Wu, J. Errington, Cell cycle regulation by the bacterial nucleoid. *Curr. Opin.*

Microbiol. **22**, 94–101 (2014).

54. M. O'Donnell, L. Langston, B. Stillman, Principles and concepts of DNA replication in bacteria, archaea, and eukarya. *Cold Spring Harb. Perspect. Biol.* **5**, 1–14 (2013).

55. P. L. Ward, W. O. Ogle, B. Roizman, Assemblons: nuclear structures defined by aggregation of immature capsids and some tegument proteins of herpes simplex virus 1. *J. Virol.* **70**, 4623–4631 (1996).

56. V. B. Rao, L. W. Black, DNA Packaging in Bacteriophage T4 in Viral Genome Packaging Machines. *Catalano CE, Ed. Plenum Press*, 40–58 (2005).

57. P. Tavares, R. Lurz, A. Stiege, B. Rückert, T. A. Trautner, Sequential headful packaging and fate of the cleaved DNA ends in bacteriophage SPP1. *J. Mol. Biol.* **264**, 954–67 (1996).

58. L. Black, DNA Packaging In DsDNA Bacteriophages. *Annu. Rev. Microbiol.* **43**, 267–292 (1989).

59. H. E. White, *et al.*, Capsid Structure and Its Stability at the Late Stages of Bacteriophage SPP1 Assembly. *J. Virol.* **86**, 6768–6777 (2012).

60. K. Miyamoto, Mechanism of Intranuclear Crystal Formation of Herpes Simplex Virus as Revealed by the Negative Staining of Thin Sections. *J. Virol.* **8**, 534–550 (1971).

61. K. D. Erickson, *et al.*, Virion assembly factories in the nucleus of polyomavirus-infected cells. *PLoS Pathog.* **8**, 1–15 (2012).

62. L. Jakutyte-Giraitiene, G. Gasiunas, Design of a CRISPR-Cas system to increase resistance of Bacillus subtilis to bacteriophage SPP1. *J. Ind. Microbiol. Biotechnol.* **43**, 1183–1188 (2016).

63. S. D. Mendoza, *et al.*, A bacteriophage nucleus-like compartment shields DNA from CRISPR nucleases. *Nature* **577**, 244–248 (2020).

64. J. A. Kraemer, *et al.*, A phage tubulin assembles dynamic filaments by a novel mechanism to center viral DNA within the host cell. *Cell* **149**, 1488–1499 (2012).

65. F. J. Rixon, M. F. Schmid, Structural similarities in DNA packaging and delivery apparatuses in Herpesvirus and dsDNA bacteriophages. *Curr. Opin. Virol.* **5**, 105–110 (2014).

66. C. São-José, M. de Frutos, E. Raspaud, M. A. Santos, P. Tavares, Pressure Built by DNA Packing Inside Virions: Enough to Drive DNA Ejection in Vitro, Largely Insufficient for Delivery into the Bacterial Cytoplasm. *J. Mol. Biol.* **374**, 346–355 (2007).

67. J. Schindelin, *et al.*, Fiji - an Open Source platform for biological image analysis. *Nat. Methods* **9**, 241–256 (2013).

Figures

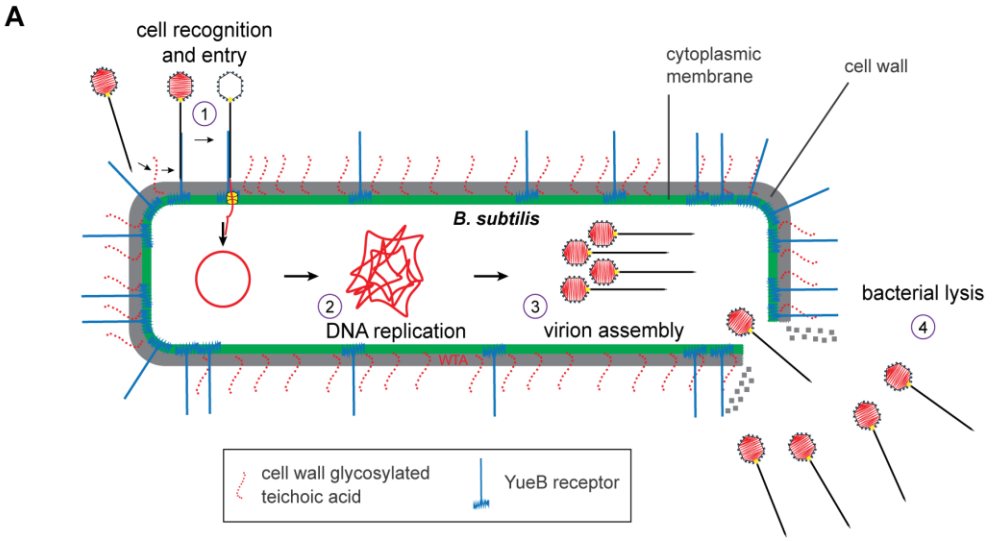

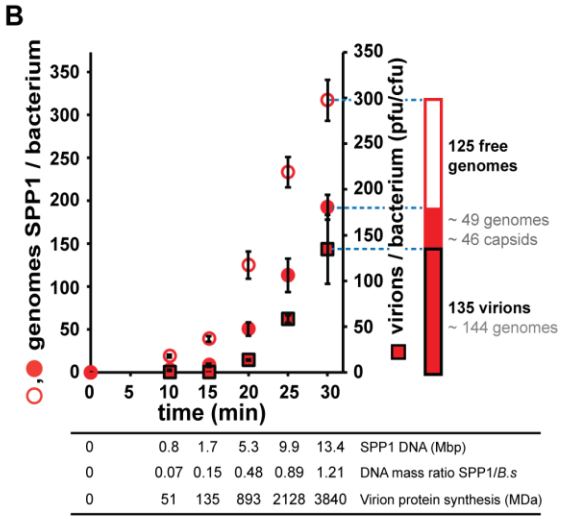

0	0.8	1.7	5.3	9.9	13.4	SPP1 DNA (Mbp)
0	0.07	0.15	0.48	0.89	1.21	DNA mass ratio SPP1/*B.s*
0	51	135	893	2128	3840	Virion protein synthesis (MDa)

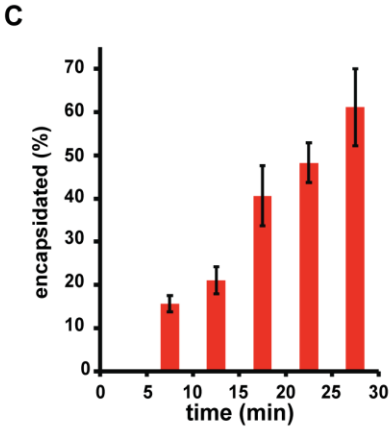

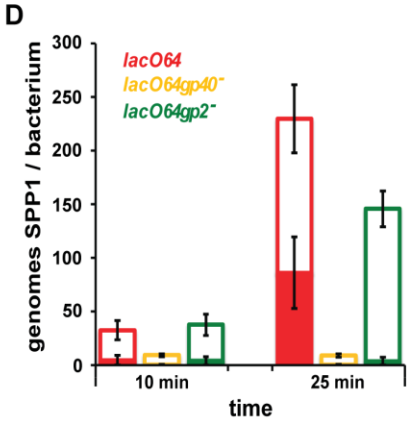

Fig. 1. SPP1 DNA replication and encapsidation.

(*A*) Schematics of the main steps on tailed bacteriophage infection exemplified by SPP1. (*B*) Quantification of SPP1 DNA synthesis (empty circles) and encapsidation (filled circles) determined by qPCR of total and DNAse-protected DNA, respectively, in *B. subtilis* GSY10004 infected with SPP1*lacO64*. The amount of SPP1 gene *6* DNA was divided by the amount of *B. subtilis gyrA* reporter DNA considering that there are 2.7 nucleoids on average *per* cell (*SI Appendix* Fig. S1 *C* and *D*) to calculate the number of SPP1 genomes *per* bacterium. The total number of infectious particles (filled squares; ordinate on the right) was quantified by phage titration of bacteria lysed with 10% chloroform. Note that the DNA molecule encapsidated in SPP1*lacO64* particles (~45.1 kbp) is 1.07-fold longer than the phage genome size (42.3 kbp) (15, 66), a factor that was used to convert phage particle counts into genome equivalents and reciprocally. A snapshot of phage DNA and particle yields at 30 min p.i., when experiments were stopped because cell lysis initiated, is displayed on the right. Values in bold were obtained experimentally and those in grey were calculated based on the figure data. Note that the calculation of ~46 capsids corresponds to particles that protect viral DNA but are non-infectious (i.e. tailless DNA-filled capsids and eventually defective tailed phage particles). The data are the average from three independent experiments. The biosynthetic effort accounting for phage DNA and virion structural proteins synthesis is depicted underneath the infection time points (Dataset S1). (*C*) Percentage of encapsidated DNA calculated from the data in *B*. (*D*) Phage DNA synthesis at 10 and 25 min p.i. in *B. subtilis* GSY10004 infected with SPP1*lacO64* (15) (red), SPP1*lacO64gp40*$^{-}$ (defective in initiation of DNA synthesis) (yellow), and SPP1*lacO64gp2*$^{-}$ (defective in DNA packaging) (green). Total DNA (bars total height) and encapsidated, DNAse-protected DNA (overlapping full bars) were quantified by qPCR. The data are the average from three independent experiments.

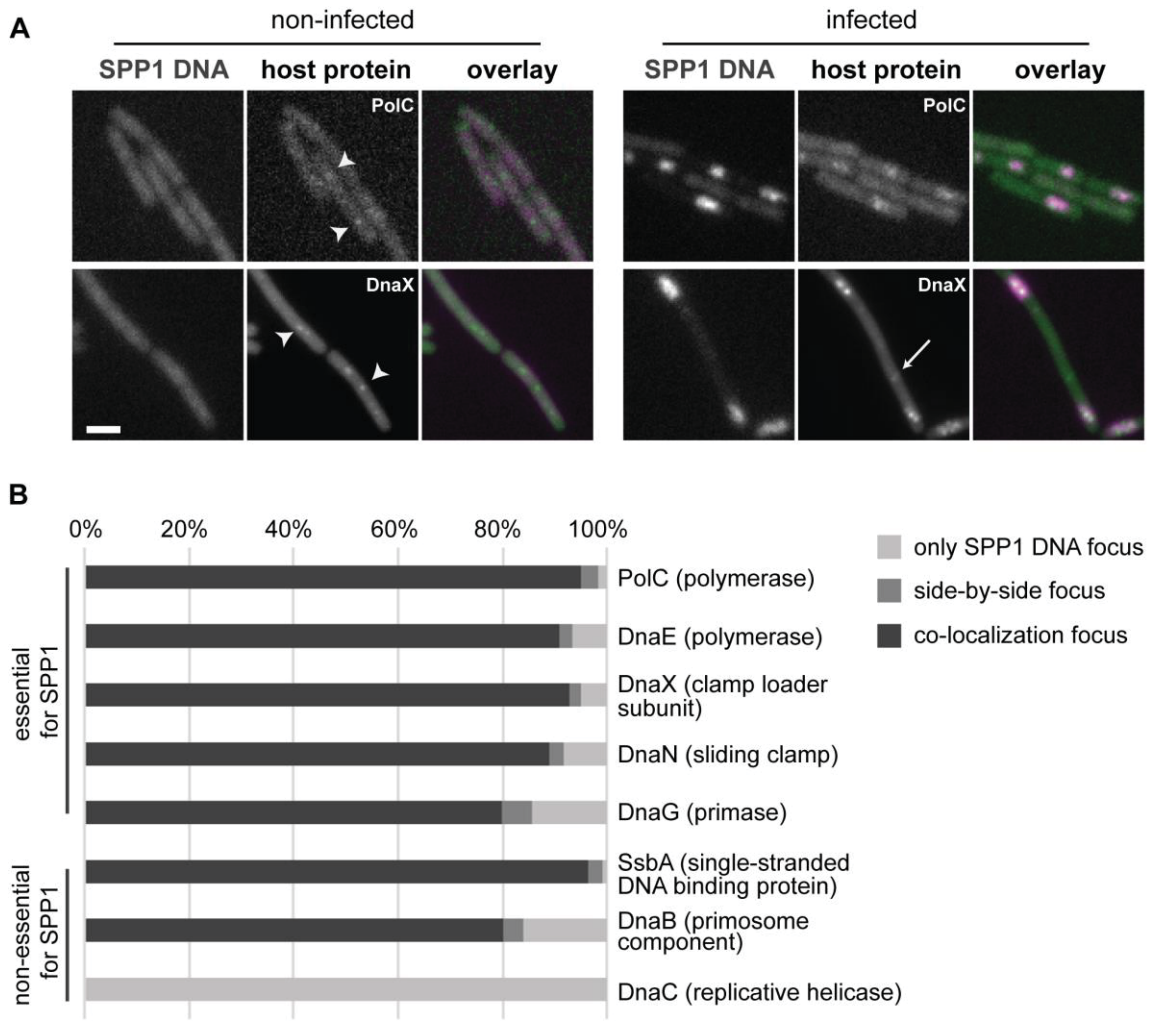

Fig. 2. Cellular localization of *B. subtilis* replisome proteins during SPP1 infection.

(*A*) PolC-GFP (top) and mCFP-DnaX (bottom) in bacteria non-infected (left) and infected with SPP1*lacO64* (right) late p.i (see *SI Appendix* Fig. S2*B* for experimental setup). The *B. subtilis* strains produce LacI-mCherry constitutively. Signals on the RFP channel are displayed in magenta while signals on GFP and CFP channels are in green on overlays, respectively. The scale bar represents 2 µm. Arrowheads show the position of host replication protein foci in non-infected bacteria and the arrow identifies a focus of mCFP-DnaX that does not colocalize with SPP1 DNA in an infected bacterium. (*B*) Quantitative analysis of *B. subtilis* replisome proteins localization relative to the SPP1 DNA focus in bacteria early p.i. according to the grey scale legend on the right. More than 100 cell counts were made for each strain.

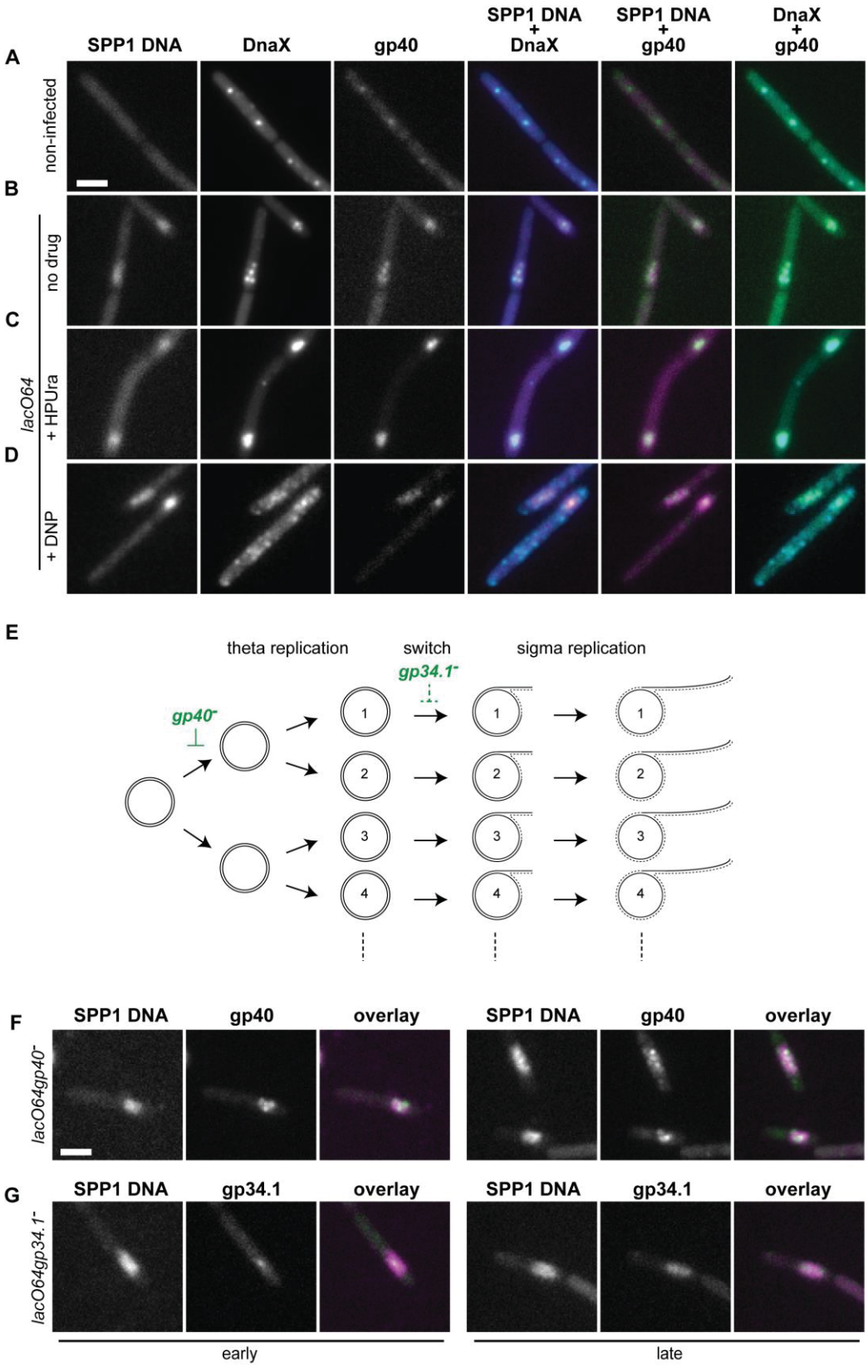
SPP1 DNA
DnaX
gp40
SPP1 DNA + DnaX
SPP1 DNA + gp40
DnaX + gp40
A
non-infected
B
no drug
C
lacO64
+ HPUra
D
+ DNP
E
theta replication
switch
sigma replication
gp34.1-
gp40-
1
2
3
4
F
lacO64gp40-
overlay
G
lacO64gp34.1-
gp34.1
early
late

Fig. 3. Cellular localization of SPP1 proteins engaged in phage DNA replication (gp40 helicase) and in the switch of genome replication mode (gp34.1 5'-3' exonuclease).

(*A*-*D*) Localization of SPP1 DNA, mCFP-DnaX (*B. subtilis* clamp loader subunit) and gp40-mCitrine in non-infected bacteria (*A*) and in SPP1*lacO64* infected bacteria untreated (*B*), incubated with 200 µM HPUra (*C*) or with 10 mM DNP (*D*). Drugs were added at 21 min p.i. to the infected culture that was spotted in the agarose pad containing the same concentration of drug 3 min later. Fluorescence microscopy acquisitions were made between 50 and 60 min p.i.. The scale bar in (*A*) represents 2 µm. (*E*) Scheme of SPP1 replication initiated by a theta mode, leading to an exponential increase of independent circular genome molecules, followed by a switch to sigma replication that generates linear concatemers for DNA packaging. SPP1 mutants blocking replication initiation (*gp40*$^{-}$) or severely affecting the switch from theta to sigma mode (*gp34.1*$^{-}$) are displayed in green. (*F,G*) Co-localization of gp40-mCitrine (*F*) and gp34.1-mCitrine (*G*) with phage DNA in infections with SPP1 mutants defective in gp40 and in gp34.1 production (trans-complementation conditions), respectively. Images at early (left) and late (right) stages of infection (*SI Appendix* Fig. S2*B*) are displayed. The scale bar in (*F*) represents 2 µm.

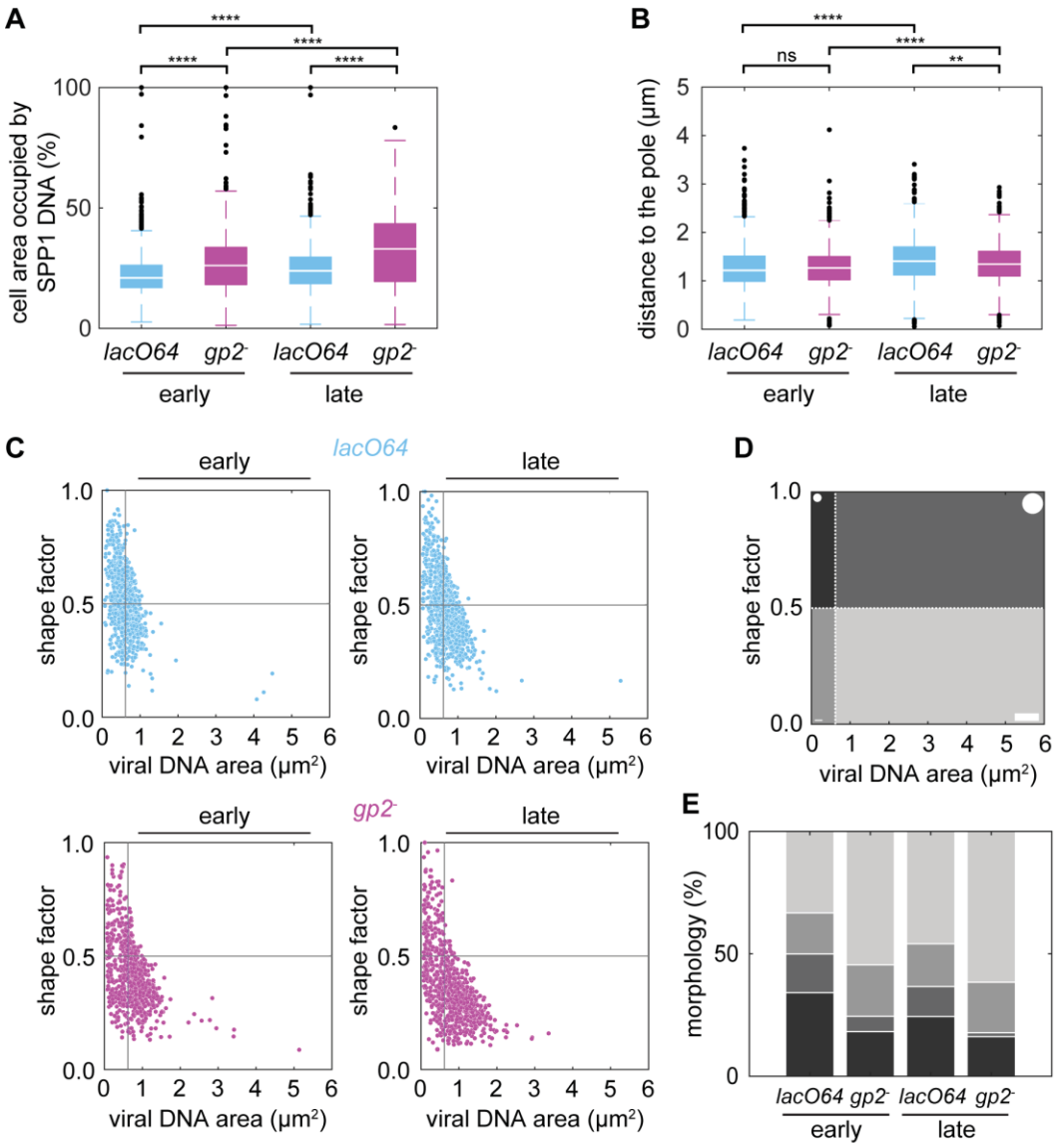

Fig. 4. Temporal evolution of the viral DNA compartment.

(*A*) Percentage of cell area occupied by the SPP1 DNA focus in *B. subtilis* GSY10025 mono-infected (one viral DNA focus per cell) with SPP1*lacO64* (blue) or with the DNA packaging-defective mutant SPP1*lacO64gp2*$^{-}$ (magenta) at early and late times p.i. (*SI Appendix* Fig. S2*B*). More than 800 cells from three independent infections were analyzed. The same datasets were used for all analyses in the figure. (*B*) Average distance of the SPP1 DNA focus center of mass to the proximal cell pole. Boxplots in (*A*) and (*B*) show the median of the sample data as a white solid line and draws point as outliers if they are greater than $q_3 + w(q_3 - q_1)$ or less than $q_1 - w(q_3 - q_1)$, where q_1 and q_3 are the 25th and 75th percentiles of the sample data, respectively, and $w = 1.5$. Statistical significance between conditions in (*A*) and in (*B*) were calculated using the Mann–Whitney non-parametric test (**** = P<0.0001; *** =

0.0001<P<0.001; ** = 0.001<P<0.01; * = 0.01<P<0.05; ns = P>0.05). (*C*) Surface aspect of the phage DNA focus. The width to length ratio (shape factor) of the segmented focus is plotted relative to its area. The vertical and horizontal limits separating all quadrants are defined, respectively, as the median values of the DNA surface and the shape factor from the dataset associated with the infection with SPP1*lacO64*. Foci shape factors were quantified when DNA encapsidation took place (blue; infection with SPP1*lacO64*, abbreviated *lacO64* in the figure) or was blocked (magenta; infection with SPP1*lacO64gp2*$^{-}$, abbreviated *gp2*$^{-}$ in the figure) at early (left) and late (right) times p.i.. (*D*) Schematic visual aid of the DNA focus shape observed in each quadrant of the plot in (*C*). (*E*) Percentage of viral DNA compartment shape types in the quadrants of (*C*) displayed according to the grey scale of (*D*).

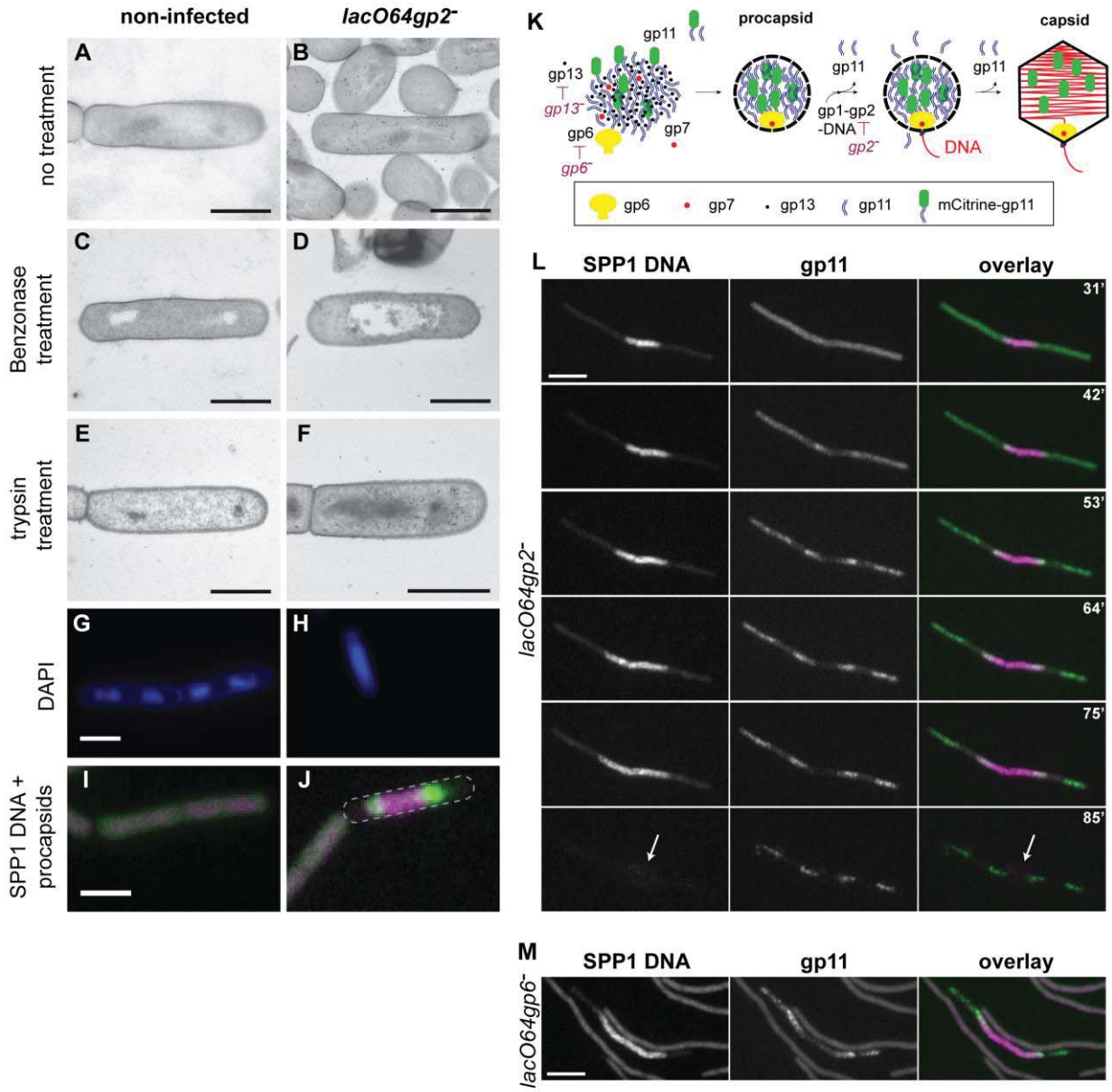

Fig. 5. Localization of SPP1 DNA and viral procapsids in infected bacteria.

(*A-F*) Ultrastructure of *B. subtilis* YB886 non-infected and infected with SPP1*lacO64gp2*$^{-}$. Sections 90-nm thick of bacteria, fixed 35 min p.i., and sectioned at cryogenic temperatures were left untreated (*A* and *B*), incubated with 25 U Benzonase (digests DNA) (*C* and *D*), or treated with 10 µg/mL trypsin (hydrolyses proteins but phage particles are resistant (43)) (*E* and *F*). Sections were labeled with a mouse monoclonal anti-DNA antibody and a rabbit polyclonal anti-procapsid serum visualized with 5 and 15 nm

colloidal gold, respectively. The scale bars represent 1 µm in the EM sections. (*G* and *H*) Epifluorescence of fixed bacteria stained with DAPI from the cultures used for immunoEM experiments. (*I* and *J*) Cytological localization of LacI-mCherry that decorates SPP1 DNA (magenta in (*J*)) and of mCitrine-gp11 that is incorporated in procapsids (green in (*J*)) in *B. subtilis* GSY10025 non-infected and infected with SPP1*lacO64gp2*$^{-}$. Grey dotted lines display the cell outline defined from brightfield imaging. The scale bars represent 2 µm in the fluorescence microscopy images of (*G*) and (*I*). (*K*) Scheme of procapsid formation and DNA packaging initiation steps during SPP1 viral particle assembly. All components of the SPP1 procapsid and of the DNA packaging apparatus are presented. The major capsid protein gp13 lattice is displayed as a dashed line delimiting the procapsid and by a thin icosahedral outline in the expanded capsid. MCitrine is displayed as a green cylinder in the mCitrine-gp11 fusion protein. Mutants, used in this study, that block synthesis of different SPP1 proteins engaged in procapsid assembly and DNA packaging are also presented. (*L*) Time-lapse of filamented *B. subtilis* GSY10025 (producing mCitrine-gp11) infected with SPP1*lacO64gp2*$^{-}$. Cell division was inhibited 1 h before infection by addition of 1 µg/mL PC190723. Signals on the RFP and YFP channels are displayed in magenta and green in overlays, respectively. Time p.i. is displayed on the right top corner of the overlay. The arrow shows dispersion of SPP1 DNA (magenta) in the agarose pad upon cell disruption at 85 min p.i. while clusters of procapsids (green) maintain their integrity. The scale bar represents 5 µm. (*M*) Infection of filamented *B. subtilis* GSY10025 with SPP1*lacO64gp6*$^{-}$ defective in production of the procapsid portal protein. Portal-less procapsids assembled during infection are not competent to package viral DNA (42). An infected cell late p.i. is presented surrounded by non-infected bacteria. Experimental conditions are as in (*L*).

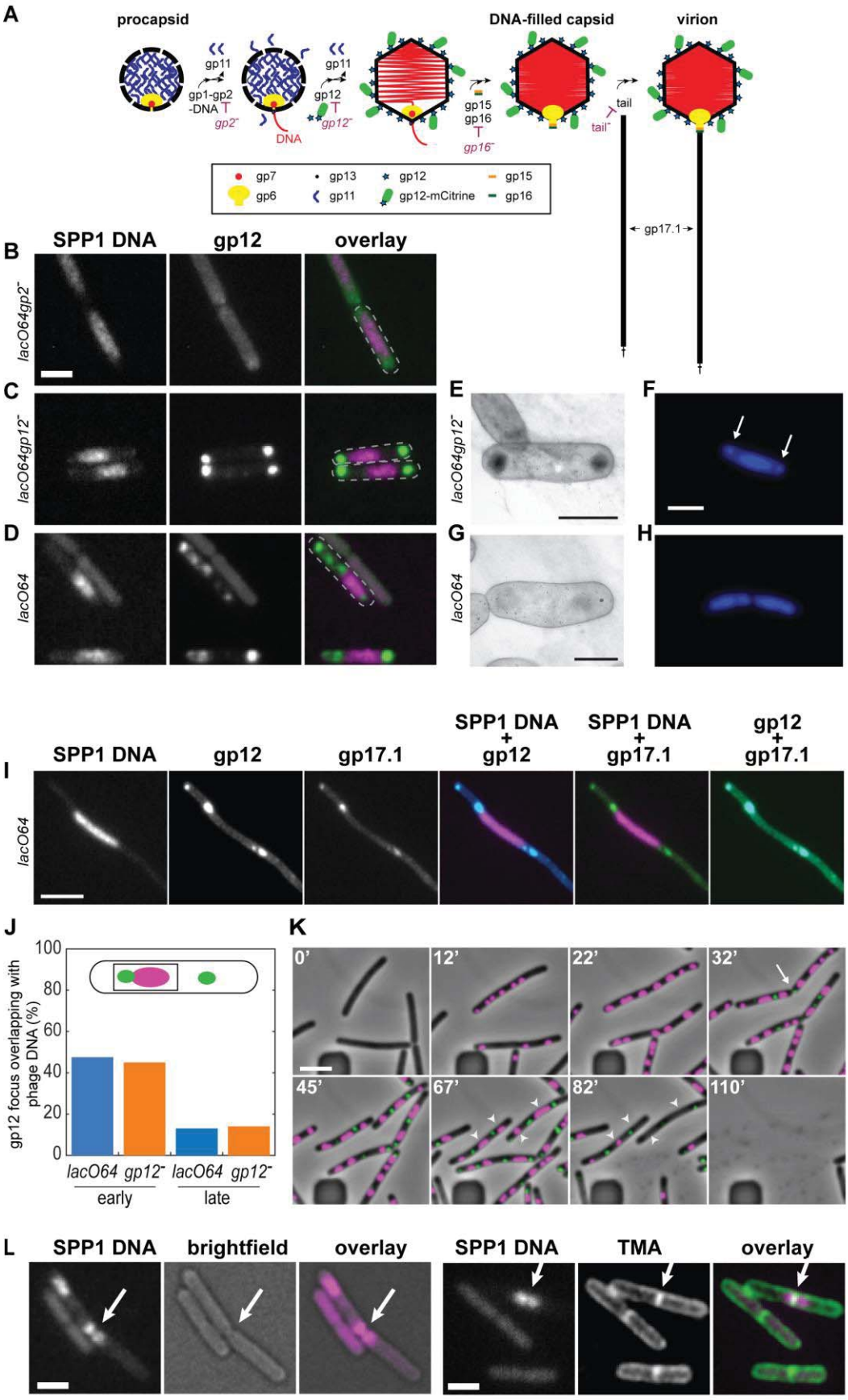
A
procapsid
DNA-filled capsid
virion
gp11
gp1-gp2
-DNA
gp2-
DNA
gp12
gp12-
gp15
gp16
gp16-
tail
tail-
gp17.1
gp7
gp6
gp13
gp11
gp12
gp12-mCitrine
gp15
gp16
B
SPP1 DNA
gp12
overlay
lacO64gp2-
C
lacO64gp12-
D
lacO64
E
lacO64gp12-
F
G
lacO64
H
I
SPP1 DNA
gp12
gp17.1
SPP1 DNA + gp12
SPP1 DNA + gp17.1
gp12 + gp17.1
lacO64
J
gp12 focus overlapping with phage DNA (%)
100
80
60
40
20
0
lacO64
gp12-
lacO64
gp12-
early
late
K
0'
12'
22'
32'
45'
67'
82'
110'
L
SPP1 DNA
brightfield
overlay
SPP1 DNA
TMA
overlay

Fig. 6. Localization of SPP1 DNA and DNA-filled particles in infected bacteria.

(*A*) Scheme of the SPP1 viral particle assembly pathway. MCitrine is displayed as a green cylinder in the gp12-mCitrine fusion protein. (*B-D*) Localization of SPP1 DNA and of capsid auxiliary protein gp12-mCitrine that decorates DNA-filled particles in *B. subtilis* GSY10024 infected with SPP1*lacO64gp2*$^{-}$ (*B*), SPP1*lacO64gp12*$^{-}$ (*C*), and SPP1*lacO64* (*D*). Images at late stages of infection (*SI Appendix* Fig. S2*B*) are displayed. Grey dotted lines display cell outlines defined from brightfield imaging. The scale bar represents 2 µm. (*E* and *G*) Thin sections of *B. subtilis* YB886 infected with SPP1*lacO64gp12*$^{-}$ (*E*) and SPP1*lacO64* (*G*) immunolabeled as in Fig. 5 *A* and *B*. The scale bars represent 1 µm. (*F* and *H*) DAPI-staining of fixed bacteria from the cultures used for immunoEM experiments. Arrows in (*F*) identify individualized DAPI foci attributed to warehouses. The scale bar in (*F*) represents 2 µm. (*I*) Infection of *B. subtilis* GSY10096 filamented cells with SPP1*lacO64*. The fluorescent reporters of SPP1 DNA, capsids, and tails were LacI-mCherry (magenta in overlays), gp12-mCFP (blue) and gp17.1-mCitrine (green), respectively. Images were taken late p.i.. The scale bar represents 5 µm. (*J*) Quantification of DNA-filled particles overlapping with the phage DNA compartment of cells mono-infected with SPP1*lacO64* and SPP1*lacO64gp12*$^{-}$ at early and late times p.i.. Datasets of >500 cells were analysed. (*K*) Snapshots from time-lapse Movie S1 of *B. subtilis* GSY10024, producing gp12-mCitrine, immobilized in a CellAsic microfluidics system and infected with SPP1*lacO64gp12*$^{-}$. The first photo shows cells before infection followed by snapshots at time points indicated on the top left corner. They illustrate the temporal and spatial program of SPP1 DNA compartment and viral particles warehouses formation (displayed in magenta and green respectively). Cells are multi-infected. The white arrow identifies a bacterium undergoing division. Arrowheads show the position of DNA compartments at 67 min p.i. that are disassembled in cell ghosts at 82 min p.i. but prior to full bacterial lysis (110 min p.i.). Images were enhanced as described in Movie S1 legend. (*L*) Cell septation through the SPP1 DNA compartment (displayed in magenta) in bacteria producing LacI-mCherry (strain GSY10004) infected with SPP1*lacO64*. Cells membrane contour is stained with TMA-DPH (rendered in green) on the right side. The white arrow shows septum formation. To enhance the signal from the membrane staining (TMA-DPH), the raw image was denoised (2D-Gaussian filter, radius = 1,25 pixel) and background was removed using a rolling ball (sigma = 10 pixel) using Fiji (67).

PNAS
www.pnas.org

Supplementary Information for
Temporal Compartmentalization of Viral Infection in Bacterial Cells

Audrey Labarde[a], Lina Jakutyte[b,1], Cyrille Billaudeau[c,1], Beatrix Fauler[d], Maria López-Sanz[e], Prishila Ponien[f], Eric Jacquet[f], Thorsten Mielke[d], Silvia Ayora[e], Rut Carballido-López[c], Paulo Tavares[a,*]

[a] Université Paris-Saclay, CEA, CNRS, Institute for Integrative Biology of the Cell (I2BC), 91198 Gif-sur-Yvette, France

[b] Laboratoire de Virologie Moléculaire et Structurale, Centre de Recherche de Gif, CNRS UPR 3296 and IFR 115, Avenue de la Terrasse, Bâtiment 14B, CNRS, 91198 Gif-sur-Yvette, France

[c] Université Paris-Saclay, INRAE, AgroParisTech, Micalis Institute, 78350 Jouy-en-Josas, France

[d] Max-Planck-Institut für Molekulare Genetik, Microscopy and Cryo-Electron Microscopy Group, Ihnestraße 63-73, 14195 Berlin, Germany

[e] Department of Microbial Biotechnology, Centro Nacional de Biotecnología, CNB-CSIC, Madrid, Spain

[f] Université Paris-Saclay, CNRS, Institut de Chimie des Substances Naturelles, UPR 2301, 91198 Gif-sur-Yvette, France

[1] - These authors contributed equally to this work.
[*] - To whom correspondence may be addressed:
Paulo Tavares, Université Paris-Saclay, CEA, CNRS, Institute for Integrative Biology of the Cell (I2BC), 91198 Gif-sur-Yvette, France, +33169823860, paulo.tavares@i2bc.paris-saclay.fr

This PDF file includes:

Other supplementary materials for this manuscript include the following:

Materials and Methods

Bacterial strains construction. Bacterial strains used in this study are listed in Table S3.

B. subtilis GSY10004 was constructed by transformation of *B. subtilis* YB886 with plasmid pPT300 linearized with XbaI. *B. subtilis* GSY10024, GSY10025, BG1829, BG1831, BG1833, BG1837, GSY10031, GSY10060 and GSY10095 were constructed by transformation of GSY10004 with plasmids pAL24, pAL25, pML1829, pML1831, pML1833, pML1839, pAL31, pAL36 and pAL53, respectively, linearized with ScaI. *B. subtilis* GSY10006, GSY10008, GSY10010, GSY10011, GSY10012 and GSY10014 were constructed by transformation of GSY10004 with chromosomal DNA from *B. subtilis* strains PolC-GFP, GFP-DnaN, GFP-SsbA, GFP-DnaB, DnaE-GFP and GFP-DnaC, respectively. GSY100050 was constructed by transformation of GSY10000 with plasmid pHM232. GSY100051 was constructed by transformation of GSY10050 with chromosomal DNA from strain HM1049. GSY10061 was constructed by transformation of GSY10060 with plasmid pML1829 linearized with ScaI. GSY10096 was constructed by transformation of GSY10095 with plasmid pAL44 linearized with ScaI.

Transformation of competent *B. subtilis* cells was performed by a two-step starvation protocol using Spizizen medium for growth (1). 1 µg of linearized plasmid or chromosomal DNA was added to 1 mL competent cells for 60 min at 37°C, plated onto appropriate selective plates, and incubated overnight at 37°C.

Growth conditions. *E. coli* and *B. subtilis* strains were grown in Luria-Bertani (LB) medium, unless stated otherwise. Antibiotics selection in *E. coli* were 100 µg/mL ampicillin and 30 µg/mL erythromycin. Antibiotics selection in *B. subtilis* were 5 µg/mL kanamycin, 0.5 µg/mL erythromycin and 12.5 µg/mL lincomycin (*mls* resistance), 100 µg/mL spectinomycin, and 5 µg/mL neomycin. *B. subtilis* BG295 and HA101B strains were cultivated in MIII minimal medium (2) supplemented with 50 µg/mL tryptophan for BG295 and 50 µg/mL tryptophan, 50 µg/mL leucine for HA101B.

Phage strains construction. Phages used in the present study are listed in Table S3. Multiple SPP1 mutants were produced by phage crosses. The two parental phages were used to infect a permissive strain in LB medium supplemented with 10 mM $CaCl_2$ at an input multiplicity of 10 pfu/cfu of each phage for 2 h at 37°C. The cell lysate was cleared by centrifugation at 12,000 *g* for 20 min at 4°C and titrated on a permissive strain. Isolated phage plaques were collected and resuspended in 200 µL TBT buffer (100 mM Tris-Cl pH 7.5, 100 mM NaCl, 10 mM $MgCl_2$) on 96-well plates. The phage clones genotype was screened initially by spot test on complementing strains. Multiple mutant candidates were then checked by titration on strains complementing or rescuing the phage *sus* mutation knock-out and by PCR for deletion and insertion mutations.

Plasmids construction. Plasmids and primers used in the present study are listed in Table S3.

pPT300 was created in two steps. First, pAL1 was generated by cloning a PCR product of *mcherry* amplified from vector pJ1 with primers 1 and 2 cut with XhoI and BamHI and ligated into plasmid pHP13 cut with the same restriction enzymes. Second, pPT300 was generated by digestion of pAL1 with EcoRI and BamHI and cloning of the fragment carrying *mcherry* in pKL190 cut with the same enzymes.

pAL24, pAL53, pML1837, pML1833, and pML1829 were constructed in three steps. First, pAL19 was generated by ligation of a PCR product coding P_{spac}, amplified from plasmid pDH88 with primers 3 and 4 cut with BamHI-XbaI to pSac-Kan cut with BglII-XbaI. Then, pAL21 was generated by ligation of a PCR product coding *mcitrine*, amplified from pJexpress404 with primers 5 and 6 cut with with EcoRI-BamHI to pAL19 cut with the same enzymes. Finally, pAL24, pAL53, pML1837, pML1833, and pML1829 were generated by ligation of a PCR product of SPP1 genes *12*, *17.1*, *34.1*, *35*, and *40* (amplified from SPP1 DNA with primers 7 and 8, 9 and 10, 11 and 12, 13 and 14, and 15 and 16, respectively), cut with ClaI-XhoI to pAL21 cut with the same enzymes.

pAL25 and pML1831 were constructed in two steps. First, pAL20 was generated by digestion of pJexpress404 with EcoRI-BamHI and ligation of the fragment coding *mcitrine* to pAL19 cut with the same enzymes. Second, pAL25 and pML1831 were generated by ligation of a PCR product coding genes *11* and *35* (amplified from SPP1 DNA with primers 17 and 18, and 13 and 19, respectively) cut with ClaI-BamHI to pAL20 cut with the same enzymes.

pAL36 and pAL37 were constructed in two steps. First, pAL28 was generated by ligation of a PCR product coding *mcfp*, amplified from pDR200 with primers 20 and 21, cut with BamHI-KpnI to pDG1190 cut with the same enzymes. Second, pAL36 and pAL37 were generated by ligation of PCR products coding *dnaG* or *dnaX* (amplified from *B. subtilis* DNA with primers 22 and 23, 24 and 25, respectively), cut with BamHI-ClaI to pAL28 cut with the same enzymes.

pAL44 was constructed in two steps. First, pAL29 was generated by ligation of a PCR product coding *mcfp*, amplified from pDR200 with primers 23 and 24, cut with EcoRI-SpeI to pDG1192 cut with the same enzymes. Second, pAL44 was generated by ligation of a PCR product coding gene *12*, amplified from SPP1 DNA with primers 28 and 29, cut with KpnI-XhoI to pAL29 cut with the same enzymes.

Plasmid constructions were transformed, selected with appropriate antibiotic concentrations (see sections Bacterial strains construction and Growth conditions) and amplified in *E. coli* DH5α using standard molecular biology protocols (3). Correctness of all constructs was confirmed by DNA sequencing.

Phage amplification. Phages SPP1*wt*, *delX110*, *lacO64* and *lacO64gp12*$^{-}$ were multiplied in *B. subtilis* YB886 as described (4). Phages SPP1*lacO64gp2*$^{-}$, *lacO64gp6*$^{-}$, *lacO64gp11*$^{-}$, *lacO64gp13*$^{-}$, and *lacO64gp16*$^{-}$ were multiplied in the permissive strain *B. subtilis* HA101B while *lacO64gp34.1*$^{-}$, *lacO64gp40*$^{-}$, and *lacO64tail*$^{-}$ were multiplied in the permissive host *B. subtilis* BG295, as described (5, 6). The *lacO* operators cassette was sequenced in SPP1*lacO64* and its stable presence was monitored by PCR during amplification of all phage strains (4). The *lacO* repeats are flanked by 10 bp random sequences to prevent recombination within the *lacO* array to ensure its genetic stability (7).

Quantification of intracellular phages. Aliquots of 100 µL of infected cells were taken at the desired time points p.i., diluted to 1 mL with TBT containing 10% chloroform and vortexed vigorously. After 2 h on ice to allow for complete cell lysis, the mix was centrifuged, and the aqueous phase was titrated to determine the intracellular phages during the infection cycle.

Purification of SPP1 particles. SPP1 procapsids and phages were produced and partially purified using a protocol adapted from (8). In brief, 300 mL cultures of *B. subtilis* GSY10004, GSY10024 and GSY10025, supplemented with 1 mM IPTG for GSY10024 and GSY10025, were infected at an OD_{600nm} of 0.8 with different SPP1 phage mutants at an input multiplicity of 5 pfu/cfu and incubated with orbital shaking at 37°C for 3 h. Cultures were centrifuged at 15,300 *g* for 15 min at 4°C to sediment intact bacteria and debris. SPP1 particles in the supernatants were sedimented by centrifugation overnight at 20,300 *g* (4°C). Supernatants were fully removed and pellets were covered with 250 µl of cold buffer R (50 mM Hepes-KOH pH 7.6, 50 mM potassium glutamate, and with a 1X protease inhibitors cocktail [Roche]) supplemented with 10 mM EDTA for procapsids purification. After incubation for 15 minutes at 4°C, pellets were resuspended very carefully, supplemented with 25 mM $MgCl_2$, 25 U Benzonase (Millipore), 100 µg/mL RNAse, and incubated for 3 h at 4°C in a rotating wheel. Debris were removed by centrifugation for 15 min at 25,900 *g* (4°C). Supernatants (200 µL) were applied to a 10-30% glycerol gradient (v/v) in buffer R and centrifuged for 90 min at 35,000 rpm (4°C). Fractions of 1 mL were collected and analyzed on 12% SDS-PAGE gels stained with Coomassie Blue. Fractions with SPP1 particles (procapsids, capsids or virions) were pooled.

To obtain highly purified SPP1 virions, lysates of infected bacteria were sedimented overnight at 12,000 *g* (4°C), resuspended in TBT buffer, and run for 6 h at 35 Krpm in a SW41 rotor (Beckman) (20°C) through a discontinuous CsCl gradient in TBT buffer (4).

Viral particles were applied to 12% SDS-PAGE gels and their composition was analysed by Coomassie Blue staining and western blotting with anti-gp11 or anti-GFP rabbit polyclonal sera (Table S3).

Preparation of cell lysates and protein composition analysis. Strains YB886, GSY10004, GSY10024 and GSY10025 were grown overnight at 30°C in LB medium. Cultures were diluted 1:100 in 25 mL of LB medium (containing 1 mM IPTG for GSY10024 and GSY10025) and grown at 37°C. At an OD_{600nm} of 0.8, cultures were supplemented with 10 mM $CaCl_2$ and infected with different phages at an input multiplicity of 5 pfu/cfu. At 25 min p.i., bacteria were centrifuged for 5 min at 8,000 *g* (4°C). Cell pellets were resuspended in 1:20 of the initial culture volume in 50 mM glucose, 1 mM EDTA, 50 mM Tris-HCl pH 8, 1 mg/mL lysozyme and 1X protease inhibitors cocktail for 5 min at room temperature. An equal volume of ice-cold lysis buffer containing 500 mM NaCl, 1% NP-40, 50 mM Tris-HCl pH 8, 5 mM $MgCl_2$, 1 µg/mL DNAse and 100 µg/mL RNAse was added and the mix was kept on ice for 30 min. Cell debris were removed by centrifugation for 30 minutes at 14,000 *g* (4°C) and supernatants were immediately run on a 12% SDS-PAGE gel. Protein composition was determined as described in the previous section. This protocol was adapted from (9).

Quantitative PCR (qPCR) experiments. An overnight culture of *B. subtilis* GSY10004 strain was diluted 1:100 in fresh LB medium and grown at 37°C to an OD_{600} of 0.8. The culture was supplemented with 10 mM $CaCl_2$ and infected at an input multiplicity of 5 pfu/cfu with phages SPP1*lacO64*, *lacO64gp2*$^-$ or *lacO64gp40*$^-$. Two aliquots of 1 mL culture were taken for each time point and for each cell treatment procedure (technical duplicates). Samples were centrifuged 3 min at 11,000 *g*. The supernatant was completely removed to eliminate extracellular phage particles and cell pellets were frozen at -20°C. Pellets were resuspended in 500 µL lysis buffer (50 mM Tris-HCl pH 8, 50 mM glucose, 50 mM NaCl, 2 mg/mL lysozyme and 1X protease inhibitors cocktail) and incubated for 10 min at room temperature. For total DNA extracts, the cell suspension was mixed with 500 µL lysis buffer A (50 mM Tris-HCl pH 8, 50 mM NaCl, 1% NP40, 10 mM EDTA and 10 µg/mL RNAse) and incubated for 30 min on ice. For DNAse-treated extracts, the cell suspension was mixed with 500 µL of lysis buffer B (50 mM Tris-HCl pH 8, 50 mM NaCl, 1% NP40, 5 mM $MgCl_2$, 100 µg/mL RNAse and 100 U Benzonase), incubated for 30 minutes at 37°C and supplemented with 10 mM EDTA. Both types of extracts were deproteinized with 0.5% SDS and 50 µg/mL proteinase K (Roche) for 1 h at 65°C. Biological duplicates were prepared for each condition and qPCR experiments were carried out for three series of samples from independent infection experiments.

Quantitative PCR was performed on a QuantStudio 12K Flex Real-Time PCR System with a SYBR green detection protocol (Life Technologies) following the manufacturer's instructions. To prepare the samples, the DNA extracts were first diluted 300-fold with water. 3 µL of diluted samples were then mixed with Fast SYBR Green Master Mix and 500 nM of each primer for a final volume of 10 µL. The reaction mixture was loaded on 384 well microplates and submitted to 40 cycles of PCR (95°C/20 s; [95°C/1 s; 60°C/20 s] x 40) followed by a fusion cycle to analyze the melting curve of the PCR products. All the qPCR reactions were made in technical duplicates. A negative control, without added sample, was included in each experiment. Primers were designed using the Primer-Blast tool from NCBI and the Primer Express 3.0 software (Life Technologies) to quantify SPP1 gene *6* and *B. subtilis* gene *gyrA* (Table S3). Specificity and the absence of multilocus matching at the primer site were verified by BLAST analysis on the genomes of SPP1 and *B. subtilis*.

Absolute quantification of the copy number from each target gene in the samples was obtained using a standard curve. The curve was prepared by a five-fold dilution series of linearized plasmid pUC19-EJ1 containing DNA sequences of the SPP1 and *B. subtilis* amplicons. The known quantity of plasmid DNA copies in the standard curve from $1x10^7$ to $6.4x10^2$ copies, allowed converting Ct values determined experimentally into the copy number for each targeted gene. These copy numbers of SPP1 and *B. subtilis* genomes present in a sample were then used to calculate the number of SPP1 phages per bacterium considering that there are an average of 2.7 copies of *B. subtilis* genomes per cell (*SI Appendix* Fig. S1 *C* and *D*). The number of SPP1 genomes protected inside viral particles was quantified in samples treated with DNAse (see above) and divided by the total number of SPP1 genomes in the sample to calculate the percentage of encapsidated SPP1.

Total DNA quantification by Qubit. Deproteinized DNA samples were prepared as described for qPCR experiments (previous section). Qubit quantifications were carried out using a Qubit™ dsDNA HS Assay kit in a Qubit™ 3.0 Fluorometer. All measurements were made in a final volume of 200 µL Qubit dsDNA HS buffer with 1 µL of fluorophore reagent and 3 µL of buffer or sample used for extraction of total DNA extracts. A standard curve was prepared with increasing quantities of the kit DNA HS Standard 2. Each sample was prepared in duplicate with 3 µL of extract and was measured twice. The DNA concentration of each sample was determined according the standard range equation and the average of the 4 measurements.

Fluorescence Microscopy. Overnight cultures of *B. subtilis* strains grown at 30°C were diluted 1:100 in fresh LB, pH 8 medium with 1 mM IPTG or/and 1% xylose, depending on the strain, and grown at 37°C.

At an OD_{600nm} of 0.8 the cultures were supplemented with 10 mM $CaCl_2$ and infected with the SPP1 strain under analysis at an input multiplicity of 1. Infected cultures were grown at 37°C with orbital shaking for 12-20 min, according to the experimental setup outlined in *SI Appendix* Fig. S2*B*. Infected cells were mounted on agarose pads and microscopy was carried out subsequently at room temperature. Image acquisitions were performed at early (20-30 min p.i.) and late (40-50 min p.i.) time-points after phage infection (*SI Appendix* Fig. S2*B*) on a Zeiss Axio Observer Z1 microscope with 63X oil objective. We noted that LacI-mCherry remained associated to the *lacO64* repeats on SPP1 DNA in presence of 1 mM IPTG.

HPUra (a gift from George Wright and Neal Brown, Glsynthesis, Worcester, USA) (200 µM final concentration) and DNP (Sigma Aldrich) (10 mM) were added to cultures at 21 min p.i., incubated for 3 min at room temperature and mounted on agarose pads for epifluorescence microscopy. HPUra and DNP were also added in the agarose pad at the same final concentration.

DAPI (Thermo Fisher Scientific) (10 mg/mL) and TMA-DPH (Thermo Fisher Scientific) (25 µM) were added to cultures for 3 min at room temperature before observation and mounted on agarose pads for epifluorescence microscopy.

Filamentated cells infection and imaging. Overnight cultures of *B. subtilis* were diluted 1:100 in fresh LB medium supplemented with 1 mM IPTG or/and 1% xylose and grown at 37°C. At an OD_{600nm} ~0.4-0.5, PC190723 (FstZ Polymer Stabilizer, Merck-Millipore) was added to a final concentration of 1 µg/mL and the cultures were further incubated for 60 min at 37°C. Then, cells were supplemented with 10 mM $CaCl_2$ and infected with the SPP1 strain to be tested for 20 min at 37°C. The input multiplicity of infection was adjusted empirically to obtain <50% infected cells. Cells were mounted in agarose pads and imaged as described in the previous section. Image acquisitions were performed every 10 min for GSY10025 and every 5 min for GSY10096.

Microfluidics experiments. An overnight culture of *B. subtilis* GSY10024 grown on LB medium was diluted 1:100 in fresh LB medium and incubated with agitation at 37°C. At an OD_{600nm} of ~0.4-0.5, cells were concentrated 5-fold and loaded into B04A microfluidic plates (ONIX, CellASIC ONIX Microfluidic Plates for Bacterial cells) at 2 psi for 12 s. The medium flow rate and temperature were maintained at 5 psi and 37°C, respectively, throughout imaging. The loading channel was subsequently washed for 20 min with LB medium supplemented with 10 mM $CaCl_2$. Phage was added to the cells for 5 min by switching the media flow channel using CellASIC ONIX FG (Version 5.0.2-Millipore). After phage infection, cells were visualized using a Nikon Ti-Eclipse microscope, stabilized at 37°C, with a 100X oil

objective (NA 1.3 WD : 0,2 mm CFI Plan Fluor - Phase - Nikon). Images were taken every 2.5 min using red and yellow fluorescence. Images and videos were processed as described in the legend of Movie S1.

Electron microscopy of cryo-sectioned infected cells. An overnight culture of *B. subtilis* YB886 was diluted 1:100 in fresh LB medium and grown at 37°C to an OD_{600nm} of 0.8. The culture was supplemented with 10 mM $CaCl_2$ and infected at a multiplicity of 5 pfu/cfu with phages SPP1*lacO64*, *lacO64gp2*$^-$ or *lacO64gp12*$^-$ at 37°C with agitation. At 35 min p.i., cells were mixed with fixation solution (4% paraformaldehyde [Electron Microscopy Sciences], 0.4% glutaraldehyde [Sigma Aldrich], 20 mM $MgCl_2$, 1X PBS pH 8) at room temperature for 2 h on a rotating wheel. Fixed cells were centrifuged for 10 min at 3,500 *g*, washed twice with wash buffer (10 mM $MgCl_2$, 1X PBS pH 8), and resuspended in TBT buffer. Cells were centrifuged and the supernatant carefully removed. Pellets were embedded in 10% gelatin dissolved in TBT. Cells embedded in gelatin beads were conserved in 2.3 M sucrose prepared in TBT at 4°C. Beads were cut in 90 nm thin sections at cryo-temperatures with an EM UC7 ultramicrotome under liquid nitrogen (10–12).

Sections were transferred to copper grids covered with carbon film, washed 5 times in TBT and incubated in buffer A (Table S4) for 1 h at room temperature. Grids were washed 3 times with TBT, twice with buffer B (1X PBS pH 8 supplemented with 10 mM $CaCl_2$), blocked with 500 µL blocking buffer for 30 min at room temperature, and incubated with 10 µL of primary antibody at 4°C (Tables S3 and S4). After 4 washes with buffer B, the grids were incubated with 10 µL of secondary antibody labelled with colloidal gold beads (Tables S3 and S4) for 2 h in a humidity chamber. They were then washed 4 times in buffer B, twice in water, and plunged in a solution of 2% uranyl acetate for 30 s. Thin-sections were imaged on a FEI Tecnai G^2 F20 electron microscope.

Automatic detection and quantification of viral compartments. Automatic detection and characterization of phage DNA compartments (LacI-mCherry), procapsids (mCitrine-gp11) and virion warehouses (gp12-mCitrine) were performed using a Matlab-based custom algorithm (Matlab R2016B version). The analysis workflow can be decomposed in three main successive steps:

1. Cell detection and identification. This step aims to generate a binary image in which cells are individualized. First, pixels associated to background were identified by applying k-means method (with 2 kernels) on the epi-fluorescence image of viral (pro-)capsids. The corresponding bright-field image was sequentially processed to (i) emphasize cells from the background (by applying a ‘top-hat’ filter using a disk with 15 pixels radius as structuring element), (ii) enhance the cell contour (by a ‘difference of Gaussian’ filter) and (iii) assign all background pixels to a unique value (lower than any pixel in the image).

By applying the k-means method (with 3 kernels) on this processed image, pixels were then classified within three groups: background, cell outline and cell inside. The binary mask of the cells was obtained by keeping only pixels associated to the inside of the cells. The absence of membrane staining in our images prevented to isolate and separate all cells without error (particularly when cells form chains). Therefore, visual inspection of each binary mask was performed to correct for cell separations (when it was obvious on bright-field image) and/or to eliminate cells for which segmentation failed. Finally, connected pixels were detected in each binary mask, allowing to generate a labeled image displaying individual bacteria in which morphological features of the cells (surface and length) were quantified.

2. Localization and morphology of the phage DNA compartment. First, the epi-fluorescence image of phage DNA was pre-processed (denoising by a 3x3 pixels median filter) and background pixels (detected on step 1) were all assigned to a unique value (lower that any value in the image). Then, the DNA foci were segmented using the k-means method (with 3 kernels) by keeping only areas greater than 7 pixels^2. The resulting binary image allowed to (i) identify, locate and measure the replication area, (ii) count replication foci per cell to identify non-infected, mono-infected or multi-infected cells, (iii) characterize the dimensions (length and width) of replication foci by fitting an ellipse around these zones, (iv) measure the distance from the center of the replication foci to the two poles of the cell, and (v) quantify the average intensity of the fluorescence in the replication zone.

3. Localization and morphology of procapsids and virion warehouses. Detection was performed only on mono-infected cells with two different approaches for procapsids and capsids foci. For viral procapsids, segmentation of mCitrine-gp11 foci was achieved by the k-means method (with 2 kernels), and by removing areas smaller than 6 pixels^2 and areas displaying less than 5% pixels with intensity above an activation threshold. The activation threshold was defined on the fluorescence intensity of non-infected cells as the average +3 standard deviation. For viral capsids, gp12-mCitrine foci were enhanced by subtraction of their own filtered images obtained by denoising (5x5 pixels 2D-median filter). Noise was removed using a grayscale morphological opening (using a disk with 2 pixel radius as structuring element). Then all pixels not associated to mono-infected cells were set to 'Not-a-Number' (NaN) value in the resulting image, and segmentation of capsid foci was achieved by the k-means method (with 2 kernels). To remove false detections, capsid signals displaying an intensity below the threshold (defined as the value presenting equal probability distributions for intensity associated to cytoplasm and capsids areas) and smaller than 6 pixels^2 were removed. For both procapsids and capsids, the resulting binary image allowed to (i) identify, count, locate and measure the area of foci per mono-infected cell, (ii) measure the distance between the (pro)capsid and the phage DNA compartment, (iii) measure the percentage of overlapping area between the (pro)capsids and the DNA compartment (in case of overlap) or the gap distance between the two areas (in case of non overlap), (iv) determine the side localization

of viral (pro)capsids in the cell as compared to phage DNA compartment, (v) characterize the morphology (length and width) of the compartment by adjusting an ellipse around these areas, and (iv) quantify their average fluorescence intensity.

Image processing used for visualization. Fig. 6*K* and Movie S1. The time-lapse was processed to highlight the phage DNA compartment and virion warehouses. Firstly, temporal lateral drift was estimated using the phase contrast channel and corrected on all channels (fluorescence and phase contrast). SPP1 DNA images were pre-processed to remove background signal (rolling ball subtraction, radius = 20 pixels) and enhanced using a Laplacian of Gaussian filter (with an increasing radius from 3 to 5 pixels to respect foci area enlargement during infection). Processed images were segmented using thresholding, converted to binary mask and blurred with a Gaussian filter (radius = 2 pixels) for visualization. Capsid warehouses were denoised using median filter (radius: 1 pixel), and enhanced using Laplacian of Gaussian filter (radius = 2 pixels). As soon as capsids appeared in the time-lapse they were segmented using thresholding, converted to binary mask after rejecting large foci (> 0.5 µm^2) to remove false detections (based on results from Fig. 4*C*), and blurred with a Gaussian filter (radius = 2 pixels) for the visualization.

For Fig. 6*L*, to enhance the signal from the membrane staining (TMA), the raw image was denoised (2D-Gaussian filter, radius = 1.25 pixel) and background was removed using a rolling ball (sigma = 10 pixel) using Fiji (13).

Multiplicity of infection quantification. Multiplicity of infection (MOI) was calculated from microscopy acquisitions of SPP1 DNA (LacI-mCherry) assuming that the fraction of cells containing virus particles is given by a Poisson distribution:

$$P(n) = \frac{m^n e^{-m}}{n!}$$

where *m* is the multiplicity of infection, *n* is the number of infectious agents that enter the host cell, and *P(n)* is the probability that a cell will get infected by *n* bacteriophages. For non-infected cells (*n= 0*), the ratio or probability can be simplified as *P(0) = exp(-m)* allowing to quantify easily the MOI as

$$m = -\log\left(\frac{N_{ni}}{N_t}\right)$$

where N_{ni} is the number of non-infected cells and $N_t$is the total number of cells.

Statistical analysis. All statistical tests were performed using GraphPad Prism 6.05 and a non-parametric statistical test (two-tailed Mann-Whitney test with an alpha level of 5%).

Supplementary Figures

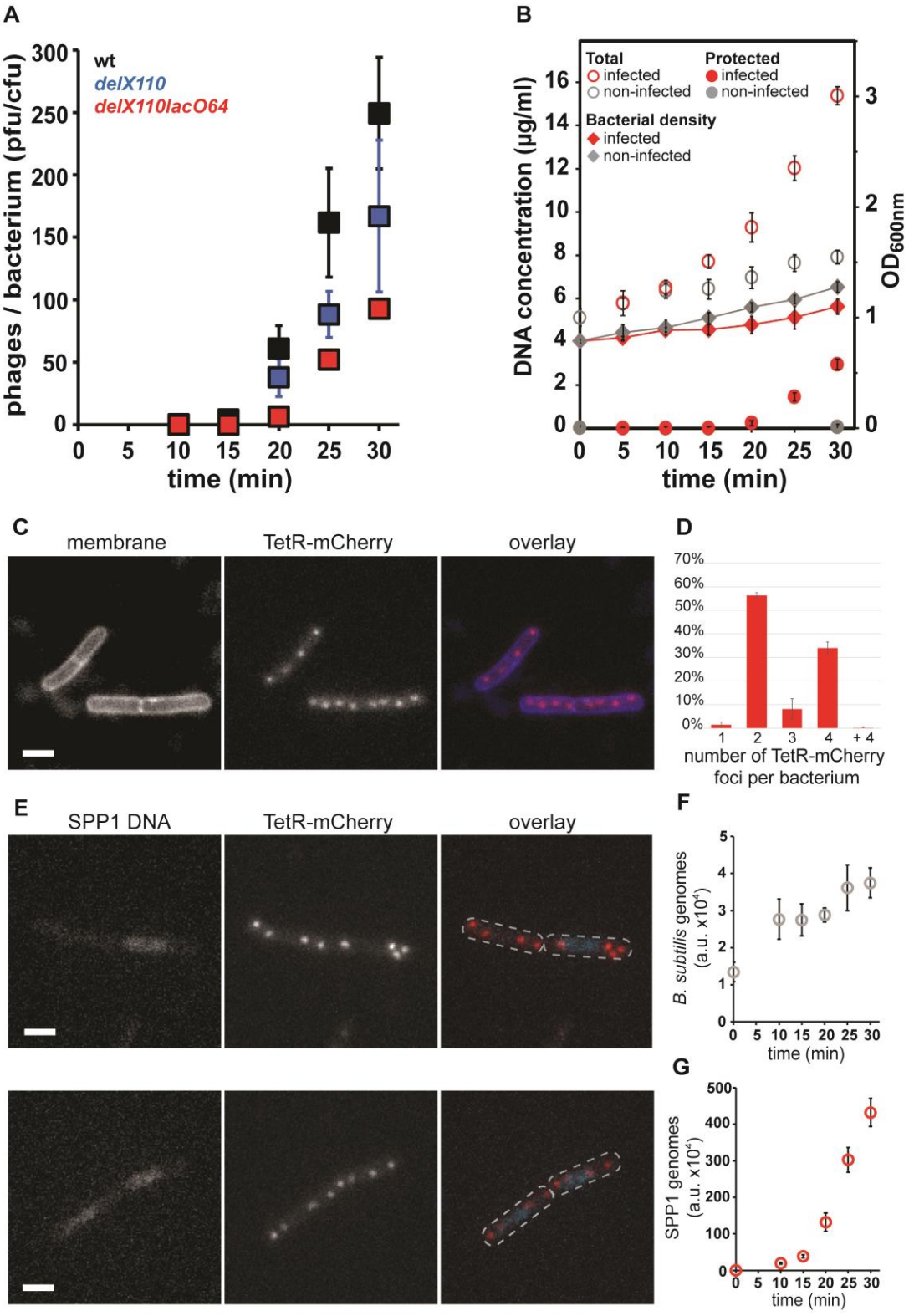

Fig. S1

Fig. S1: Phage yield and DNA replication in SPP1-infected bacteria.

(*A*) Number of intracellular infectious particles in *B. subtilis* GSY10004 (producing LacI-mCherry) cells infected with SPP1 wild-type (black), SPP1*delX110* (blue), and SPP1*delX110lacO64* (also abbreviated SPP1*lacO64* in this work) (red). Infectious particles were scored by titration after lysis of bacteria with 10% chloroform at different time points p.i. and divided by the number of bacteria infected at an OD_{600nm} of 0.8 (10^8 cfu/mL). The results are the average of three independent experiments. (*B*) Quantification of total DNA (empty circles) and DNAse-protected DNA (filled circles) by Qubit in cell extracts from *B. subtilis* GSY10004 non-infected (grey) and infected with SPP1*lacO64* (red) prepared at different time points p.i.. Non-infected and infected bacteria originated from the same culture split prior to infection. Diamonds connected with eye guiding lines display the culture optical density at 600nm. The results are the average of three independent experiments. (*C*) Localization of TetR-mCherry (red in the overlay) binding to an array of *tetO* repeats, inserted between the *soj* and *spo0J* loci in a region proximal to the *B. subtilis* origin of replication, during exponential growth in LB medium at 37°C. The cells membrane contour is stained with TMA-DPH (blue in the overlay). The scale bar represents 2 µm. (*D*) Distribution of TetR-mCherry foci per bacterium in the reporter system of (*C*). Data are the average of counts from three independent experiments. Around 200 bacteria were scored in each experiment. The average number of TetR-mCherry foci per bacterium is 2.7. (*E*) Localization of *B. subtilis* replication origin region (red in the overlay) and of SPP1 DNA (blue in the overlay) using the reporter system of (*C*) combined with a LacI-CFP fusion protein in *B. subtilis* GSY10051 cells infected with SPP1*lacO64gp2*$^-$. Grey dotted lines display cell outlines defined from phase imaging. (*F*) Change in *B. subtilis* GSY10004 bacterial genome copy number during infection with SPP1*lacO64* determined by qPCR of bacterial gene *gyrA*. (*G*) SPP1 genome copy number during the infection in (*F*) determined by qPCR of SPP1 gene *6*.

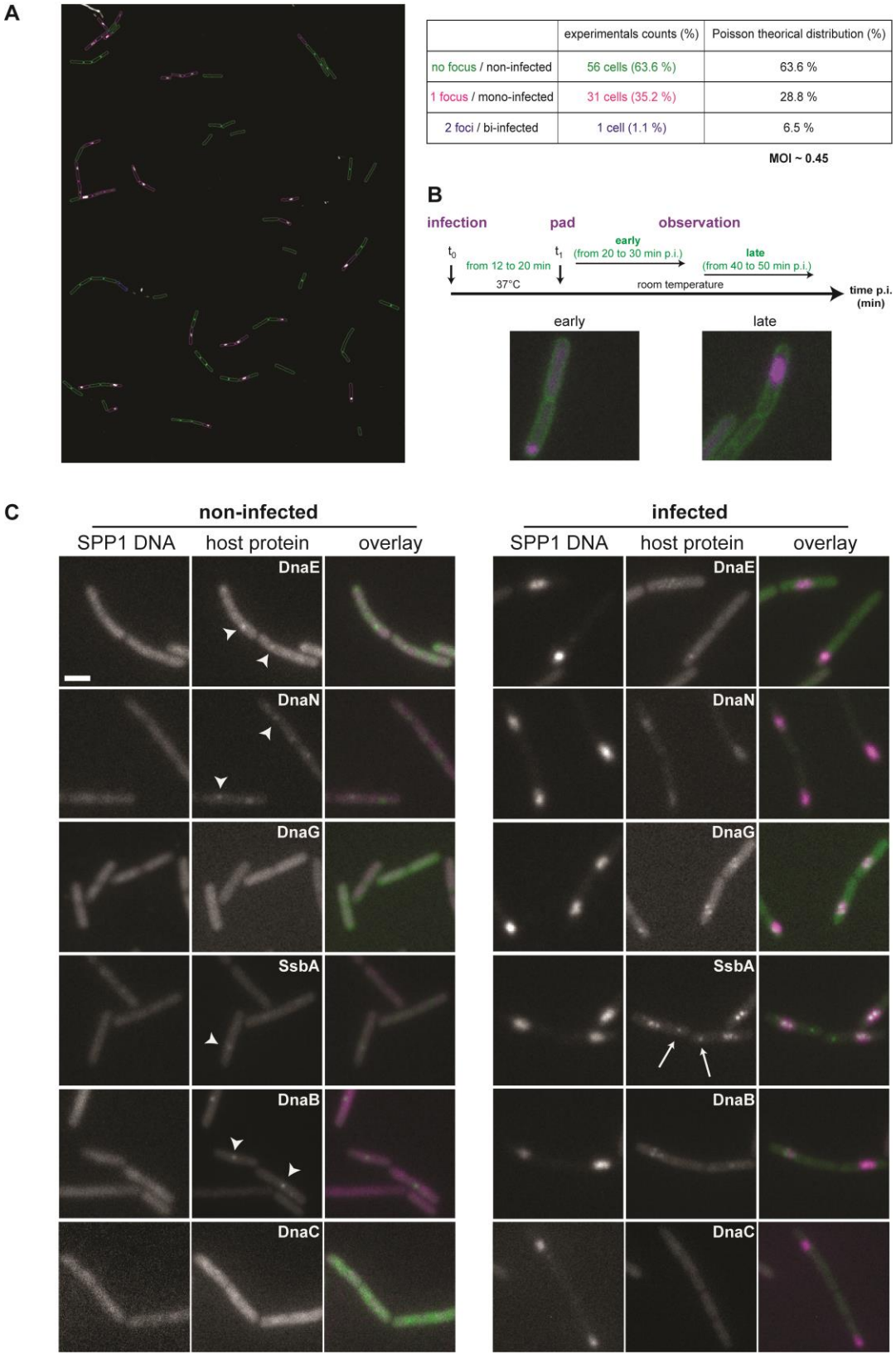
A
experimentals counts (%)
Poisson theorical distribution (%)
no focus / non-infected
56 cells (63.6 %)
63.6 %
1 focus / mono-infected
31 cells (35.2 %)
28.8 %
2 foci / bi-infected
1 cell (1.1 %)
6.5 %
MOI ~ 0.45
B
infection
pad
observation
early
(from 20 to 30 min p.i.)
late
(from 40 to 50 min p.i.)
from 12 to 20 min
37°C
room temperature
time p.i. (min)
early
late
C
non-infected
infected
SPP1 DNA
host protein
overlay
DnaE
DnaN
DnaG
SsbA
DnaB
DnaC

Fig. S2

Fig. S2. Imaging of the SPP1 DNA compartment and of *B. subtilis* replisome proteins during SPP1 infection.

(*A*) Determination of the multiplicity of infection (MOI) in a population of SPP1-infected bacteria following a Poisson distribution and computed from the number of non-infected bacteria (segmented in green on the left) (see *SI Appendix, Materials and Methods*). The experimental counts of cells with one (segmented in magenta) and two (blue) SPP1 DNA foci fit to the theoretical distribution of mono-infected and bi-infected bacteria, respectively (right). (*B*) Experimental setup to image SPP1-infected cells in agarose pads illustrated by visualization of the DNA compartment in *B. subtilis* GSY10004 mono-infected with SPP1*lacO64* at early and late times p.i.. SPP1 DNA is in magenta and the cells membrane contour is stained with TMA-DPH displayed in green. (*C*) Localization of host replisome proteins in non-infected (left) and in SPP1*lacO64*-infected (right) bacteria late p.i. (see (*B*)). All strains produce constitutively LacI-mCherry to label phage DNA and one GFP (DnaE, DnaN, SsbA, DnaB and DnaC) or mCFP (DnaG) fusion to label a bacterial replisome protein. The display is as in Fig. 2*A*. The scale bar represents 2 µm. Arrowheads show the position of host proteins foci in non-infected bacteria and arrows identify foci of SsbA not-colocalizing with SPP1 DNA in infected bacteria. Quantification of replisome proteins foci co-localization with SPP1 DNA is presented in Fig. 2*B* while function and features of each protein are compiled in Table S2.

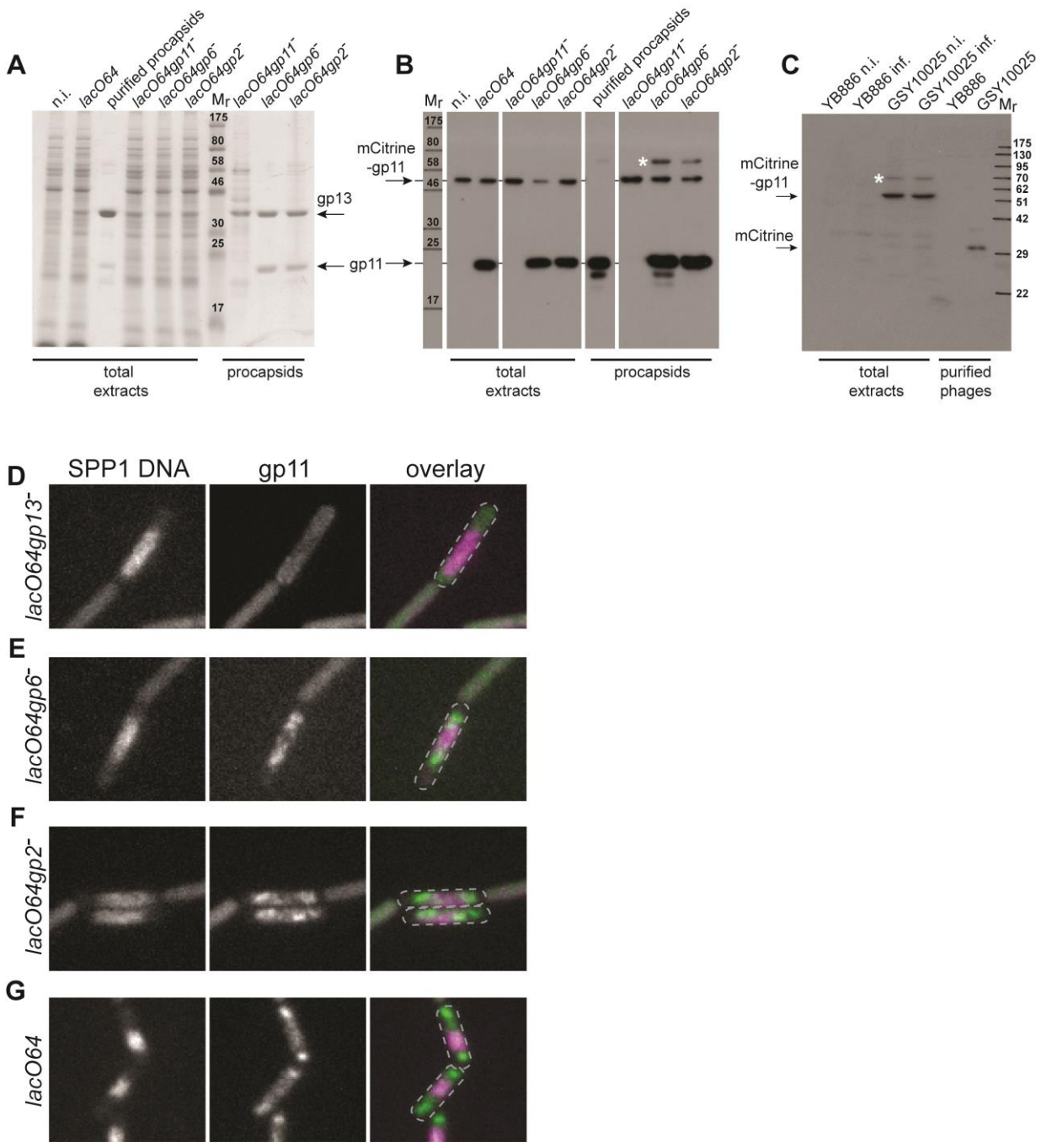

Fig. S3. Presence of gp11 and mCitrine-gp11 in phage structures.

(*A-C*) Analysis of extracts from *B. subtilis* GSY10025 cells infected with different SPP1 phage mutants and of viral structures purified from infected GSY10025 cells. Phage mutants used for infection are labeled above the gel lanes. Lysates of non-infected bacteria (n.i.) and purified procapsids competent for DNA packaging *in vitro* are controls. (*A*) Coomassie Blue-stained gel. Bands of the major capsid protein gp13 and of the scaffolding protein gp11 are labeled. M_r, molecular weight marker. (*B*) Anti-gp11 western

blot detecting gp11 and mCitrine-gp11. Note that particles sedimenting at the position of procapsids from lysates of SPP1*lacO64gp11*$^{-}$ infection of strain GSY10025 contain only a small amount of mCitrine-gp11 and no gp11, resulting on gp13 polymorphic structures that spread through the glycerol gradient used for particles separation (see *SI Appendix, Materials and Methods*). The white asterisk indicates a band of unknown origin recognized by anti-gp11 polyclonal antibodies. (*C*) Anti-GFP western blot to detect presence of mCitrine in extracts of *B. subtilis* strains producing mCitrine-gp11 (GSY10025) or not (YB886) infected with SPP1*lacO64* (left) and in phage particles purified from both cell types (right). The white asterisk indicates a band of unknown origin recognized by anti-GFP antibodies. (*D*-*G*) Localization of SPP1 DNA (magenta in overlay) and of mCitrine-gp11 (green in overlay) in *B. subtilis* GSY10025 infected with SPP1*lacO64gp13*$^{-}$ (defective in procapsid assembly) (*D*), SPP1*lacO64gp6*$^{-}$ (defective in portal protein production; leads to assembly of procapsids without portal that do not package DNA) (*E*), SPP1*lacO64gp2*$^{-}$ (defective in DNA packaging) (*F*) and SPP1*lacO64* (*G*). Images were taken at late stages of infection. Grey dotted lines display cell outlines defined from brightfield imaging. The scale bar represents 2 µm.

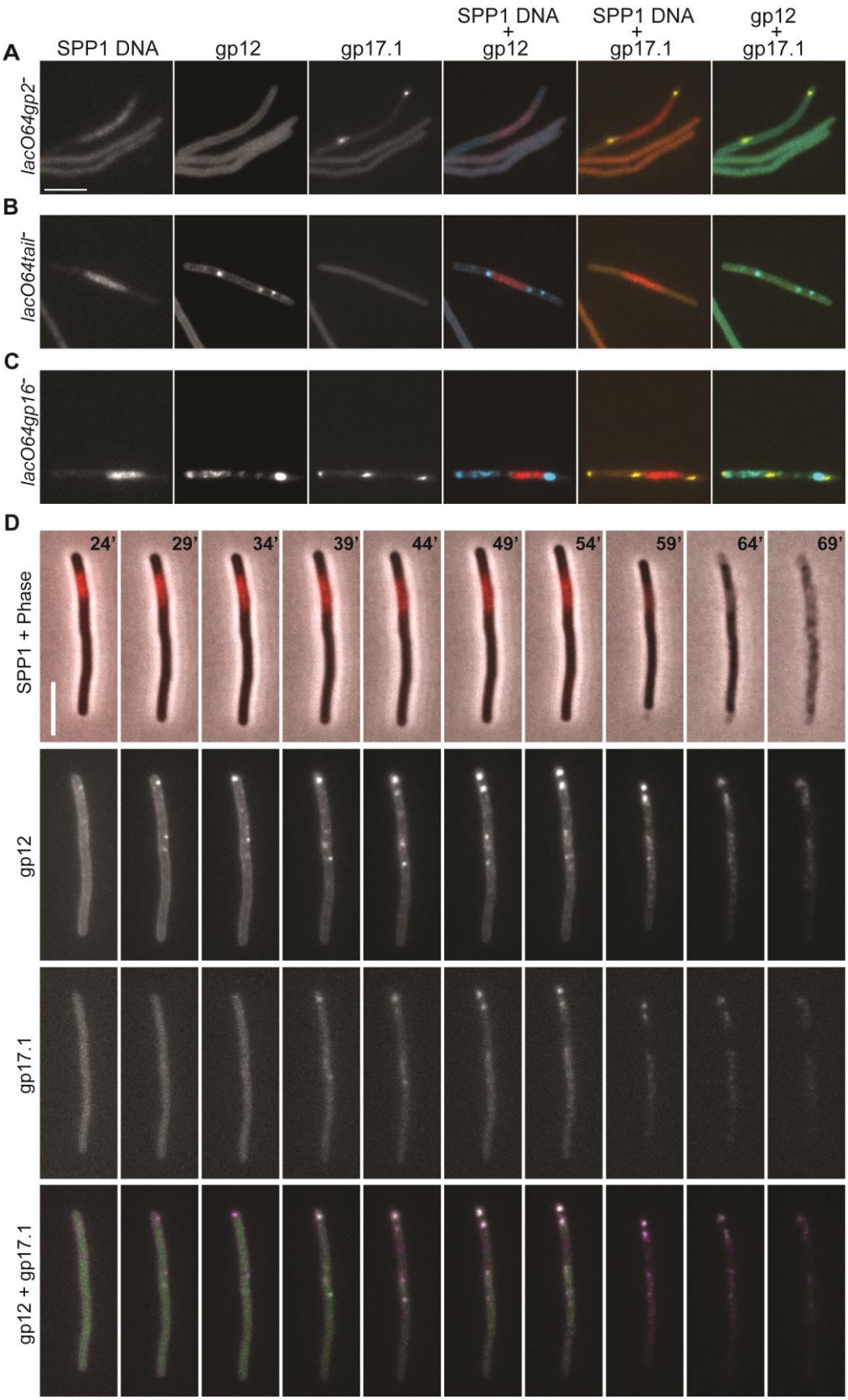
A
SPP1 DNA
gp12
gp17.1
SPP1 DNA + gp12
SPP1 DNA + gp17.1
gp12 + gp17.1
lacO64gp2-
B
lacO64tail-
C
lacO64gp16-
D
24'
29'
34'
39'
44'
49'
54'
59'
64'
69'
SPP1 + Phase
gp12
gp17.1
gp12 + gp17.1

Fig. S4

Fig. S4. Localization of the SPP1 DNA compartment, capsids and tails in infected bacteria.

(*A*-*C*) Infection of *B. subtilis* GSY10096 filamented cells with SPP1*lacO64gp2*$^{-}$ (defective in DNA packaging) (*A*), SPP1*lacO64tail*$^{-}$ (defective in tail assembly) (*B*), and SPP1*lacO64gp16*$^{-}$ (defective in formation of the capsid connector interface for phage tail binding) (*C*). The fluorescent reporters of SPP1 DNA, capsids, and tails were LacI-mCherry (red in overlays), gp12-mCFP (blue) and gp17.1-mCitrine (yellow), respectively. Images were taken late p.i. (*SI Appendix* Fig. S2*B*). (*D*) Time-lapse of *B. subtilis* GSY10096 infection with SPP1*lacO64*. SPP1 DNA imaging (red) and phase contrast are overlaid on the figure top row to show the phage DNA compartment and its loss of organization at the onset of cell lysis. Time p.i. is displayed on the top right corner of each image in the top row. Gp12-mCFP (displayed in magenta in the bottom row overlay) and gp17.1-mCitrine (green in the overlay) fluorescence signals are presented in the rows underneath. The scale bars represent 5 µm.

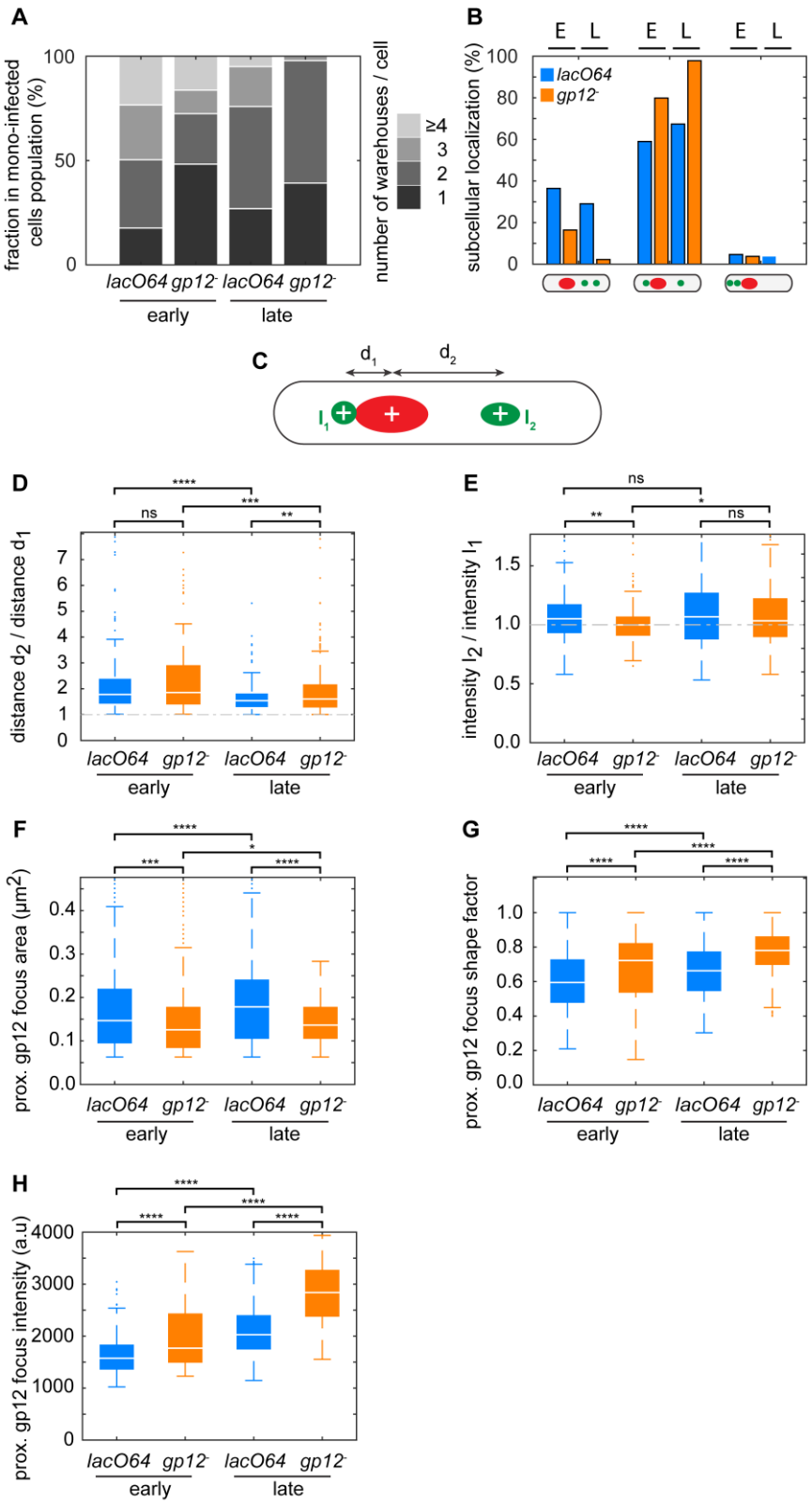
A
fraction in mono-infected cells population (%)
100
50
0
lacO64 gp12- lacO64 gp12-
early
late
number of warehouses / cell
≥4
3
2
1
B
E L E L E L
subcellular localization (%)
100
80
60
40
20
0
lacO64
gp12-
C
d1
d2
I1
I2
D
distance d2 / distance d1
7
6
5
4
3
2
1
0
****
***
ns
**
lacO64 gp12- lacO64 gp12-
early
late
E
intensity I2 / intensity I1
1.5
1.0
0.5
0.0
ns
**
*
ns
lacO64 gp12- lacO64 gp12-
early
late
F
prox. gp12 focus area (µm2)
0.4
0.3
0.2
0.1
0.0
****
***
*
****
lacO64 gp12- lacO64 gp12-
early
late
G
prox. gp12 focus shape factor
1.0
0.8
0.6
0.4
0.2
0.0
****
****
****
****
lacO64 gp12- lacO64 gp12-
early
late
H
prox. gp12 focus intensity (a.u)
4000
3000
2000
1000
0
****
****
****
****
lacO64 gp12- lacO64 gp12-
early
late

Fig. S5

Fig. S5. Spatial organization of the SPP1 DNA compartment and of warehouses in the cell.

(*A*) Distribution of the number of warehouses (foci of gp12-mCitrine-containing particles) in GSY10024 mono-infected cells (one SPP1 DNA focus) with SPP1*lacO64* (abbreviated *lacO64* in the figure) or with SPP1*lacO64gp12*$^{-}$ (abbreviated *gp12*$^{-}$ in the figure) at early and late times p.i.. Analysis was carried out with Fig. 6*J* datasets, including more than 500 cells from three independent infections. (*B*) Localization of warehouses relative to the SPP1 DNA compartment position in the subset of cells in (*A*) with two warehouses at early (E) and late (L) times p.i., according to the topology depicted underneath the histogram bars. More than 130 cells from three independent infections were analysed. Red, DNA compartment; green, warehouse. (*C*) Scheme illustrating measurements of distance and fluorescence intensity parameters in mono-infected bacteria whose viral DNA compartment is flanked by one warehouse on each side, the most frequent topology found in cells with two warehouses (*B*). "+" is the center of mass of the fluorescent focus. (*D*) Ratio between distances of the two warehouse centers of mass to the SPP1 DNA compartment center of mass (d_2/d_1; see (*C*)) in the sub-set of cells from (*B*). (*E*) Ratio of fluorescence average intensity between the warehouses from cells in (*B*) (I_2/I_1; see (*C*)). More than 130 cells from three independent infections were analyzed in (*B,D* and *E*). (*F-H*) Average area (*F*), shape factor (minimal/maximal diameters) (*G*) and average fluorescence intensity (*H*) of the warehouse proximal to the DNA compartment in all cells from (*A*). More than 500 cells from three independent infections were analyzed. In panels (*D-H*), the boxplot shows median of the sample data as a white solid line and draws point as outliers if they are greater than $q_3 + w(q_3 - q_1)$ or less than $q_1 - w(q_3 - q_1)$, where q_1 and q_3 are the 25th and 75th percentiles of the sample data, respectively and $w = 1.5$. Statistical significance between conditions was calculated using the Mann–Whitney non-parametric test (**** = P<0.0001; *** = 0.0001<P<0.001; ** = 0.001<P<0.01; * = 0.01<P<0.05; ns = P>0.05). a.u., arbitrary units.

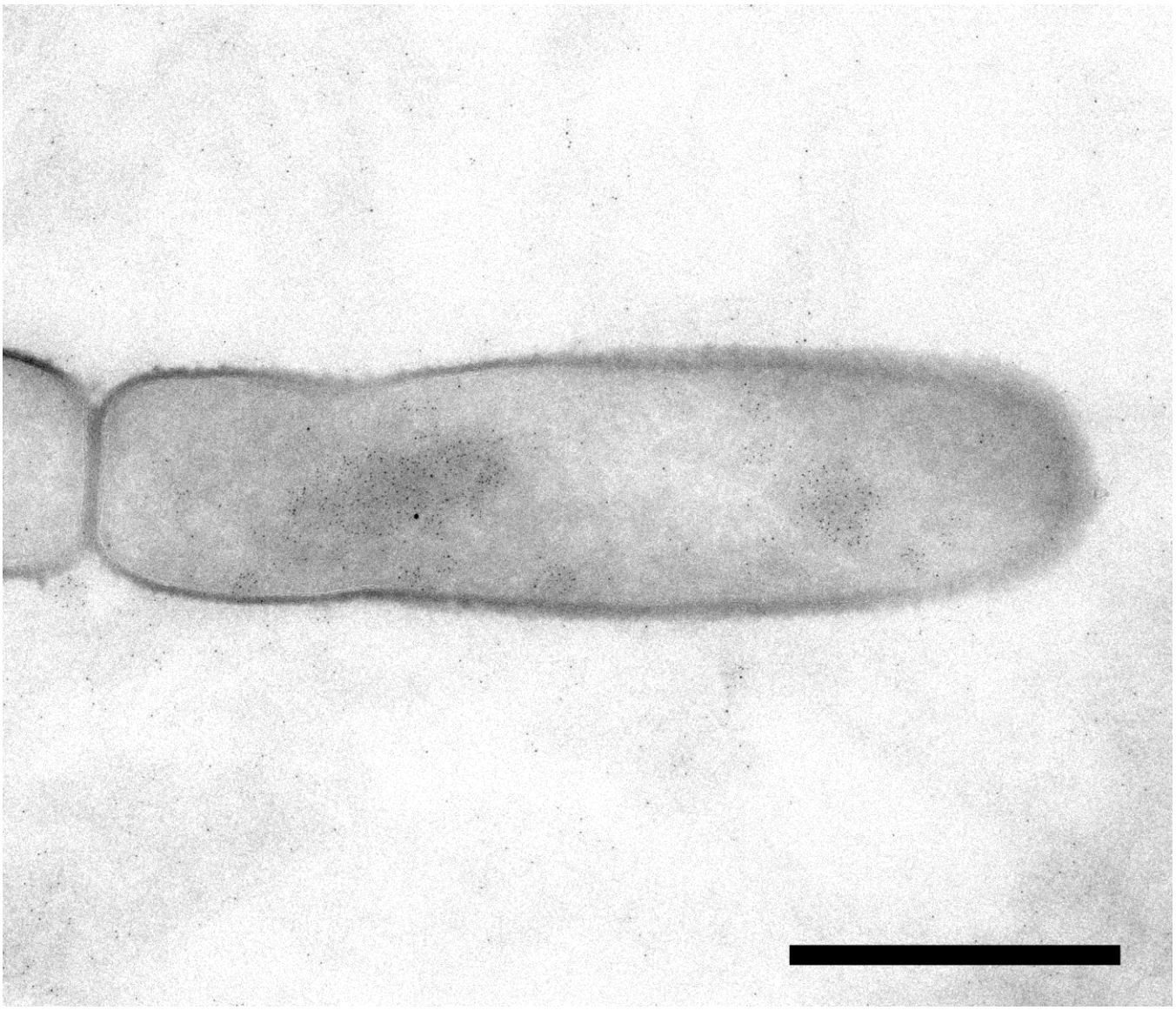

High resolution Fig. 5A

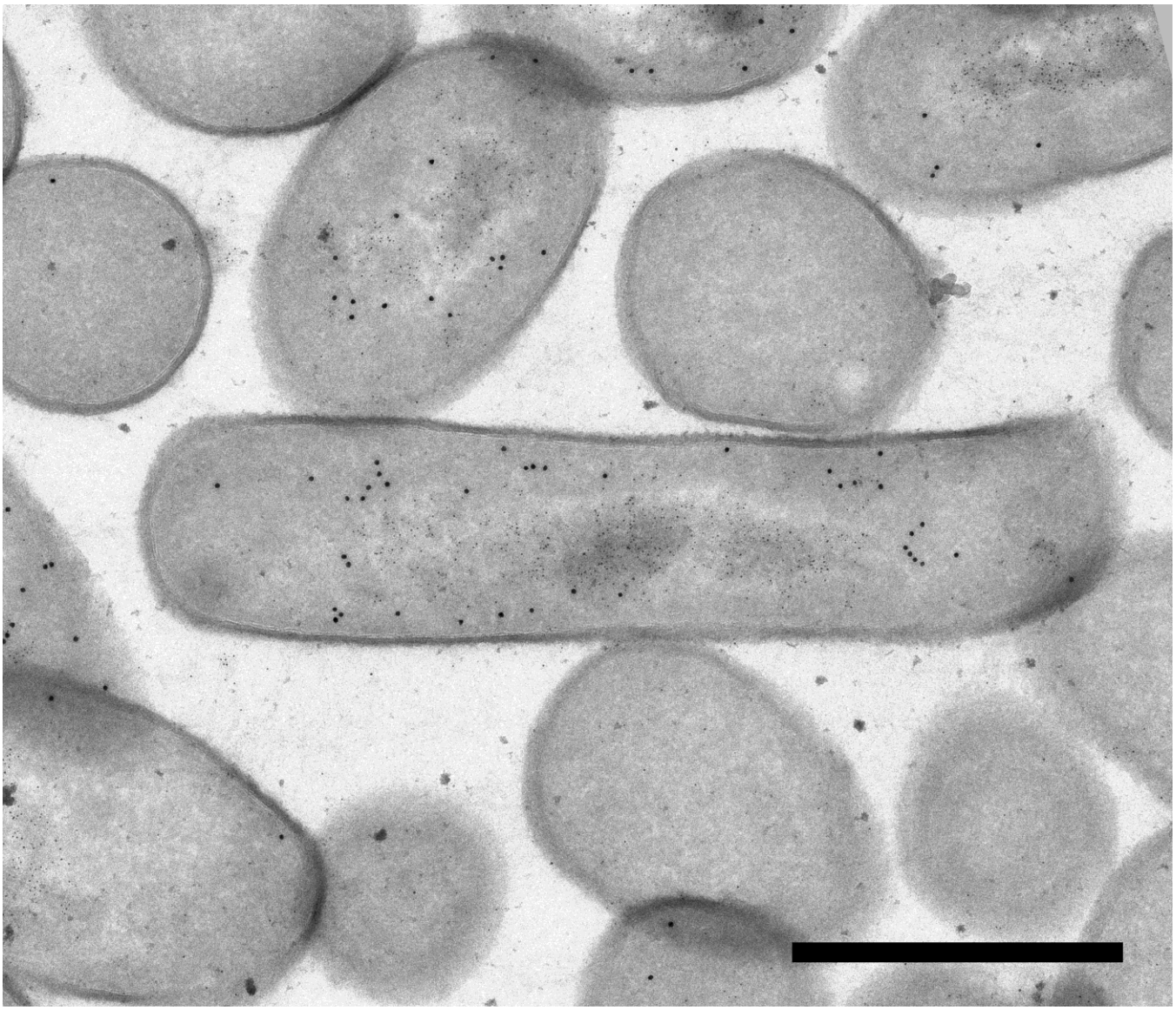

High resolution Fig. 5B

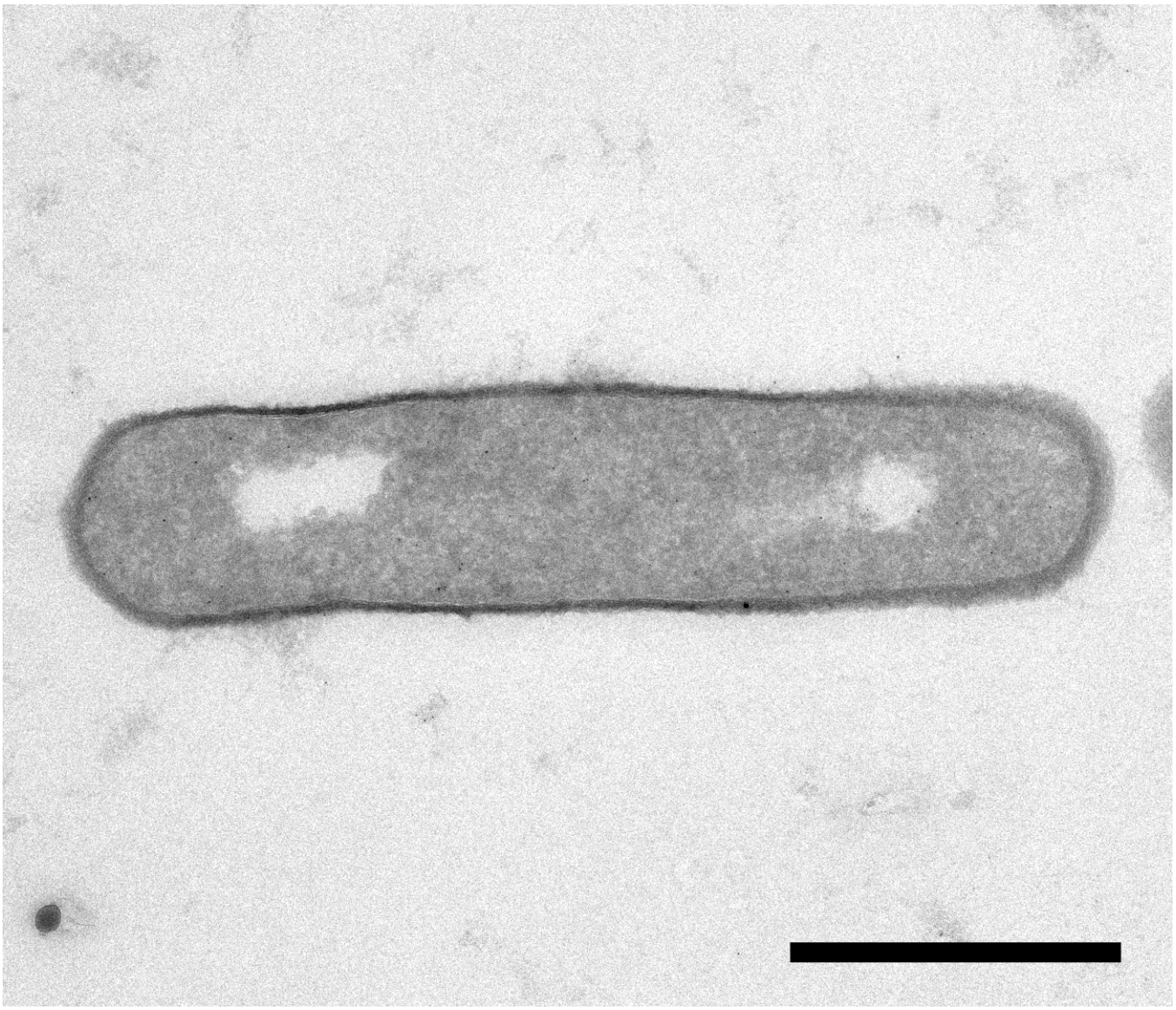

High resolution Fig. 5C

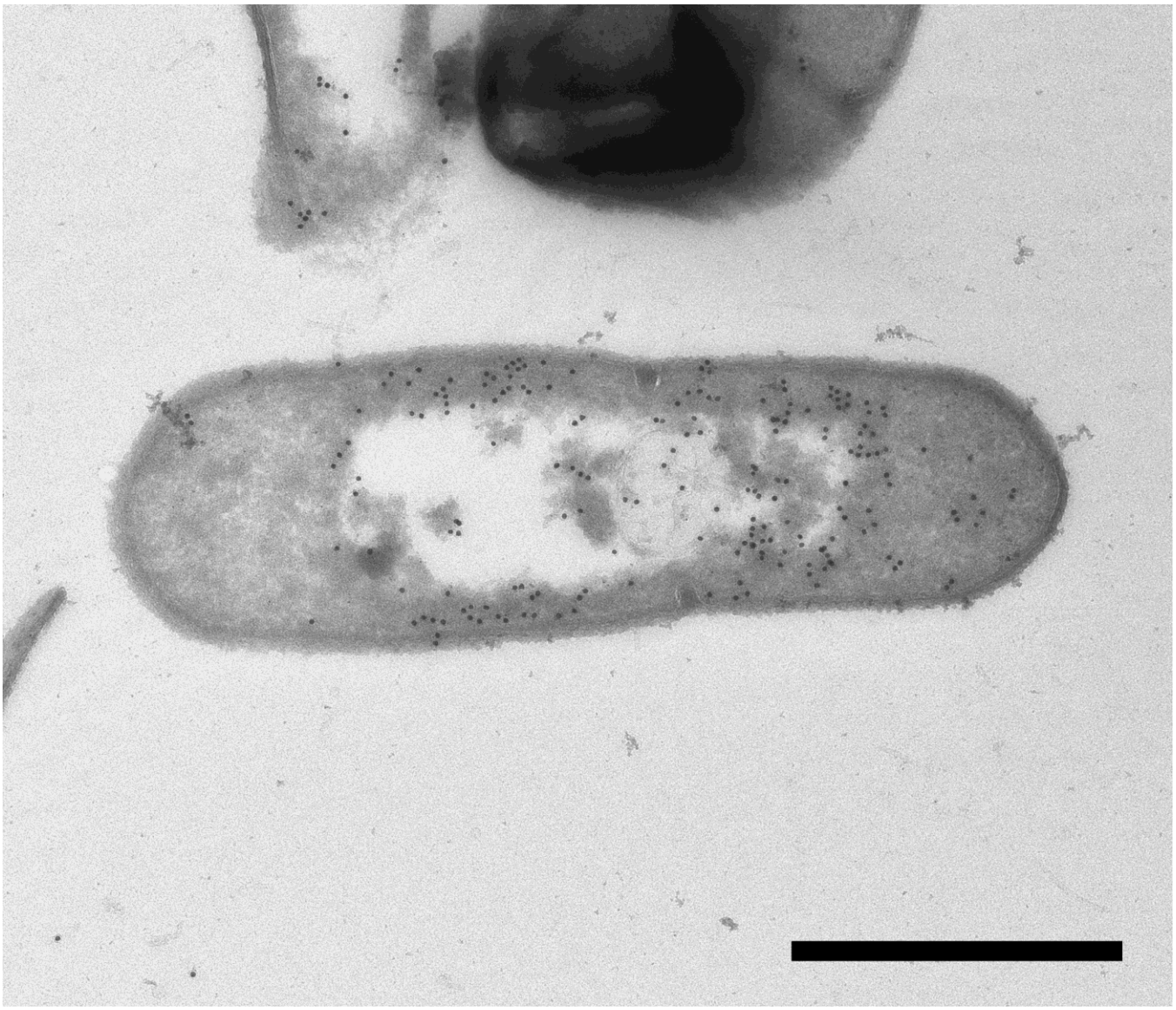

High resolution Fig. 5D

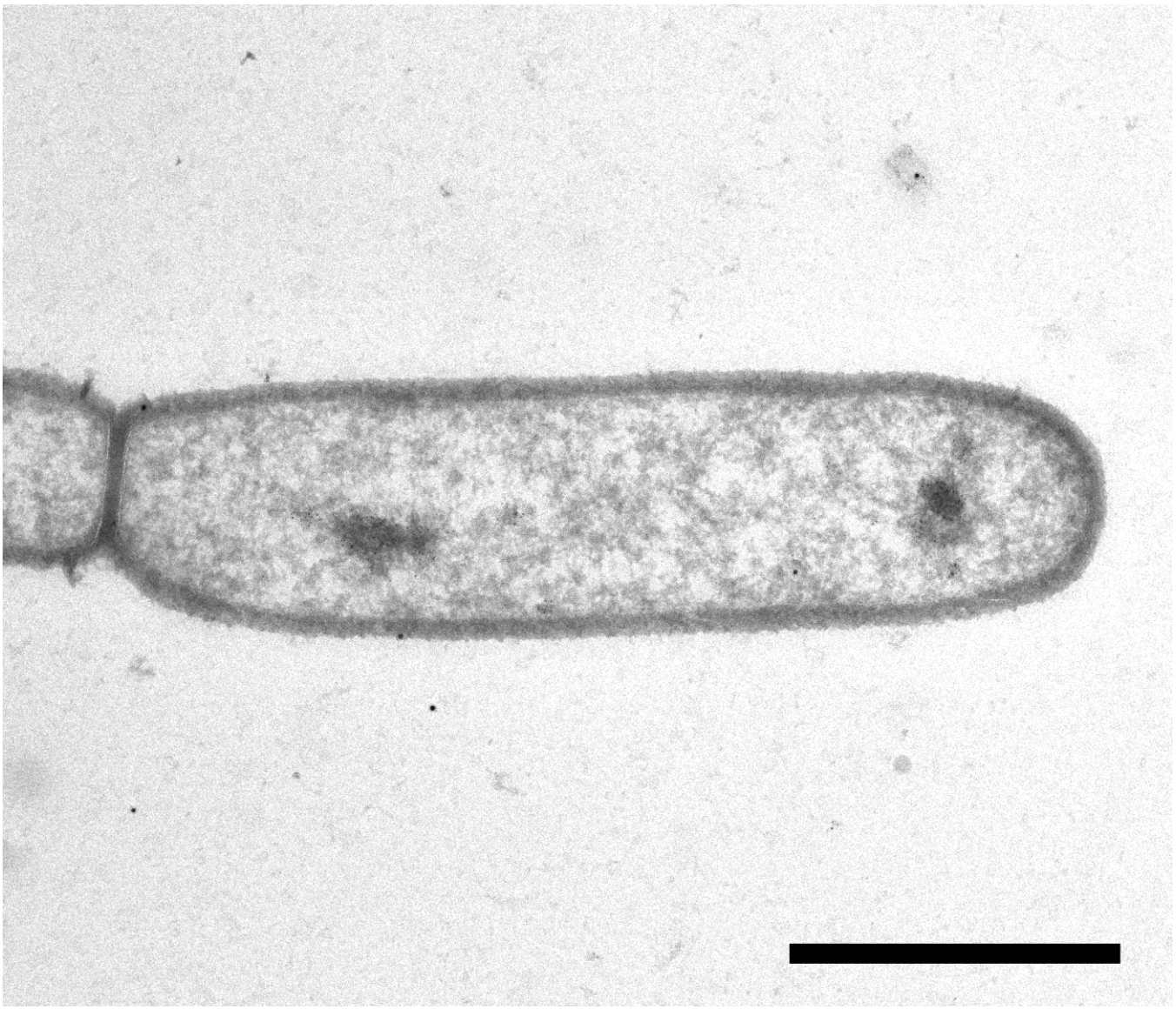

High resolution Fig. 5E

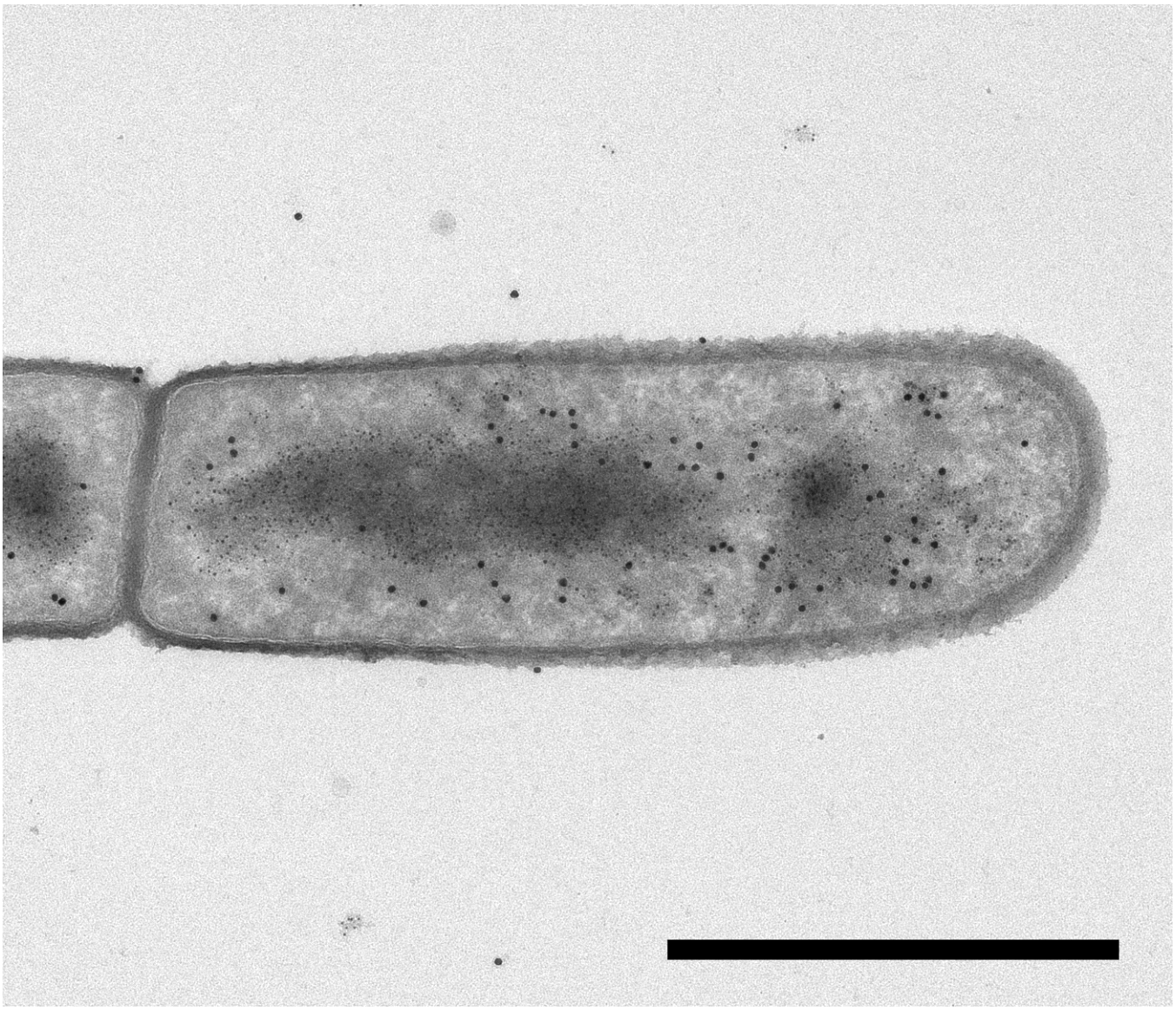

High resolution Fig. 5F

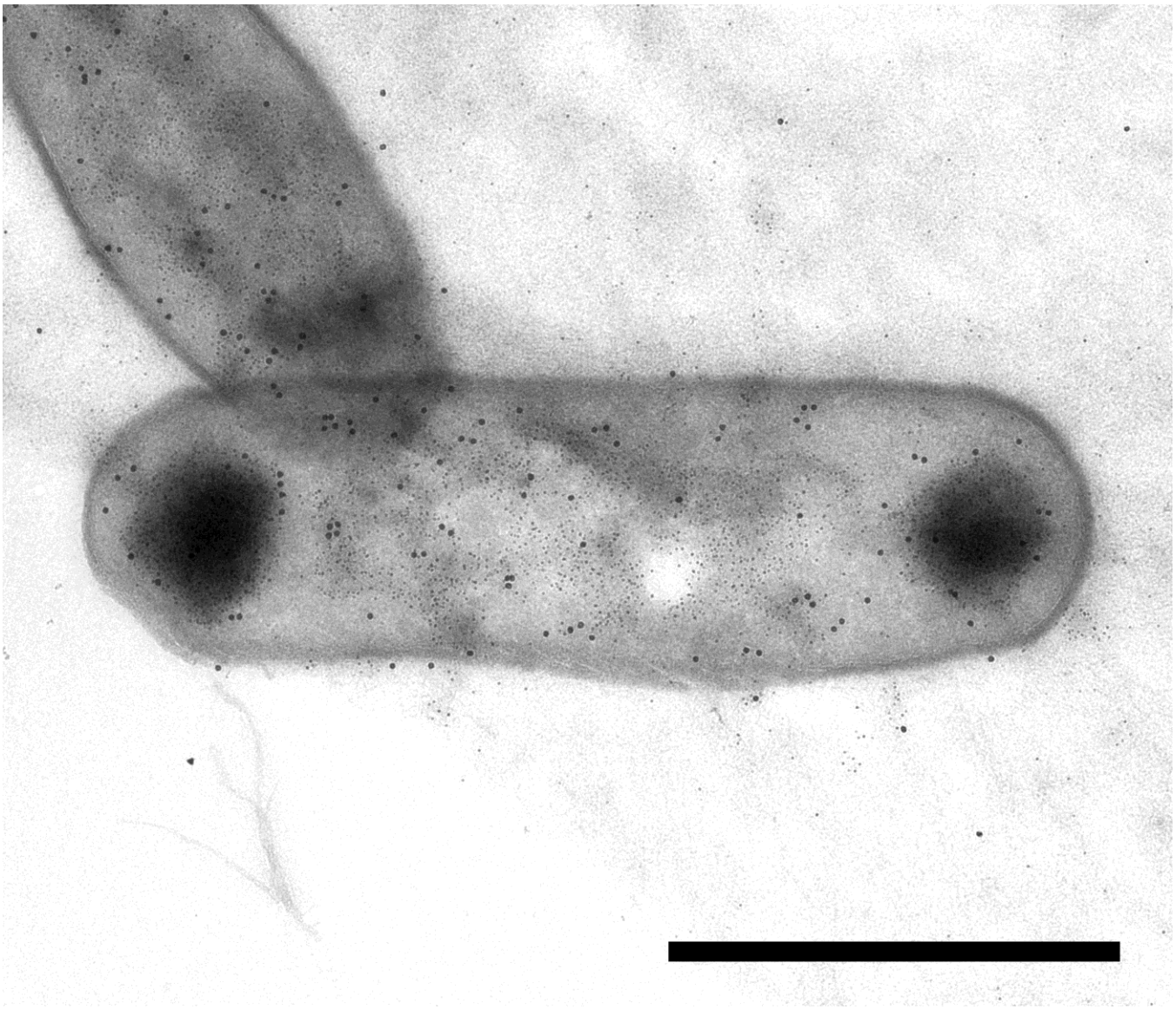

High resolution Fig. 6E

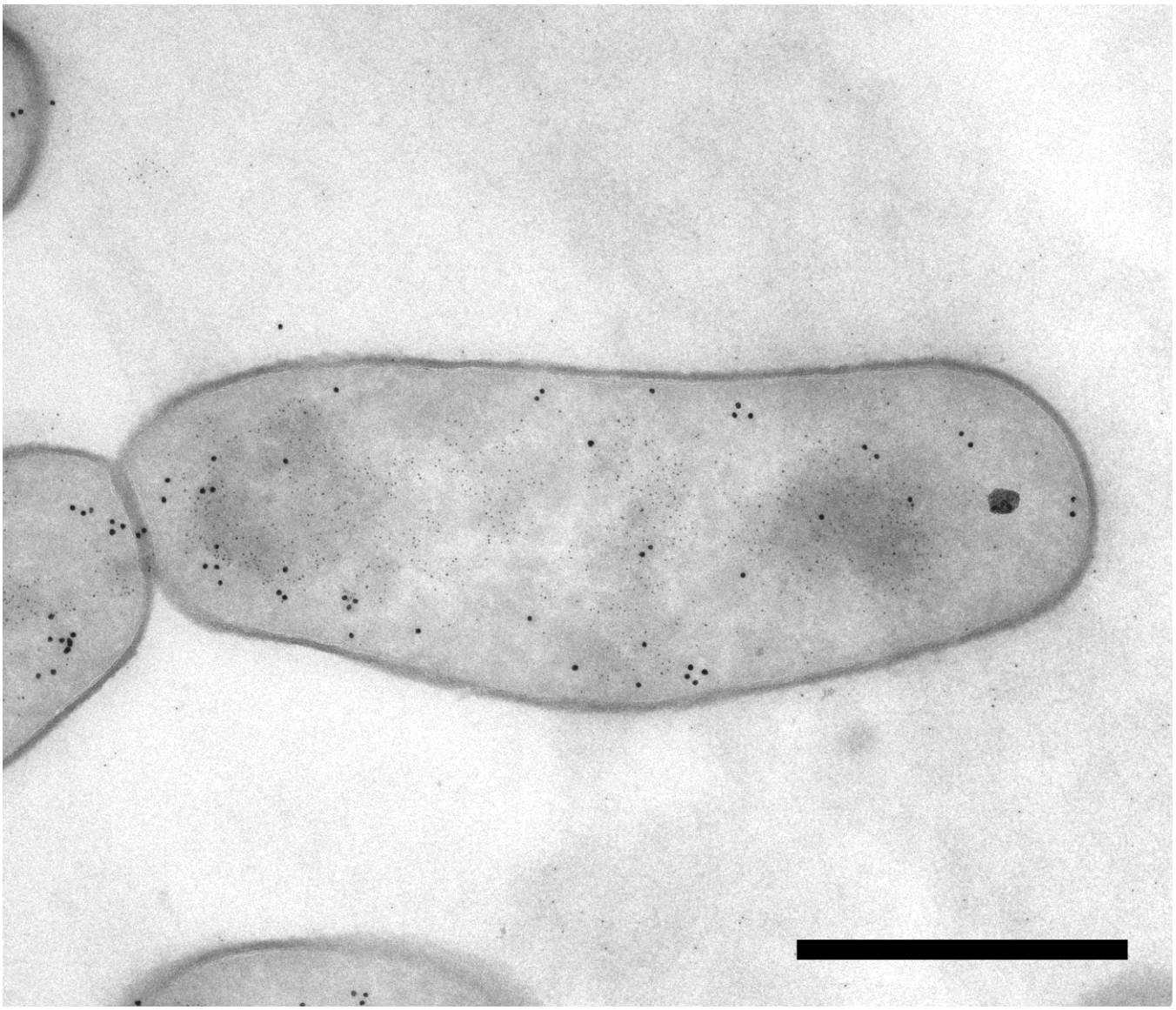

High resolution Fig. 6G

Table S1: **SPP1 proteins studied in this work involved in phage DNA replication and viral particle assembly.**

Their function (14), role on SPP1 multiplication (14), and type of FP fusion used in this work (Figs. 3,5 and 6 and *SI Appendix* Figs. S3 and S4) are presented.

SPP1 protein	Function	Essential for SPP1	FP fusion
Viral particle assembly			
gp1	SPP1 TerS; phage DNA recognition and packaging	yes	NA
gp2	SPP1 TerL; phage DNA packaging	yes	NA
gp6	procapsid and capsid portal protein, DNA packaging	yes	NA
gp7	procapsid and capsid minor protein ; DNA transfer to host cell	no	NA
gp11	internal procapsid scaffolding protein	yes	N-Ter
gp12	DNA-filled capsid auxiliary protein	no	C-Ter
gp13	major capsid protein	yes	NA
gp15	capsid connector adaptor protein	yes	NA
gp16	capsid connector stopper protein	yes	NA
gp17.1	major tail tube protein	yes	C-Ter
DNA replication			
gp34.1	5'-3' exonuclease ; switch theta to sigma mode of replication	no	C-Ter
gp35	recT-like recombinase	yes	N and C-Ter
gp38	SPP1 replication origin binding binding protein and replication re-start	yes	NA
gp39	gp40 helicase loader	yes	NA
gp40	replicative DNA helicase	yes	C-Ter

Table S2. *B. subtilis* replisome proteins.

Function, essential role in SPP1 replication (15), localization in non-infected ((16) and this work) and in infected bacteria (this work), and type of FP fusion used in this work (Figs. 2,3 and *SI Appendix* Fig. S2).

***B. subtilis* protein**	**function**	**essential for SPP1**	**localization in non-infected bacterium**	**localization change to SPP1 DNA**	**FP fusion**
PolC	DNA polymerase	yes	mid cell	yes	C-Ter
DnaE	DNA polymerase	yes	mid cell	yes	C-Ter
DnaX	DNA pol III τ subunit, assembly of the replisome, clamp loader	yes	mid cell	yes	N-Ter
DnaN	DNA pol III β subunit, sliding clamp	yes	mid cell	yes	N-Ter
DnaG	primase	yes	homogeneous	yes	N-Ter
SsbA	single-stranded DNA-binding protein	no	mid cell	yes	N-Ter
DnaB	initiation of DNA replication, primosome component	no	mid cell	yes	N-Ter
DnaC	replicative helicase	no	homogeneous	no	N-Ter

Table S3. Bacterial strains, phages, plasmids, antibodies and primers used in this study.

Bacterial strains		
E. coli F⁻ Φ80lacZΔM15 Δ(lacZYA-argF) U169 recA1 endA1 hsdR17 (rk⁻, mk⁺) phoA supE44 λ⁻thi⁻1 gyrA96 relA1	(17)	DH5α
*B. subtilis amyE trpC2 metB5 xin-1 att*SPβ	(18)	YB886
B. subtilis [*his met*] *sup- leu trpC2*	(19)	HA101B
B. subtilis [*metB5*] *sup-3 amyE trpC2 xin-1 att*SPβ	(20)	BG295
*B. subtilis amyE trpC2 metB5 xin-1 att*SPβ *thrC::(P$_{pen}$-lacIΔ11-cfp mls)*	(4)	GSY10000
*B. subtilis amyE trpC2 metB5 xin-1 att*SPβ *thrC::(P$_{pen}$-lacIΔ11-mcherry mls)*	This work	GSY10004
*B. subtilis amyE trpC2 metB5 xin-1 att*SPβ *thrC::(P$_{pen}$-lacIΔ11-mcherry mls) sacA::(P$_{spac}$-12-mcitrine kan)*	This work	GSY10024
*B. subtilis amyE trpC2 metB5 xin-1 att*SPβ *thrC::(P$_{pen}$-lacIΔ11-mcherry mls) sacA::(P$_{spac}$-mcitrine-11 kan)*	This work	GSY10025
*B. subtilis amyE trpC2 metB5 xin-1 att*SPβ *thrC::(P$_{pen}$-lacIΔ11-mcherry mls) sacA::(P$_{spac}$-34.1-mcitrine kan)*	This work	BG1837
*B. subtilis amyE trpC2 metB5 xin-1 att*SPβ *thrC::(P$_{pen}$-lacIΔ11-mcherry mls) sacA::(P$_{spac}$-mcitrine-35 kan)*	This work	BG1831
*B. subtilis amyE trpC2 metB5 xin-1 att*SPβ *thrC::(P$_{pen}$-lacIΔ11-mcherry mls) sacA::(P$_{spac}$-35-mcitrine kan)*	This work	BG1833
*B. subtilis amyE trpC2 metB5 xin-1 att*SPβ *thrC::(P$_{pen}$-lacIΔ11-mcherry mls) sacA::(P$_{spac}$-40-mcitrine kan)*	This work	BG1829
*B. subtilis amyE trpC2 metB5 xin-1 att*SPβ *thrC::(P$_{pen}$-lacIΔ11-mcherry mls) sacA::(P$_{spac}$-mcfp-dnaG spc)*	This work	GSY10031
*B. subtilis amyE trpC2 metB5 xin-1 att*SPβ *thrC::(P$_{pen}$-lacIΔ11-mcherry mls) sacA::(P$_{spac}$-mcfp-dnaX spc)*	This work	GSY10060
B. subtilis JJS59 *amyE::(P$_{xyl}$-polC-gfp spc)*	(16)	PolC-GFP
*B. subtilis trpC2 metB5 xin-1 att*SPβ *thrC::(P$_{pen}$-lacIΔ11-mcherry mls) amyE::(P$_{xyl}$-polC-gfp spc)*	This work	GSY10006
B. subtilis JJS59 *amyE::(P$_{xyl}$-gfp-dnaN spc)*	(16)	GFP-DnaN
*B. subtilis trpC2 metB5 xin-1 att*SPβ *thrC::(P$_{pen}$-lacIΔ11-mcherry mls) amyE::(P$_{xyl}$-gfp-dnaN spc)*	This work	GSY10008
B. subtilis JJS59 *amyE::(P$_{xyl}$-gfp-ssbA spc)*	(16)	GFP-SsbA
*B. subtilis trpC2 metB5 xin-1 att*SPβ *thrC::(P$_{pen}$-lacIΔ11-mcherry mls) amyE::(P$_{xyl}$-gfp-ssbA spc)*	This work	GSY10010
B. subtilis JJS59 *amyE::(P$_{xyl}$-gfp-dnaB spc)*	(16)	GFP-DnaB
*B. subtilis trpC2 metB5 xin-1 att*SPβ *thrC::(P$_{pen}$-lacIΔ11-mcherry mls) amyE::(P$_{xyl}$-gfp-dnaB spc)*	This work	GSY10011
B. subtilis JJS59 *amyE::(P$_{xyl}$-dnaE-gfp spc)*	(16)	DnaE-GFP

*B. subtilis trpC2 metB5 xin-1 att*SPβ *thrC::(*P_{pen}*-lacIΔ11-mcherry mls) amyE::(*P_{xyl}*-dnaE-gfp spc)*	This work	GSY10012
B. subtilis JJS59 *amyE::(*P_{xyl}*-gfp-dnaC spc)*	(16)	GFP-DnaC
*B. subtilis trpC2 metB5 xin-1 att*SPβ *thrC::(*P_{pen}*-lacIΔ11-mcherry mls) amyE::(*P_{xyl}*-gfp-dnaC spc)*	This work	GSY10014
*B. subtilis trpC2 metB5 xin-1 att*SPβ *thrC::(*P_{pen}*-lacIΔ11-mcherry mls) sacA::(*P_{spac}*-40-mcitrine kan) amyE::(*P_{xyl}*-mcfp-dnaX spc)*	This work	GSY10061
*B. subtilis trpC2 metB5 xin-1 att*SPβ *thrC::(*P_{pen}*-lacIΔ11-mcherry mls) sacA::(*P_{spac}*-17.1-mcitrine kan)*	This work	GSY10095
*B. subtilis trpC2 metB5 xin-1 att*SPβ *thrC::(*P_{pen}*-lacIΔ11-mcherry mls) sacA::(*P_{spac}*-17.1-mcitrine kan) amyE::(*P_{xyl}*-gp12-mcfp spc)*	This work	GSY10096
B. subtilis trpC2 spo0J::(tetO167 neo) amyE::(P_{xyl}*-tetR-mcherry spc)*	Kindly provided by Heath Murray BGSC 1A1087	HM1049
*B. subtilis trpC2 metB5 xin-1 att*SPβ *trpC2 thrC::(*P_{pen}*-lacIΔ11-cfp mls) amyE::(*P_{xyl}*-tetR-mcherry spc)*	This work	GSY10050
*B. subtilis trpC2 metB5 xin-1 att*SPβ *trpC2 thrC::(*P_{pen}*-lacIΔ11-cfp mls) spo0J::(tetO167 neo) amyE::(*P_{xyl}*-tetR-mcherry spc)*	This work	GSY10051

Phages		
SPP1*wt*: SPP1 wild-type lytic siphophage	(21)	*wt*
SPP1*delX110*: SPP1*wt* derivative carrying deletion *delX110*	(22)	*delX110*
SPP1*delX110lacO64*: SPP1*delX110* derivative carrying an array of *lacO* operators	(4)	*lacO64*
SPP1*sus34.1*: phage SPP1 defective in gene *34.1*	(23)	$gp34.1^-$
SPP1*delX110lacO64sus34.1*: SPP1*sus34.1* derivative carrying an array of *lacO* operators	This work	$lacO64gp34.1^-$
SPP1*sus12*: phage SPP1 defective in gene *40*	(15)	$gp40^-$
SPP1*delX110lacO64sus12*: SPP1*sus12* derivative carrying an array of *lacO* operators	This work	$lacO64gp40^-$
SPP1*sus31*: phage SPP1 defective in gene *13*	(8)	$gp13^-$
SPP1*delX110lacO64sus31*: SPP1*sus31* derivative carrying an array of *lacO* operators	This work	$lacO64gp13^-$
SPP1*sus19*: phage SPP1 defective in gene *2*	(6)	$gp2^-$
SPP1*delX110lacO64sus19*: SPP1*sus19* derivative carrying an array of *lacO* operators	This work	$lacO64gp2^-$
SPP1*del12*: phage SPP1 with a deletion in gene *12*	(24)	$gp12^-$
SPP1*delX110lacO64del12*: SPP1*del12* derivative carrying an array of *lacO* operators	This work	$lacO64gp12^-$
SPP1*sus115*: phage SPP1 defective in gene *6*	(22)	$gp6^-$

SPP1*delX110lacO64sus115*: SPP1*sus115* derivative carrying an array of *lacO* operators	This work	*lacO64gp6*$^-$
SPP1*sus7*: phage SPP1 defective in gene *11*	(8)	*gp11*$^-$
SPP1*delX110lacO64sus7*: SPP1*sus7* derivative carrying an array of *lacO* operators	This work	*lacO64gp11*$^-$
SPP1*sus117*: phage SPP1 defective in gene *16*	(5, 25)	*gp16*$^-$
SPP1*delX110lacO64sus117*: SPP1*sus117* derivative carrying an array of *lacO* operators	This work	*lacO64g16*$^-$
SPP1*sus9*: phage SPP1 defective in tail assembly gene	(8, 26)	*tail*$^-$
SPP1*delX110lacO64sus9*: SPP1*sus9* derivative carrying an array of *lacO* operators	This work	*lacO64tail*$^-$

Plasmids		
pHP13	(27)	NA
pJ1 *(kan:mcherry)*	Kindly provided by A.O. Henriques	NA
pKL190	(28)	NA
pDH88	(29)	NA
pJexpress404 (*bla:mcitrine*)	This work (DNA2:0)	NA
pDR200 *(bla:mcfp)*	Kindly provided by T. Doan and D. Rudner	NA
pSacKan *bla sacA::(kan*)	Kindly provided by D. Zeigler from BGSC	NA
pSG1190 *bla amyE:(P$_{xyl}$-mcfp spc)*	Kindly provided by D. Zeigler from BGSC	NA
pSG1192 *bla amyE:(P$_{xyl}$-mcfp spc)*	Kindly provided by D. Zeigler from BGSC	NA
pAL1 P$_{pen}$*-lacIΔ11-mcherry erm*	This work	NA
pPT300 *bla thrC::(*P$_{pen}$*-lacIΔ11-mcherry erm)*	This work	NA
pAL19 *bla sacA::(*P$_{spac}$ *kan)*	This work	NA
pAL20 *bla sacA::(*P$_{spac}$*-mcitrine kan)*	This work	NA
pAL21 *bla sacA::(*P$_{spac}$*-mcitrine kan)*	This work	NA
pAL24 *bla sacA::(*P$_{spac}$*-12-mcitrine kan)*	This work	NA
pAL25 *bla sacA::(*P$_{spac}$*-mcitrine-11 kan)*	This work	NA
pML1837 *bla sacA::(*P$_{spac}$*-34.1-mcitrine kan)*	This work	NA
pML1831 *bla sacA::(*P$_{spac}$*-mcitrine-35 kan)*	This work	NA
pML1833 *bla sacA::(*P$_{spac}$*-35-mcitrine kan)*	This work	NA
pML1829 *bla sacA::(*P$_{spac}$*-40-mcitrine kan)*	This work	NA
pAL28 *bla amyE::(*P$_{xyl}$*-mcfp spc)*	This work	NA

pAL29 *bla amyE::(*P_{xyl}*-mcfp spc)*	This work	NA
pAL31 *bla amyE::(*P_{xyl}*-mcfp-dnaG spc)*	This work	NA
pAL36 *bla amyE::(*P_{xyl}*-mcfp-dnaX spc)*	This work	NA
pAL44 *bla amyE::(*P_{xyl}*-12-mcfp spc)*	This work	NA
pAL53 *bla sacA::(*P_{spac}*-17.1-mcitrine kan)*	This work	NA
pHM232 *bla amyE::(*P_{xyl}*-tetR-mcherry spc)*	(30)	NA
pUC19-EJ1 vector with amplicons of SPP1, *B.s* and T7	This work	NA

Antibodies		
Anti-Rabbit IgG	Sigma Aldrich	Cat#A6667
Anti-SPP1 gp11 rabbit polyclonal serum	(8)	NA
Anti-SPP1 gp12 rabbit polyclonal serum	(24)	NA
Anti-SPP1 gp17.1 rabbit polyclonal serum	(31)	NA
Anti-SPP1 procapsids rabbit polyclonal serum	Kindly provided by S. Brasilès	NA
GFP Rabbit anti-Tag, polyclonal	Invitrogen	Cat#A6455
Goat Anti-Mouse IgG (H+L) Antibody, 5 nm Gold Conjugated	BBI Solutions	Cat#EM.GMHL5
Goat Anti-Rabbit IgG Antibody, 15 nm Gold Conjugated	BBI Solutions	Cat#EM.GAR15
Mouse Monoclonal against dsDNA	Abcam	Cat#ab27156

Primers	**Sequence (5'-3')**
For cloning	
Primer 1	CTG**CTCGAG**GGTTCCGGAATGGTCAGCAAGGGAGAGG
Primer 2	TTC**GGATCC**GCATGCTTATTTGTATAATTCGTCCATTCC
Primer 3	CGC**GGATCC**AGCCCGCCTAATGAGCGGGCTTTTTTTTTACACAGCCCAG
Primer 4	GGCCGGATCCATTAATGATGATGATGATGATGACCAGAACCTTCTAA CAGCTGCATTAATGAATCG
Primer 5	CCG**GAATTC**AAAGGAGAAATCGATTAGACGCTCGAGCTCGAAGGCA GTGGAATGGTAAGCAAAGGCGAGGAACTCTTCACAGGCG
Primer 6	CG**GGATCC**TTATTATTTATACAGTTCATCCATACCATGAGTTATGCCA GCTGCCG
Primer 7	CCCC**ATCGAT**ATGTCTAAGCGTATACCGCGTTTCTTGC
Primer 8	CGC**GGATCC**TTATTACTCGAGAGTCGTTCCGCCGCCGC
Primer 9	CCCC**ATCGAT**ATGCCAGAAACGCCTATTATGGGACAAGATG
Primer 10	CGC**GGATCC**TTATTACTCGAGAGGAGCAGGAACAGTTCCCGGTG
Primer 11	TAGG**ATCGAT**AAAATGGCGAG

Primer 12	CTATACA**CTCGAG**TGCCTTTTGC
Primer 13	CCCC**ATCGAT**ATGGCAACTAAAAAACAAGAGG
Primer 14	CCCC**CTCGAG**TTCATTTGTTTCCCCTC
Primer 15	CCCC**ATCGAT**ATGAATCCAGAAGAAAAAACG
Primer 16	CCCC**CTCGAG**ACGATCATCAAAACGAC
Primer 17	CCCC**ATCGAT**ATGAGTTTGAAAGAGCAGTTAGGTGAAGAGTTGTACG
Primer 18	CGC**GGATCC**TTATTACTCGAGCTGTGCTTCTGCTTGTAGCTTCT TCGC
Primer 19	CGC**GGATCC**CTATTCATTTGTTTCCC
Primer 20	CCGA**GGTACC**ATGGTTTCAAAAGGCG
Primer 21	CGA**GGATCC**CCTTATAAAGTTCGTCCATGCC
Primer 22	CGC**GGATCC**ACTTAGAAGGATCTGGAATGGGAAATCGGATACC
Primer 23	CGAATTC**ATCGAT**TTATTTTAAAGATCGGTTCAATGTAACG
Primer 24	CGC**GGATCC**ACTTAGAAGGATCTGGAATGAGTTACCAAGCTTTATATCG
Primer 25	CCG**CTCGAG**TTAGTCTTTTATTTCAATTAAATCC
Primer 26	CGA**GAATTC**ATGGTTTCAAAAGGCG
Primer 27	CGA**ACTAGT**TTATTACTTATAAAGTTCGTCCATGCC
Primer 28	CCG**GGTACC**ATGTCTAAGCGTATACCGCGTTTCTTGC
Primer 29	CCG**CTCGAG**CGGTCCAGATCCTTCTAA AGTCGTTCCGCCGCCGCTTG
For qPCR experiments	
SPP1-Fw	CGGGCTGAAATACCTGTGGA
SPP1-Rv	TAGCCCCTCCTCCGATTGTT
Bs-Fw	GAATACGGCAGAACGGCAAA
Bs-Rv	TTCGTTTTGAAACCCCATGC

Table S4. Treatment and immunolabeling of thin sections of *B. subtilis* cells.

Buffers, enzymatic treatment, antibodies labelling, and incubation conditions are presented.

	no treatment	**Benzonase treatment**	**trypsin treatment**	**incubation time**
buffer A	TBT	TBT + 25 U Benzonase	TBT + 10 µg.ml^{-1} trypsin (Sigma Aldrich)	1 hour at room temperature
blocking buffer	buffer for labelling + 0.4% BSA-c^{TM} (Aurion) + 0.1% CWFG gelatin (Sigma-Aldrich)	buffer for labelling + 0.4% BSA	buffer for labelling + 0.4% BSA-c^{TM} + 0.1% CWFG gelatin	30 minutes at room temperature
primary antibody	buffer for labelling + anti-sus70 (1 :150) serum + anti-dsDNA (1:200) + 0.4% BSA-c^{TM}			overnight at 4°C
secondary antibody	buffer for labelling + anti-IgG-rabbit-gold 15 nm (1:200) + anti-IgG-mouse-gold 5 nm (1:200) + 0.4% BSA-c^{TM}			2 hours in an humidity chamber

Movie S1. Time-lapse of SPP1 viral-induced compartmentalization of the *B. subtilis* cytoplasm.
B. subtilis GSY10024, producing LacI-mCherry and gp12-mCitrine, was immobilized in a CellAsic microfluidics system and infected with SPP1*lacO64gp12*$^{-}$. Note that cells are multi-infected. The time-lapse was processed to highlight the phage DNA compartment and virion warehouses as in Fig. 6*K* (displayed in magenta and green, respectively). Firstly, temporal lateral drift was estimated using the phase contrast channel and corrected on all channels (fluorescence and phase contrast). SPP1 DNA images were pre-processed to remove background signal (rolling ball subtraction, radius = 20 pixels) and enhanced using a Laplacian of Gaussian filter (with an increasing radius from 3 to 5 pixels to respect foci area enlargement during infection). Processed images were segmented using thresholding, converted to binary mask and blurred with a Gaussian filter (radius = 2 pixels) for visualization. Virion warehouses were denoised using median filter (radius: 1 pixel), and enhanced using Laplacian of Gaussian filter (radius = 2 pixels). As soon as warehouses appeared in the time-lapse they were segmented using thresholding, converted to binary mask after rejecting large foci (> 0.5 μm^2) to remove false detections based on results from Fig. 4*C*, and blurred with a Gaussian filter (radius = 2 pixels) for the visualization.

Dataset S1: Protein and DNA composition of SPP1 viral particles.
The mass of each protein was calculated from translation of their encoding genes (14). Stoichiometry was derived from structural (32–38) and/or biochemical data (8, 20, 24, 26, 31, 39–43). The mass of DNA encapsidated in SPP1*lacO64* is identical to SPP1 wild-type (45.1 kbp on average) (44) because SPP1 packages its DNA by a headful packaging mechanism. The genome length of SPP1*lacO64* used to calculate the mass of non-encapsidated genomes in infected bacteria is 42.3 kbp. An average cell volume of 1.59 μm^3 was derived from measurements of *B. subtilis* cells in our experimental conditions. Protein concentrations were then calculated for the total number of subunits engaged in virion assembly. These values aim to provide an order of magnitude of viral polypeptide numbers present in the cell. However, they are not free in the cytoplasm, rapidly assembling into large macromolecular complexes in normal infection conditions. Cumulative numbers for virion components are provided for the SPP1*lacO64* infection using data from Fig. 1*B*. Proteins function in viral assembly and their topology in the viral particle are also listed. NA - not applied; NS - non-structural. # - There is an average of 3 gp7 molecules per virion (39). ## - There are 415-420 copies of scaffolding protein gp11 per precursor procapsid (32) but it is not known if the protein is recycled for procapsid assembly after release from procapsids. The mass of gp11 is thus not included in this calculation. ### - The number of subunits of the tape measure gp18 in SPP1 particles is low but not precisely known (37). #### - An encapsidated SPP1 DNA molecule of ~45.1 kbp (44) has a molecular mass of ~45100 x 0.65 = ~29315 kDa considering that a base pair has an average molecular mass of 0.65 kDa. A SPP1 genome of 42.3 kbp has a molecular mass of ~42300 x 0.65 = ~27495 kDa.

SI References

1. R. J. Boylan, N. H. Mendelson, D. Brooks, F. E. Young, Regulation of the Bacterial Cell Wall : Analysis of a Mutant of Bacillus subtilis Defective in Biosynthesis of Teichoic Acid. *J. Bacteriol.* **110**, 281–290 (1972).
2. H. Esche, Gene expression of bacteriophage SPP1. II. Regulatory aspects. *Mol. Gen. Genet.* **142**, 57–66 (1975).
3. J. Sambrook, E. F. Fritsch, T. Maniatis, Molecular Cloning: A Laboratory Manual, 2nd edn. *Cold Spring Harb. NY Cold Spring Harb. Lab. Press.* (1989).
4. L. Jakutyte, *et al.*, Bacteriophage infection in rod-shaped Gram-positive bacteria: Evidence for a preferential polar route for phage SPP1 entry in Bacillus subtilis. *J. Bacteriol.* **193**, 4893–4903 (2011).
5. B. Behrens, G. Lüder, M. Behncke, T. A. Trautner, The Genome of B. subtilis Phage SPP1: Physical Arrangement of Phage genes. *MGG Mol. Gen. Genet.* **175**, 351–357 (1979).
6. S. Chai, *et al.*, Molecular Analysis of the Bacillus subtilis Bacteriophage SPP1 Region Encompassing Genes 1 to 6 SPP1 - The Products of Gene 1 and Gene 2 are Required for pac Cleavage. *J. Mol. Biol.* **224**, 87–102 (1992).
7. I. F. Lau, *et al.*, Spatial and temporal organization of replicating Escherichia coli chromosomes. *Mol. Microbiol.* **49**, 731–743 (2003).
8. B. Becker, *et al.*, Head morphogenesis genes of the Bacillus subtilis bacteriophage SPP1. *J. Mol. Biol.* **268**, 822–839 (1997).
9. A. Isidro, M. A. Santos, A. O. Henriques, P. Tavares, The high-resolution functional map of bacteriophage SPP1 portal protein. *Mol. Microbiol.* **51**, 949–962 (2004).
10. G. Griffiths, A. McDowall, R. Back, J. Dubochet, On the preparation of cryosections for immunocytochemistry. *J. Ultrastruct. Res.* **89**, 65–78 (1984).
11. K. T. Tokuyasu, A technique for ultracryotomy of cell suspensions and tissues. *J. Cell Biol.* **57**, 551–565 (1973).
12. E. Bos, *et al.*, Vitrification of Tokuyasu-style immuno-labelled sections for correlative cryo light microscopy and cryo electron tomography. *J. Struct. Biol.* **186**, 273–282 (2014).
13. J. Schindelin, *et al.*, Fiji - an Open Source platform for biological image analysis. *Nat. Methods* **9**, 241–256 (2013).
14. L. M. Godinho, *et al.*, The Revisited Genome of Bacillus subtilis Bacteriophage SPP1. *Viruses* **10**, 1–28 (2018).
15. X. Pedré, F. Weise, S. Chai, G. Lüder, J. C. Alonso, Analysis of Cis and Trans acting elements

required for the initiation of DNA replication in the Bacillus subtilis bacteriophage SPP1. *J. Mol. Biol.* **236**, 1324–1340 (1994).

16. J. C. Meile, L. J. Wu, S. D. Ehrlich, J. Errington, P. Noirot, Systematic localisation of proteins fused to the green fluorescent protein in Bacillus subtilis: Identification of new proteins at the DNA replication factory. *Proteomics* **6**, 2135–2146 (2006).
17. D. Hanahan, Studies on Transformation of Escherichia coli with Plasmids. *J. Mol. Biol.* **166**, 557–580 (1983).
18. R. E. Yasbin, P. I. Fields, B. J. Andersen, Properties of Bacillus subtilis 168 derivatives freed of their natural prophages. *Gene* **12**, 155-159 (1980).
19. S. Okubo, T. Yanagida, Isolation of a suppressible mutant in Bacillus subtilis. *J Bacteriol* **95**, 1187–1188 (1968).
20. A. Dröge, *et al.*, Shape and DNA packaging activity of bacteriophage SPP1 procapsid: protein components and interactions during assembly. *J. Mol. Biol.* **296**, 117–132 (2000).
21. S. Riva, M. Polsinelli, A. Falaschi, A new phage of Bacillus subtilis with infectious DNA having separable strands. *J. Mol. Biol.* **35**, 347–356 (1968).
22. P. Tavares, *et al.*, Identification of a gene in Bacillus subtilis bacteriophage SPP1 determining the amount of packaged DNA. *J. Mol. Biol.* **225**, 81–92 (1992).
23. A. Valero-Rello, M. López-Sanz, A. Quevedo-Olmos, A. Sorokin, S. Ayora, Molecular Mechanisms That Contribute to Horizontal Transfer of Plasmids by the Bacteriophage SPP1. *Front. Microbiol.* **8**, 1–13 (2017).
24. M. Zairi, A. C. Stiege, N. Nhiri, E. Jacquet, P. Tavares, The Collagen-like Protein gp12 is a Temperature-dependent Reversible Binder of SPP1 Viral Capsids. *J. Biol. Chem.* **289**, 27169–27181 (2014).
25. E. V. Orlova, *et al.*, Structure of a viral DNA gatekeeper at 10 Å resolution by cryo-electron microscopy. *EMBO J.* **22**, 1255–1262 (2003).
26. R. Lurz, *et al.*, Structural organisation of the head-to-tail Interface of a bacterial virus. *J. Mol. Biol.* **310**, 1027–1037 (2001).
27. P. Haima, S. Bron, G. Venema, The effect of restriction on shotgun cloning and plasmid stability in Bacillus subtilis Marburg. *Mol Microbiol* **209**, 335–342 (1987).
28. K. P. Lemon, A. D. Grossman, Movement of replicating DNA through a stationary replisome. *Mol. Cell* **6**, 1321–1330 (2000).
29. D. J. Henner, Inducible Expression of Regulatory Genes in Bacillus subtilis. *Methods Enzymol.* **185**, 223–228 (1990).
30. H. Murray, J. Errington, Dynamic Control of the DNA Replication Initiation Protein DnaA by

Soj/ParA. *Cell* **135**, 74–84 (2008).

31. I. Auzat, A. Dröge, F. Weise, R. Lurz, P. Tavares, Origin and function of the two major tail proteins of bacteriophage SPP1. *Mol. Microbiol.* **70**, 557–569 (2008).
32. A. Ignatiou, *et al.*, Structural transitions during the scaffolding-driven assembly of a viral capsid. *Nat. Commun.* **10**, 1–11 (2019).
33. H. E. White, *et al.*, Capsid Structure and Its Stability at the Late Stages of Bacteriophage SPP1 Assembly. *J. Virol.* **86**, 6768–6777 (2012).
34. Y. Chaban, *et al.*, Structural rearrangements in the phage head-to-tail interface during assembly and infection. *Proc. Natl. Acad. Sci. U. S. A.* **112**, 7009–7014 (2015).
35. B. Chagot, *et al.*, Solution structure of gp17 from the Siphoviridae bacteriophage SPP1: Insights into its role in virion assembly. *Proteins Struct. Funct. Bioinforma.* **80**, 319–326 (2012).
36. A. Goulet, *et al.*, The opening of the SPP1 bacteriophage tail, a prevalent mechanism in Gram-positive-infecting siphophages. *J. Biol. Chem.* **286**, 25397–25405 (2011).
37. C. Plisson, *et al.*, Structure of bacteriophage SPP1 tail reveals trigger for DNA ejection. *EMBO J.* **26**, 3720–3728 (2007).
38. S. Lhuillier, *et al.*, Structure of bacteriophage SPP1 head-to-tail connection reveals mechanism for viral DNA gating. *Proc. Natl. Acad. Sci. U. S. A.* **106**, 8507–8512 (2009).
39. A. C. Stiege, A. Isidro, A. Dröge, P. Tavares, Specific targeting of a DNA-binding protein to the SPP1 procapsid by interaction with the portal oligomer. *Mol. Microbiol.* **49**, 1201–1212 (2003).
40. D. Veesler, *et al.*, Crystal structure of bacteriophage SPP1 distal tail protein (gp19.1): A baseplate hub paradigm in gram-positive infecting phages. *J. Biol. Chem.* **285**, 36666–36673 (2010).
41. I. Vinga, *et al.*, Role of bacteriophage SPP1 tail spike protein gp21 on host cell receptor binding and trigger of phage DNA ejection. *Mol. Microbiol.* **83**, 289–303 (2012).
42. I. Auzat, I. Petitpas, R. Lurz, F. Weise, P. Tavares, A touch of glue to complete bacteriophage assembly: The tail-to-head joining protein (THJP) family. *Mol. Microbiol.* **91**, 1164–1178 (2014).
43. S. L. Poh, *et al.*, Oligomerization of the SPP1 Scaffolding Protein. *J. Mol. Biol.* **378**, 551–564 (2008).
44. C. São-José, M. de Frutos, E. Raspaud, M. A. Santos, P. Tavares, Pressure Built by DNA Packing Inside Virions: Enough to Drive DNA Ejection in Vitro, Largely Insufficient for Delivery into the Bacterial Cytoplasm. *J. Mol. Biol.* **374**, 346–355 (2007).